

ISSN 1881-7815 Online ISSN 1881-7823

BST

BioScience Trends

Volume 5 • Number 1 • 2011



www.biosciencetrends.com

BST

BioScience Trends



ISSN: 1881-7815
Online ISSN: 1881-7823
CODEN: BTIRCZ
Issues/Year: 6
Language: English
Publisher: IACMHR Co., Ltd.

BioScience Trends is one of a series of peer-reviewed journals of the International Research and Cooperation Association for Bio & Socio-Sciences Advancement (IRCA-BSSA) Group and is published bimonthly by the International Advancement Center for Medicine & Health Research Co., Ltd. (IACMHR Co., Ltd.) and supported by the IRCA-BSSA and Shandong University China-Japan Cooperation Center for Drug Discovery & Screening (SDU-DDSC).

BioScience Trends devotes to publishing the latest and most exciting advances in scientific research. Articles cover fields of life science such as biochemistry, molecular biology, clinical research, public health, medical care system, and social science in order to encourage cooperation and exchange among scientists and clinical researchers.

BioScience Trends publishes Original Articles, Brief Reports, Reviews, Policy Forum articles, Case Reports, News, and Letters on all aspects of the field of life science. All contributions should seek to promote international collaboration.

Editorial Board

Editor-in-Chief:

Masatoshi MAKUUCHI
Japanese Red Cross Medical Center, Tokyo, Japan

Co-Editors-in-Chief:

Xue-Tao CAO
Chinese Academy of Medical Sciences, Beijing, China
Rajendra PRASAD
King George's Medical University, Lucknow, India
Arthur D. RIGGS
Beckman Research Institute of the City of Hope, Duarte, CA, USA

Chief Director & Executive Editor:

Wei TANG
The University of Tokyo, Tokyo, Japan

Managing Editor:

Munehiro NAKATA
Tokai University, Hiratsuka, Japan

Senior Editors:

Xunjia CHENG
Fudan University, Shanghai, China
Yoko FUJITA-YAMAGUCHI
Tokai University, Hiratsuka, Japan
Kiyoshi KITAMURA
The University of Tokyo, Tokyo, Japan

Chushi KUROIWA
Yotsukaidou Tokushukai Medical Center, Yotsukaido, Japan
Misao MATSUSHITA
Tokai University, Hiratsuka, Japan
Takashi SEKINE
The University of Tokyo, Tokyo, Japan
Yasuhiko SUGAWARA
The University of Tokyo, Tokyo, Japan

Web Editor:

Yu CHEN
The University of Tokyo, Tokyo, Japan

Proofreaders:

Curtis BENTLEY
Roswell, GA, USA
Christopher HOLMES
The University of Tokyo, Tokyo, Japan
Thomas R. LEBON
Los Angeles Trade Technical College, Los Angeles, CA, USA

Editorial Office

Pearl City Koishikawa 603,
2-4-5 Kasuga, Bunkyo-ku,
Tokyo 112-0003, Japan
Tel: 03-5840-8764
Fax: 03-5840-8765
E-mail: office@biosciencetrends.com

BioScience Trends

Editorial and Head Office

Pearl City Koishikawa 603, 2-4-5 Kasuga, Bunkyo-ku,
Tokyo 112-0003, Japan

Tel: 03-5840-8764, Fax: 03-5840-8765
E-mail: office@biosciencetrends.com
URL: www.biosciencetrends.com

Editorial Board Members

Girdhar G. AGARWAL (Lucknow, India)	Na HE (Shanghai, China)	Qingyue MENG (Beijing, China)	Puay Hoon TAN (Singapore, Singapore)
Hirotsugu AIGA (Geneva, Switzerland)	David M. HELFMAN (Daejeon, Korea)	Mark MEUTH (Sheffield, UK)	John TERMINI (Duarte, CA, USA)
Hidechika AKASHI (Tokyo, Japan)	De-Xing HOU (Kagoshima, Japan)	Yutaka MOROHOSHI (Tokyo, Japan)	Usa C. THISYAKORN (Bangkok, Thailand)
Moazzam ALI (Geneva, Switzerland)	Sheng-Tao HOU (Ottawa, Canada)	Satoko NAGATA (Tokyo, Japan)	Toshifumi TSUKAHARA (Nomi, Japan)
Michael E. BARISH (Duarte, CA, USA)	Yong HUANG (Ji'ning, China)	Miho OBA (Odawara, Japan)	Kohjiro UEKI (Tokyo, Japan)
Boon-Huat BAY (Singapore, Singapore)	Hirofumi INAGAKI (Tokyo, Japan)	Xianjun QU (Ji'nan, China)	Masahiro UMEZAKI (Tokyo, Japan)
Yasumasa BESSHO (Nara, Japan)	Masamine JIMBA (Tokyo, Japan)	Sergei N. RODIN (Duarte, CA, USA)	Junming WANG (Jackson, MS, USA)
Generoso BEVILACQUA (Pisa, Italy)	Kimitaka KAGA (Tokyo, Japan)	John J. ROSSI (Duarte, CA, USA)	Stephen G. WARD (Bath, UK)
Shiuan CHEN (Duarte, CA, USA)	Ichiro KAI (Tokyo, Japan)	Carlos SAINZ-FERNANDEZ (Santander, Spain)	Hisashi WATANABE (Tokyo, Japan)
Yuan CHEN (Duarte, CA, USA)	Kazuhiro KAKIMOTO (Osaka, Japan)	Takehito SATO (Isehara, Japan)	Masatake YAMAUCHI (Chiba, Japan)
Naoshi DOHMAE (Wako, Japan)	Kiyoko KAMIBEPPU (Tokyo, Japan)	Akihito SHIMAZU (Tokyo, Japan)	Yun YEN (Duarte, CA, USA)
Zhen FAN (Houston, TX, USA)	Bok-Luel LEE (Busan, Korea)	Judith SINGER-SAM (Duarte, CA, USA)	George W-C. YIP (Singapore, Singapore)
Ding-Zhi FANG (Chengdu, China)	Mingjie LI (St. Louis, MO, USA)	Raj K. SINGH (Dehradun, India)	Benny C-Y ZEE (Hong Kong, China)
Yoshiharu FUKUDA (Ube, Japan)	Ren-Jang LIN (Duarte, CA, USA)	Junko SUGAMA (Kanazawa, Japan)	(as of February 2011)
Rajiv GARG (Lucknow, India)	Hongxiang LOU (Ji'nan, China)	Hiroshi TACHIBANA (Isehara, Japan)	
Ravindra K. GARG (Lucknow, India)	Daru LU (Shanghai, China)	Tomoko TAKAMURA (Tokyo, Japan)	
Makoto GOTO (Yokohama, Japan)	Duan MA (Shanghai, China)	Tadatashi TAKAYAMA (Tokyo, Japan)	
Demin HAN (Beijing, China)	Yutaka MATSUYAMA (Tokyo, Japan)	Sumihito TAMURA (Tokyo, Japan)	

Original Articles

- 1 - 9** **Multiple viral coinfections among HIV/AIDS patients in China.**
Na He, Li Chen, Haijiang Lin, Man Zhang, Jun Wei, Jianhua Yang, Jenna Gabrio, Baoling Rui, Zuo-Feng Zhang, Zhuohua Fu, Yingying Ding, Genming Zhao, Qingwu Jiang, Roger Detels
- 10 - 16** **Invasion of carcinoma cells into reconstituted type I collagen gels: Visual real-time analysis by time-lapse microscopy.**
Keiko Sakai, Taisuke Kurokawa, Yoshihiro Furui, Yuh Kuronuma, Masaru Sekiguchi, Jun Ando, Yoshinori Inagaki, Wei Tang, Munehiro Nakata, Yoko Fujita-Yamaguchi
- 17 - 22** **Expression, purification, and S-nitrosylation of recombinant histone deacetylase 8 in *Escherichia coli*.**
Jinhong Feng, Fanbo Jing, Hao Fang, Lichuan Gu, Wenfang Xu
- 23 - 29** **Nrf2-mediated protection against UVA radiation in human skin keratinocytes.**
Feifei Tian, Feifei Zhang, Xiangdong Lai, Lijuan Wang, Li Yang, Xiang Wang, Gurinder Singh, Julia Li Zhong
- 30 - 37** **Influence of glutathione levels and activity of glutathione-related enzymes in the brains of tumor-bearing mice.**
Kaikai Shen, Lili Ji, Ying Chen, Qianming Yu, Zhengtao Wang
- 38 - 43** **Environmental lead exposure as a risk for childhood aplastic anemia.**
Maqsood Ahamed, Mohd Javed Akhtar, Sanjeev Verma, Archana Kumar, Mohammad K.J. Siddiqui

Case Report

- 44 - 45** **Dengue causing fulminant hepatitis in a hepatitis B virus carrier.**
Mukul P. Agarwal, Subhash Giri, Vishal Sharma, Ujjawal Roy, Komal Gharsangi

CONTENTS

(Continued)

Guide for Authors

Copyright

Multiple viral coinfections among HIV/AIDS patients in China

Na He^{1,*}, Li Chen¹, Haijiang Lin^{1,2}, Man Zhang³, Jun Wei⁴, Jianhua Yang⁵, Jenna Gabrio⁶, Baoling Rui³, Zuo-Feng Zhang⁷, Zhuohua Fu¹, Yingying Ding^{1,7}, Genming Zhao¹, Qingwu Jiang¹, Roger Detels⁷

¹ Department of Epidemiology, School of Public Health, Fudan University; Key Laboratory of Public Health Safety of Ministry of Education, Shanghai, China;

² Taizhou City Center for Disease Control and Prevention, Taizhou, Zhejiang Province, China;

³ Urumqi City Center for Disease Control and Prevention, Urumqi, Xinjiang Uygur Autonomous Region, China;

⁴ Yuncheng Prefecture Center for Disease Control and Prevention, Yuncheng, Shanxi Province, China;

⁵ Yingjiang County Center for Disease Control and Prevention, Yingjiang, Yunnan Province, China;

⁶ Department of International Health, School of Nursing and Health Sciences, Georgetown University, Washington, DC, USA;

⁷ Department of Epidemiology, School of Public Health, University of California, Los Angeles, CA, USA.

Summary

A cross-sectional survey was conducted to determine seroprevalence and correlates of coinfections of hepatitis B virus (HBV), hepatitis C virus (HCV), Epstein-Bar virus (EBV), herpes simplex virus including type 1 (HSV-1) and type 2 (HSV-2) among human immunodeficiency virus (HIV)/acquired immunodeficiency syndrome (AIDS) patients in China. A total of 1,110 HIV/AIDS patients from Shanxi (Central area, $n = 287$), Zhejiang (Eastern area, $n = 163$), Yunnan (Southwestern area, $n = 300$) and Xinjiang (Northwestern area, $n = 360$) provinces were analyzed. The overall seroprevalence was 6.3% for HBsAg, 59.0% for anti-HCV IgG, 96.6% for anti-EBV IgG, 91.5% for anti-HSV-1 IgG, and 34.1% for anti-HSV-2 IgG. Eleven (1.0%) HIV/AIDS patients were coinfecting with all five viruses, 177 (15.9%) with four viruses, 611 (55.0%) with three viruses, 288 (25.9%) with two viruses, 23 (2.1%) with single virus, and 1 (0.1%) with none of the five viruses. Multiple logistic regression analyses indicated that neither HBV, nor EBV and HSV-1 coinfection was associated with sociodemographic characteristics and HIV transmission mode, but HCV coinfection was associated with geographic region, age, gender, ethnicity, marital status, and HIV transmission mode, whereas HSV-2 coinfection was associated with geographic region, ethnicity and HIV transmission mode. This study suggests that HIV/AIDS patients with different regional and sociodemographic backgrounds and HIV transmission mode in China have different profiles of viral coinfections and should be subject to differential considerations in related health care programs.

Keywords: Coinfection, HSV, EBV, HBV/HCV, HIV, Chinese

1. Introduction

The issue of viral coinfection among human immunodeficiency virus (HIV)/acquired immunodeficiency syndrome (AIDS) patients

represents a growing public health concern worldwide. Viral coinfections among an HIV-infected individual may affect the disease progression of HIV/AIDS and may accelerate the progression of these other viral infections to more severe illness due to HIV coinfection (1-10). Among the list of viruses that are likely to be co-infected with HIV, hepatitis B virus (HBV), hepatitis C virus (HCV), herpes simplex virus including type 1 (HSV-1) and type 2 (HSV-2), and the Epstein-Bar virus (EBV) are the most important coinfections among HIV/AIDS patients due to their pathogenicity and relatively high prevalence in populations affected by HIV.

*Address correspondence to:

Dr. Na He, Department of Epidemiology, School of Public Health, Fudan University; Key Laboratory of Public Health Safety of Ministry of Education, Shanghai, China.

e-mail: nhe@shmu.edu.cn

HBV and HCV are of concerns because both viruses compromise liver function, which may further affect the metabolism and therapeutic effect of antiretroviral drugs (ARV) for AIDS patients (11-13). They are also classified as group one causative agents of hepatocellular carcinoma (HCC) by International Agency for Research on Cancer (IARC). Worldwide it is estimated that 10-30% of the 40 million people infected with HIV are co-infected with HCV due to similar transmission routes between HIV and HCV (14). In China, high prevalence of HIV and HCV coinfection has been reported among injection drug users (IDU) and plasma/blood donors (15,16).

HSV also plays an important role in the disease progression of HIV infection. Chronic infection of HSV-1 has been regarded by the World Health Organization (WHO) as an important factor affecting the disease progression of HIV/AIDS. HSV-1 infection is usually transmitted during childhood and adolescence and is most often transmitted *via* nonsexual contact (17). On the other hand, HSV-2 is most likely to be sexually transmitted and is the leading cause of the genital ulcer disease. Studies have suggested that there is a strong association between HSV-2 and HIV serostatus and that diagnosis of HSV-2 infection can help to identify individuals at greater risk for contracting HIV (18). In China, HSV-2 infection is relatively uncommon in the general population but is very common among female sex workers (19-24).

EBV is the causal agent of non-Hodgkin's lymphoma (NHL) which is an AIDS-defining malignancy. It is also the causal agent of Hodgkin's lymphoma (HL) and nasopharyngeal cancer, both of which are non-AIDS defining malignancies but have been increasingly observed among HIV/AIDS patients who have experienced long-term immunodeficiency (25,26). EBV is also highly prevalent around the world (27).

In China, there has been no study specifically designed to examine the seroprevalence of viral coinfections among HIV/AIDS patients. We hypothesize that multiple pathogenic viral coinfections may negatively impact HIV-infected individuals. Therefore, as the first step to test the hypothesis, we conducted a cross-sectional seroprevalence survey of HBV, HCV, HSV-1, HSV-2, and EBV among HIV/AIDS patients from four geographical areas representing different HIV transmission routes in China. The knowledge gained from this study will shed a light on the disease progression of HIV infection in Chinese populations and will be valuable for designing effective antiretroviral treatment (ART) programs for Chinese HIV/AIDS patients.

2. Materials

2.1. HIV/AIDS reporting and managing system in China

In China, it is required by law that all newly identified HIV-infected cases must be reported to local centers

for disease prevention and control (CDC) first and then to the national CDC through the AIDS Network Direct Reporting Information System. The local CDC is also obligated to conduct a nationwide standardized epidemiological investigation on each newly reported HIV-infected case which ascertains sociodemographic characteristics and HIV-related risky behaviors. Once the HIV-infected cases are registered in the national reporting information system, they will be regularly followed up by local CDC for behavioral interventions, provision of health care services and social support. At each follow-up visit, venous blood is drawn for testing CD4⁺ cell counts as an index of disease progression. The data obtained from the initial and all follow-up epidemiological investigation, interviews and medical examinations constitute the patient's personal HIV/AIDS file or database, which is located in both local and national CDC.

2.2. Study sites

The present study was conducted in four regions which were selected to represent the overall epidemiological pattern of the HIV/AIDS epidemic in China: (i) Yuncheng city in Shanxi province in Central China where the HIV epidemic was first reported in 1996 and predominantly transmitted through plasma/blood donation or transfusion. By the end of 2008, 1,436 HIV/AIDS cases had been reported. Among them, 515 died and 715 were alive and traceable. (ii) Taizhou city in Zhejiang province in the Eastern coast of China where HIV was primarily transmitted through unprotected sexual behaviors. The first HIV case was reported in 1996. By the end of 2008, 365 HIV/AIDS cases had been reported. Among them, 45 died and 172 were alive and traceable. (iii) Urumqi city, the capital city of Xinjiang Uygur Autonomous Region in Northwestern China where drug injection and to a less extent, heterosexual transmission were the two major modes of HIV transmission. The first HIV case was reported in 1995 and by the end of 2008, 9,068 HIV/AIDS cases had been reported. Among them, 258 died and 1,129 were alive and traceable. (iv) Yingjiang county in Yunnan province in Southwestern China where HIV was formerly predominantly transmitted through injecting drugs but now is almost equally likely to be transmitted through drug injection or unprotected sexual contacts. The first HIV case in Yingjiang county was reported in 1990. By the end of 2008, 3,335 HIV/AIDS cases had been reported. Among them, 1,069 died and 1,679 were alive and traceable.

Each of the four sites had a qualified laboratory equipped with a flow cytometer for CD4⁺ cell counting of HIV/AIDS patients.

2.3. Subject selection

Due to limited resources and unaffordable expenses for

laboratory tests, we decided not to include all alive and traceable HIV/AIDS patients in these four study sites for this study. Instead, we selected all adult HIV/AIDS patients in these four study sites who visited local CDC for routine follow-up tests of CD4⁺ cell count during a specified two-week sample collection period for each site from late 2008 through early 2009. The specific two-week sample collection period designated to each site was chosen primarily based on our experience that it would allow for obtaining a reasonable size of the study sample. A total of 1,110 HIV/AIDS patients who visited local CDC during the sample collection period were included in the present study. Among them, 288 HIV/AIDS patients were from Yuncheng city, 163 were from Taizhou, 360 were from Urumqi, and 300 were from Yingjiang. These patients shown up within the two-week sample collection period represented 40% of all alive and traceable HIV patients in Yuncheng, 95% in Taizhou, 32% in Urumqi, and 18% in Yingjiang, respectively. The low representativeness in Yingjiang, Yunnan province, was due to the fact that it had a large number of alive HIV/AIDS patients and the majority of them were living in remote mountainous villages and did not visit the local CDC as often as their counterparts in other areas. Sociodemographic characteristics and HIV transmission route of the study subjects were abstracted from their individual epidemiological HIV/AIDS files. This study was approved by the Institutional Review Board (IRB) of the corresponding institution in China.

2.4. Blood testing

To avoid drop of antibody titers due to long distance transportation, all aliquots of serum samples were cryopreserved at -20°C or -70°C and tested in the local CDC. CD4⁺ cell counts were measured by local CDC laboratory staff using a flow cytometry (BD FACSCount™; BD Biosciences, San Jose, CA, USA), who had been strictly trained and certified following the national guidelines set by the national center for AIDS and sexually transmitted disease (STD) prevention and control (NCAIDS) of China CDC. HBV surface antigen (HBsAg) and anti-HCV IgG antibody were tested using an enzyme-linked immunosorbant assay (ELISA) (Wantai Biological Pharmacy Enterprise Co., Beijing, China). HSV-1- and HSV-2-specific IgG antibodies were tested using the HerpeSelect ELISA Kit (Focus Technologies, Cypress, CA, USA). Anti-EBV nucleic antigen (EBNA) IgG antibody was tested by ELISA (Euroimmun, Lübeck, Germany). All above serological tests were performed by the same two experienced technicians from the key laboratory of the leading institution of this study, according to the manufacturers' standard protocols. Duplicate negative, positive and blank controls were always used.

2.5. Data analysis

Seroprevalence of each viral coinfection was tabulated by geographic region and sociodemographic characteristics of study subjects, followed by chi-squared tests to determine statistical significance. Five separate multiple logistic regression analyses were performed to identify independent sociodemographic correlates of HBV, HCV, HSV-1, HSV-2, and EBV infection respectively among HIV/AIDS patients. Their respective odds ratios (ORs) and 95% confidence intervals were calculated. All statistical analyses were carried out using the SAS System for Windows (Cary, NC, USA), version 8.0.

3. Results

3.1. Sociodemographic characteristics

Table 1 presents sociodemographic characteristics of the study participants. About 45.3% of the study subjects were between 30 to 39 years and 61.5% were males. The majority of them were married and almost a half was either illiterate or educated only at primary schools. All Yuncheng patients and 93.2% of Taizhou patients were ethnic Han, whereas 92.2% of Urumqi patients and 55.7% of Yingjiang patients were ethnic minorities. Table 1 presents a detailed description of their socio-demographic characteristics which varied significantly by geographic region.

3.2. HIV transmission mode and disease status

As shown in Table 1, the means of HIV transmission varied widely by geographic region. In Yuncheng the most frequent mode of transmission was through plasma/blood donation or transfusion (85.1%). In Taizhou the majority of transmission was heterosexual (69.9%), however all modes of transmission were reported among the sample. In Urumqi the majority of the transmission reported was through injection drug use (52.8%), however the rate of heterosexual transmission was also relatively high (30.0%). In Yingjiang injection drug use was the most common transmission route (50.0%), which was followed closely by heterosexual transmission (42.0%).

About 42.7% of the patients were receiving ART, and 32.1% had 200-349 CD4⁺ cells/ μL and 23.4% had less than 200 CD4⁺ cells/ μL (Table 1).

3.3. Prevalence of viral coinfections

The overall seroprevalence was 6.3% for HBV, 59.0% for HCV, 96.6% for EBV, 91.5% for HSV-1, and 34.1% for HSV-2 (Table 2). The seroprevalence of all five viruses except for HBV varied significantly by geographic region, most sociodemographic

Table 1. Sociodemographic characteristics, transmission modes and current CD4⁺ T-cell counts of HIV/AIDS patients in four geographical areas in China

	Yuncheng, Central China (n ₁ = 287) No. (%)	Taizhou, Eastern China (n ₂ = 163) No. (%)	Urumqi, Northwestern China (n ₃ = 360) No. (%)	Yingjiang, Southwestern China (n ₄ = 300) No. (%)	Total (n = 1,110) No. (%)
Age (years, <i>p</i> < 0.001)					
18-29	23 (8.0)	47 (28.8)	75 (20.8)	46 (15.3)	191 (17.2)
30-39	81 (28.2)	68 (41.7)	216 (60.0)	138 (46.0)	503 (45.3)
40-49	117 (40.8)	29 (17.8)	54 (15.0)	90 (30.0)	290 (26.1)
50-59	60 (20.9)	12 (7.4)	3 (0.8)	21 (7.0)	96 (8.6)
60-94	6 (2.1)	7 (4.3)	12 (3.3)	5 (1.7)	30 (2.7)
Gender (<i>p</i> < 0.001)					
Male	155 (54.0)	109 (66.9)	188 (52.4)	230 (76.7)	682 (61.5)
Female	132 (46.0)	54 (33.1)	171 (47.6)	70 (23.3)	427 (38.5)
Ethnicity (<i>p</i> < 0.001)					
Han	287 (100.0)	152 (93.2)	28 (7.8)	133 (44.3)	600 (54.1)
Uygur	0	1 (0.6)	317 (88.0)	0	318 (28.6)
Dai	0	0	0	112 (37.3)	112 (10.1)
Jingpo	0	1 (0.6)	0	48 (16.0)	49 (4.4)
Other minorities	0	9 (5.5)	15 (4.2)	7 (2.3)	31 (2.8)
Occupation (<i>p</i> < 0.001)					
Peasant	282 (98.2)	51 (31.3)	4 (1.1)	245 (81.7)	582 (52.5)
Commercial service	0	73 (44.8)	47 (13.1)	8 (2.7)	128 (11.5)
Other employees	5 (1.8)	39 (23.9)	77 (21.4)	14 (4.7)	135 (12.2)
Unemployed	0	0	232 (64.4)	33 (11.0)	265 (23.8)
Marital status (<i>p</i> < 0.001)					
Never married	2 (0.7)	30 (18.9)	65 (18.1)	61 (20.3)	158 (14.3)
Married	275 (95.8)	115 (72.3)	251 (69.9)	180 (60.0)	821 (74.3)
Divorced/Widowed	10 (3.5)	14 (8.8)	43 (12.0)	59 (19.7)	126 (11.4)
Education (<i>p</i> < 0.001)					
Illiterate	74 (25.8)	12 (7.4)	10 (2.8)	36 (12.0)	132 (12.0)
Primary school	119 (41.5)	53 (32.9)	62 (17.5)	176 (58.9)	410 (37.3)
Secondary school	83 (28.9)	73 (45.3)	160 (45.1)	67 (22.4)	383 (34.7)
High school or equal	10 (3.5)	17 (10.6)	90 (25.4)	17 (5.7)	134 (12.1)
College/University	1 (0.3)	6 (3.7)	33 (9.3)	3 (1.0)	43 (3.9)
Transmission route (<i>p</i> < 0.001)					
Heterosexual	39 (13.6)	114 (69.9)	108 (30.0)	126 (42.0)	387 (34.8)
Injection drugs	0	13 (8.0)	190 (52.8)	150 (50.0)	353 (31.8)
Plasma/blood donation or transfusion	244 (85.0)	10 (6.1)	0	1 (0.3)	255 (23.0)
Homosexual	0	10 (6.1)	3 (0.8)	0	13 (1.2)
Unidentified	4 (1.4)	16 (9.8)	59 (16.4)	23 (7.7)	102 (9.2)
Receiving ART (<i>p</i> < 0.001)					
Yes	190 (66.2)	42 (25.8)	89 (24.7)	153 (51.0)	474 (42.7)
No	97 (33.8)	121 (74.2)	271 (75.3)	147 (49.0)	636 (57.3)
CD4 ⁺ counts (<i>p</i> < 0.001)					
< 200	96 (34.2)	33 (26.0)	62 (17.3)	57 (19.2)	248 (23.4)
200-349	84 (29.9)	39 (30.7)	108 (30.1)	111 (37.4)	342 (32.1)
350-499	53 (18.9)	33 (26.0)	88 (24.5)	68 (22.9)	242 (22.7)
500-749	41 (14.6)	18 (14.2)	64 (17.8)	48 (16.2)	171 (16.0)
750-	7 (2.5)	4 (3.1)	37 (10.3)	13 (4.4)	61 (5.7)

characteristics and transmission route but not by CD4⁺ cell counts, according to chi-squared tests. The HBV prevalence varied only among different ethnicities and occupations.

3.4. Concurrency of multiple viral coinfections

Eleven (1.0%) HIV-infected individuals were co-infected with all five viruses, 177 (15.9%) with four viruses, 611 (55.0%) with three viruses, 288 (25.9%) with two viruses, and 23 (2.1%) with a single virus. Only one (0.1%) was not co-infected with any of

the five viruses. The most common combination of coinfections was with HCV, EBV, and HSV-1, which accounted for 36.8% of study subjects (Table 3).

3.5. Correlates of viral coinfections

The results of multiple logistic regression analyses were shown in Table 4. Sociodemographic characteristics and HIV transmission mode were not significantly correlated with coinfections of HBV, EBV, and HSV-1 among the study subjects (data not shown). However, coinfection with HCV was independently associated

Table 2. Seroprevalence of HBV, HCV, EBV, HSV-1, and HSV-2 among HIV/AIDS patients of four geographical areas in China

	No. of tested	HBV (%)	HCV (%)	EBV (%)	HSV-1 (%)	HSV-2 (%)
Geographic area		<i>p</i> = 0.210	<i>p</i> < 0.001	<i>p</i> < 0.001	<i>p</i> < 0.001	<i>p</i> < 0.001
Yuncheng, Central China	287	8.0	76.0	93.4	85.8	13.2
Taizhou, Eastern China	163	7.3	21.3	93.9	86.6	53.0
Urumqi, Northwestern China	360	4.2	61.4	98.1	97.5	41.4
YingJiang, Southwestern China	300	6.7	60.3	99.3	92.7	35.0
Age (years)		<i>p</i> = 0.209	<i>p</i> < 0.001	<i>p</i> = 0.194	<i>p</i> = 0.069	<i>p</i> = 0.001
18-29	191	6.3	37.5	95.3	94.3	43.8
30-39	503	6.4	62.2	97.6	92.6	34.8
40-49	290	4.8	66.3	96.2	89.7	30.2
50-59	96	11.5	67.7	93.8	85.4	20.8
60-94	30	3.3	43.3	100.0	93.3	40.0
Gender		<i>p</i> = 0.322	<i>p</i> < 0.001	<i>p</i> < 0.001	<i>p</i> = 0.007	<i>p</i> < 0.001
Male	682	6.9	69.6	98.1	89.8	26.5
Female	427	5.4	42.2	94.1	94.4	46.4
Ethnicity		<i>p</i> = 0.050	<i>p</i> < 0.001	<i>p</i> = 0.024	<i>p</i> < 0.001	<i>p</i> < 0.001
Han (the major ethnic in China)	600	8.0	53.8	95.0	87.5	32.4
Uyгур	318	3.8	63.2	97.8	98.4	41.8
Dai	112	3.6	74.1	100.0	95.5	17.9
Jingpo	49	10.2	65.3	98.0	87.8	28.6
Other minorities	31	3.2	51.6	100.0	90.3	54.8
Occupation		<i>p</i> = 0.058	<i>p</i> < 0.001	<i>p</i> = 0.327	<i>p</i> < 0.001	<i>p</i> < 0.001
Peasant	582	8.1	65.0	96.2	88.7	24.9
Commercial service	128	4.7	37.2	94.6	92.2	48.8
Other employees	135	5.9	47.4	97.8	91.1	39.3
Unemployed	265	3.4	62.3	97.7	97.7	44.5
Marital status		<i>p</i> = 0.315	<i>p</i> = 0.027	<i>p</i> = 0.646	<i>p</i> = 0.889	<i>p</i> = 0.001
Never married	158	6.3	64.8	95.6	91.8	32.1
Married	821	6.7	59.2	96.6	91.7	32.1
Divorced/Widowed	126	3.2	49.2	97.6	90.5	48.4
Education		<i>p</i> = 0.364	<i>p</i> < 0.001	<i>p</i> = 0.025	<i>p</i> = 0.040	<i>p</i> = 0.009
Illiterate	132	4.5	66.7	94.7	87.9	25.0
Primary school	410	6.6	64.2	97.1	89.3	32.4
Secondary school	383	7.3	56.5	96.1	93.8	33.9
High school or equal	134	6.0	50.0	100.0	94.8	44.8
College/University	43	0.0	39.5	90.7	95.3	41.9
Transmission route		<i>p</i> = 0.621	<i>p</i> < 0.001	<i>p</i> = 0.003	<i>p</i> < 0.001	<i>p</i> < 0.001
Heterosexual	387	7.0	23.0	96.6	92.0	49.4
Injection drugs	353	5.4	87.3	99.2	94.3	29.7
Plasma/blood donation or transfusion	255	7.4	84.0	93.4	85.2	11.3
Homosexual	13	0.0	0.0	100.0	100.0	21.4
Unidentified	102	4.9	43.1	95.1	95.1	50.0
Receiving ART		<i>p</i> = 0.305	<i>p</i> = 0.482	<i>p</i> = 0.796	<i>p</i> = 0.005	<i>p</i> = 0.043
Yes	474	7.2	57.8	96.4	88.8	30.8
No	636	5.7	59.9	96.7	93.6	36.6
CD4 ⁺ counts		<i>p</i> = 0.755	<i>p</i> = 0.836	<i>p</i> = 0.154	<i>p</i> = 0.188	<i>p</i> = 0.588
< 200	248	6.8	61.0	95.6	89.6	29.3
200-349	342	7.6	61.2	98.8	91.5	35.6
350-499	242	5.4	59.1	96.7	93.4	34.3
500-749	171	5.3	58.5	96.5	92.4	32.7
750-	61	4.9	54.1	95.1	98.4	31.1
Total	1,110	6.3	59.0	96.6	91.5	34.1

* All *p*-values in the table were generated from Bivariate chi-squared tests for associations between viral infections and independent variables listed in the table.

with geographic region, age, gender, ethnicity, marital status, and HIV transmission mode. HIV patients who were living in Taizhou, Eastern China, were female or divorced/widowed, were less likely to have an HCV coinfection. Those who aged more than 30 years, were ethnic Jingpo or infected with HIV through drug injection or plasma/blood donation or transfusion were more likely to be co-infected with HCV. On the contrary,

coinfection with HSV-2 was significantly higher among those who were living in areas other than Yuncheng city in central China or female. However, those who were ethnic Dai or Jingpo were less likely to have an HSV-2 coinfection than ethnic Han. Those who became infected with HIV through plasma/blood donation or transfusion were less likely to have an HSV-2 coinfection than those who were heterosexually infected with HIV.

Table 3. Combinations of the five viral coinfections among HIV-infected patients in China

No. of virus	HBV	HCV	EBV	HSV-1	HSV-2	No. of patients	Proportion (%)
5	+	+	+	+	+	11	1.0
4	+	+	+	+	-	20	1.8
4	+	+	+	-	+	-	-
4	+	+	-	+	+	-	-
4	+	-	+	+	+	13	1.2
4	-	+	+	+	+	144	13.0
3	+	+	+	-	-	5	0.4
3	+	+	-	+	-	-	-
3	+	+	-	-	+	-	-
3	-	+	+	+	-	408	36.8
3	-	+	+	-	+	13	1.2
3	-	-	+	+	+	163	14.7
3	-	+	-	+	+	4	0.4
3	+	-	-	+	+	-	-
3	+	-	+	+	-	16	1.4
3	+	-	+	-	+	1	0.1
2	+	+	-	-	-	-	-
2	-	+	+	-	-	37	3.3
2	-	-	+	+	-	206	18.5
2	-	-	-	+	+	9	0.8
2	+	-	+	-	-	2	0.2
2	+	-	-	+	-	2	0.2
2	+	-	-	-	+	-	-
2	-	+	-	+	-	12	1.1
2	-	+	-	-	+	1	0.1
2	-	-	+	-	+	19	1.7
1	+	-	-	-	-	-	-
1	-	+	-	-	-	-	-
1	-	-	+	-	-	14	1.3
1	-	-	-	+	-	8	0.7
1	-	-	-	-	+	1	0.1
0	-	-	-	-	-	1	0.1

+, testing positive; -, testing negative.

4. Discussion

The present study, for the first time, examined prevalence and combinations of five pathogenic viral infections amongst Chinese HIV/AIDS patients. The prevalence of coinfections with HBV, HCV, EBV, HSV-1, and HSV-2 amongst HIV/AIDS patients was generally high. About 96% of the study subjects were infected with EBV and more than 90% of them were infected with HSV-1. This might be due to the high background prevalence of EBV and HSV-1 in the general Chinese population (28-30). The prevalence of HBsAg among the HIV/AIDS patients was comparable to that in the general Chinese population which was 7.18% for those aged 1-59 years in a nationwide survey completed in 2006 among 81,775 participants (China Ministry of Health, April 21, 2008). Although HCV and HSV-2 are both relatively uncommon in the general Chinese population (31,19-21), a high prevalence of HCV coinfection was observed among the study subjects who had contracted HIV through drug injections and plasma/blood donation or transfusion but a high prevalence of HSV-2 coinfection was also observed among those who had become HIV-infected through heterosexual transmission. Previous studies have reported that HCV infection is prevalent among

former plasma donors and injection drug users and that HSV-2 infection is prevalent among commercial sex workers in China (15-16,22-24).

In this study, geographic region was also independently correlated with HCV and HSV-2 coinfection among HIV/AIDS patients. This may be due to different background levels of HCV and HSV-2 infections in different geographic regions (14-16,19-24). Thus HCV and HSV-2 coinfections should be considered in areas where these viruses are common.

Gender was also found to be independently associated with HCV and HSV-2 coinfections among HIV/AIDS patients in this study. Females were less likely than males to have a HCV coinfection. This is probably related to the fact that in China females are generally less likely than males to be an IDU. A 2009 meta-analysis found that 84% of all IDU participating in the 1997-2007 studies included in the meta-analysis were men (32). The present study found that female HIV patients were more likely than males to have an HSV-2 coinfection. This finding is consistent with a meta-analysis of HSV-1 and HSV-2 infections in regions throughout the globe which indicates that there tend to be a higher HSV-2 seroprevalence among females (17). Other studies in China have also suggested that the increased prevalence of

Table 4. Logistic regression analyses for identifying sociodemographic correlates of HCV or HSV-2 coinfection among HIV/AIDS patients in China

	HCV		HSV-2	
	OR* (95% CI**)	p value	OR* (95% CI**)	p value
Geographic area				
Yuncheng, Central China	1.00		1.00	
Taizhou, Eastern China	0.29 (0.12-0.69)	0.005	4.69 (2.17-10.13)	0.000
Urumqi, Northwestern China	0.71 (0.20-2.44)	0.582	2.18 (0.73-6.49)	0.162
Yingjiang, Southwestern China	0.60 (0.26-1.36)	0.221	4.01 (1.88-8.55)	0.000
Age (years)				
18-29	1.00		1.00	
30-39	2.09 (1.28-3.42)	0.003	0.95 (0.64-1.42)	0.799
40-49	2.30 (1.32-4.03)	0.003	1.10 (0.69-1.75)	0.697
50-59	1.89 (0.88-4.06)	0.102	0.76 (0.37-1.54)	0.442
60-94	2.19 (0.78-6.18)	0.139	0.98 (0.39-2.50)	0.969
Gender				
Male	1.00		1.00	
Female	0.43 (0.30-0.61)	0.000	2.50 (1.79-3.50)	0.000
Ethnicity				
Han (the major ethnic in China)	1.00		1.00	
Uygur	2.23 (0.89-5.59)	0.087	0.97 (0.45-2.13)	0.946
Dai	1.81 (0.88-3.70)	0.107	0.24 (0.12-0.44)	0.000
Jingpo	3.30 (1.35-8.05)	0.009	0.29 (0.14-0.63)	0.002
Other minorities	1.86 (0.67-5.17)	0.234	1.24 (0.52-2.96)	0.623
Occupation				
Peasant	1.00		1.00	
Commercial service	1.28 (0.63-2.60)	0.498	1.08 (0.61-1.90)	0.794
Other employees	1.04 (0.51-2.12)	0.908	0.88 (0.49-1.57)	0.654
Unemployed	0.93 (0.47-1.86)	0.843	1.31 (0.74-2.32)	0.348
Marital status				
Never married	1.00		1.00	
Married	0.67 (0.38-1.16)	0.154	1.15 (0.74-1.79)	0.536
Divorced/Widowed	0.47 (0.24-0.94)	0.033	1.70 (0.97-2.99)	0.063
Education				
Illiterate	1.00		1.00	
Primary school	1.19 (0.66-2.16)	0.566	0.96 (0.56-1.64)	0.881
Secondary school	0.65 (0.35-1.22)	0.184	0.79 (0.44-1.41)	0.422
High school or equal	0.56 (0.26-1.18)	0.128	0.96 (0.50-1.86)	0.912
College/University	0.75 (0.27-2.03)	0.568	0.88 (0.36-2.11)	0.767
Transmission route				
Heterosexual	1.00		1.00	
Injection drugs	13.76 (8.61-22.00)	0.000	0.78 (0.52-1.16)	0.217
Plasma/blood donation or transfusion	12.87 (6.37-25.98)	0.000	0.36 (0.18-0.72)	0.004
Homosexual	0.004 (0.00-N.A)	0.565	0.38 (0.10-1.48)	0.161
Unidentified	2.06 (1.23-3.45)	0.006	1.20 (0.74-1.96)	0.461

* OR: odds ratio, adjusted for potential confounding effects of other variables listed in the table; ** 95% CI: 95% confidence interval.

HSV-2 among women is associated with the growing commercial sex industry (19,22-24). Since HSV-2 is the major cause of genital herpes and HSV-2 coinfection can significantly accelerate sexual transmission of HIV, female HIV patients, particularly those who become HIV-infected through heterosexual transmission, should be tested for HSV-2 and treated if infected.

The present study also identified an association between ethnicity and an HCV or HSV-2 coinfection in HIV/AIDS patients. Those of Uygur, Dai and especially Jingpo ethnicities were more likely than ethnic Han to have an HCV coinfection and those of Dai and Jingpo ethnicities were less likely than ethnic Han to have an HSV-2 coinfection. Compared with ethnic Hans, these minorities have a higher percentage infected with HIV through injection drug use but have a lower percentage infected with HIV through sexual transmission. These

findings suggest that minority HIV patients are more likely to contract viral coinfections from needle sharing than from heterosexual contacts.

An important finding of this study is that a combined total of 71.8% of the study subjects were co-infected with at least three other viruses which put them at risk for developing other diseases and malignancies that could significantly reduce their level of general health. The results of the present study also suggest the need to look for coinfections with other viruses such as EBV and HSV-1 which further threaten the immune response.

This study has certain limitations. First, the determination of viral coinfections was based on cross-sectional measurement of surface antigen for HBV and IgG antibody for HCV, EBV, HSV-1 and HSV-2 which only reflect historical exposure to the viruses. Thus,

it is difficult to determine the temporal relationship between infections with HIV and the other viruses, limiting our ability to draw causal inferences about these viral coinfections. Second, we only tested for coinfections with HBV, HCV, EBV, HSV-1, and HSV-2. Due to the unavailability of blood-based, type-specific commercial products for testing, we did not test for human papillomavirus (HPV) which is also prevalent in China and is the causal agent of invasive cervical cancer, an important AIDS-defining disease. Also, due to lack of qualified commercial products for testing, we did not test for human herpes virus type 8 (HHV8) which was first identified in 1994 and has been demonstrated to be prevalent in the Mediterranean region and the causal agent of Kaposi's Sarcoma (KS), another important AIDS-defining disease (33-36). This limited our ability to draw conclusions with regard to the spectrum of viral coinfections that are of most significance to Chinese HIV/AIDS patients. Third, we only included HIV patients visiting local CDC for follow-up within the specified two-week sample collection period in the study, which compromised the representativeness of the study sample.

In conclusion, this study has demonstrated that most Chinese HIV/AIDS patients are living with multiple pathogenic viruses that may play important roles in their disease progression, responses to antiretroviral treatment and general health. It is foreseeable that the incidence of HIV-related malignancies such as HCC, NHL, HL, and nasopharyngeal cancer in China will increase given the high prevalence of HCV and EBV coinfections among HIV/AIDS patients and their extended lifetime gained from the nationwide antiretroviral treatment campaign. Moreover, Chinese HIV/AIDS patients with different backgrounds in terms of HIV transmission route, residential geographic region, gender and ethnicity may have different profiles of viral coinfections and thus should be subject to differential considerations in designing public health and clinical care programs for both HIV and other co-infected pathogenic viruses.

Acknowledgements

This study was supported by grants from Chinese National Natural Science Foundation (grant No. 30671880; 81072345), Shanghai Municipal Education Committee (grant No. 08ZZ02), Shanghai Leading Disciplinary Project (grant No. B118), and the United States National Institutes of Health Fogarty International Center (R01TW007298; D43TW000013-21S2). This study was approved by the Institutional Review Board (IRB) of Fudan University, Shanghai, China.

References

1. Sulkowski MS, Moore RD, Mehta SH, Chaisson RE, Thomas DL. Hepatitis C and progression of HIV disease. *JAMA*. 2002; 288:199-206.
2. Rossi SJ, Volberding PA, Wright TL. Does hepatitis C virus infection increase the risk of HIV disease progression? *JAMA*. 2002; 288:241-243.
3. Nikolopoulos GK, Paraskevis D, Hatzitheodorou E, Moschidis Z, Sypsa V, Zavitsanos X, Kalapothaki V, Hatzakis A. Impact of hepatitis B virus infection on the progression of AIDS and mortality in HIV-infected individuals: A cohort study and meta-analysis. *Clin Infect Dis*. 2009; 48:1763-1771.
4. Graham CS, Baden LR, Yu E, Mrus JM, Carnie J, Heeren T, Koziel MJ. Influence of human immunodeficiency virus infection on the course of hepatitis C virus infection: A meta-analysis. *Clin Infect Dis*. 2001; 33:562-569.
5. Thein HH, Yi Q, Dore GJ, Krahn MD. Natural history of hepatitis C virus infection in HIV-infected individuals and the impact of HIV in the era of highly active antiretroviral therapy: A meta-analysis. *AIDS*. 2008; 22:1979-1991.
6. Calistri A, Parolin C, Palù G. Herpes simplex virus type 1 can either suppress or enhance human immunodeficiency virus type 1 replication in CD4-positive T lymphocytes. *J Med Virol*. 2003; 70:163-170.
7. Kucera LS, Leake E, Iyer N, Raben D, Myrvik QN. Human immunodeficiency virus type 1 (HIV-1) and herpes simplex virus type 2 (HSV-2) can coinfect and simultaneously replicate in the same human CD4⁺ cell: Effect of coinfection on infectious HSV-2 and HIV-1 replication. *AIDS Res Hum Retroviruses*. 1990; 6:641-647.
8. Sheth PM, Sunderji S, Shin LY, Rebbapragada A, Huibner S, Kimani J, Macdonald KS, Ngugi E, Bwayo JJ, Moses S, Kovacs C, Loutfy M, Kaul R. Coinfection with herpes simplex virus type 2 is associated with reduced HIV-specific T cell responses and systemic immune activation. *J Infect Dis*. 2008; 197:1394-1401.
9. Sculley TB, Apolloni A, Hurren L, Moss DJ, Cooper DA. Coinfection with A- and B-type Epstein-Barr virus in human immunodeficiency virus-positive subjects. *J Infect Dis*. 1990; 162:643-648.
10. Engels EA, Biggar RJ, Marshall VA, Walters MA, Gamache CJ, Whitby D, Goedert JJ. Detection and quantification of Kaposi's sarcoma-associated herpesvirus to predict AIDS-associated Kaposi's sarcoma. *AIDS*. 2003; 17:1847-1851.
11. Omland LH, Weis N, Skinhoj P, Laursen A, Christensen PB, Nielsen HI, Møller A, Engsig F, Sørensen HT, Obel N. Impact of hepatitis B virus coinfection on response to highly active antiretroviral treatment and outcome in HIV-infected individuals: A nationwide cohort study. *HIV Med*. 2008; 9:300-306.
12. Santin M, Mestre M, Shaw E, Barbera MJ, Casanova A, Niubo J, Bolao F, Podzamczar D, Gudiol F. Impact of hepatitis C virus coinfection on immune restoration during successful antiretroviral therapy in chronic human immunodeficiency virus type 1 disease. *Eur J Clin Microbiol Infect Dis*. 2008; 27:65-73.
13. Weis N, Lindhardt BO, Kronborg G, Hansen AB, Laursen AL, Christensen PB, Nielsen H, Møller A, Sørensen HT, Obel N. Impact of hepatitis C virus coinfection on response to highly active antiretroviral therapy and outcome in HIV-infected individuals: A nationwide cohort study. *Clin Infect Dis*. 2006; 42:1481-1487.

14. Lu Y, Robinson M, Zhang FJ. Human immunodeficiency virus and hepatitis C virus co-infection: Epidemiology, natural history and the situation in China. *Chin Med J (Engl)*. 2009; 122:93-97.
15. Garten RJ, Zhang J, Lai S, Liu W, Chen J, Yu XF. Coinfection with HIV and hepatitis C virus among injection drug users in southern China. *Clin Infect Dis*. 2005; 41 (Suppl 1):S18-S24.
16. Qian HZ, Vermund SH, Kaslow RA, Coffey CS, Chamot E, Yang Z, Qiao X, Zhang Y, Shi X, Jiang Y, Shao Y, Wang N. Co-infection with HIV and hepatitis C virus in former plasma/blood donors: Challenge for patient care in rural China. *AIDS*. 2006; 20:1429-1435.
17. Smith JS, Robinson NJ. Age-specific prevalence of infection with herpes simplex virus types 2 and 1: A global review. *J Infect Dis*. 2002; 186 (Suppl 1):S3-S28.
18. Wald A, Link K. Risk of human immunodeficiency virus infection in herpes simplex virus type 2-seropositive persons: A meta-analysis. *J Infect Dis*. 2002; 185:45-52.
19. Detels R, Wu Z, Rotheram MJ, Li L, Guan J, Yin Y, Liang G, Lee M, Hu L; The National Institute of Mental Health (NIMH) Collaborative HIV Prevention Trial Group. Sexually transmitted disease prevalence and characteristics of market vendors in eastern China. *Sex Transm Dis*. 2003; 30:803-808.
20. Chen XS, Yin YP, Chen LP, Yu YH, Wei WH, Thuy NT, Smith JS. Herpes simplex virus 2 infection in women attending an antenatal clinic in Fuzhou, China. *Sex Transm Infect*. 2007; 83:369-370.
21. He N, Cao HJ, Yin YP, Gao MY, Zhang T, Detels R. Herpes simplex virus-2 infection in male rural migrants in Shanghai, China. *Int J STD AIDS*. 2009; 20:112-114.
22. Chen XS, Yin YP, Liang GJ, Gong XD, Li HS, Pomeroy G, Thuy N, Shi MQ, Yu YH. Sexually transmitted infections among female sex workers in Yunnan, China. *AIDS Patient Care STDS*. 2005; 19:853-860.
23. Wang H, Wang N, Chen RY, Sharp GB, Ma Y, Wang G, Ding G, Wu Z. Prevalence and predictors of herpes simplex virus type 2 infection among female sex workers in Yunnan Province, China. *Int J STD AIDS*. 2008; 19:635-659.
24. Ngo TD, Laeyendecker O, Li C, Tai H, Cui M, Lai S, Quinn TC. Herpes simplex virus type 2 infection among commercial sex workers in Kunming, Yunnan Province, China. *Int J STD AIDS*. 2008; 19:694-697.
25. Guiguet M, Boué F, Cadranel J, Lang JM, Rosenthal E, Costagliola D; Clinical Epidemiology Group of the FHDH-ANRS CO4 cohort. Effect of immunodeficiency, HIV viral load, and antiretroviral therapy on the risk of individual malignancies (FHDH-ANRS CO4): A prospective cohort study. *Lancet Oncol*. 2009; 10:1152-1159.
26. Long JL, Engels EA, Moore RD, Gebo KA. Incidence and outcomes of malignancy in the HAART era in an urban cohort of HIV-infected individuals. *AIDS*. 2008; 22:489-496.
27. Young LS, Rickinson AB. Epstein-Barr virus: 40 years on. *Nat Rev Cancer*. 2004; 4:757-768.
28. Liu YT. A serological study on anti-CMV and anti-EBV antibodies in population of Beijing, Changzhi Shanxi and Yichang Hubei. *Zhonghua Liu Xing Bing Xue Za Zhi*. 1989; 10:277-281. (in Chinese)
29. Li YY, Hidaka Y, Kino Y, Mori R. Seroepidemiology of herpes simplex virus type 1 in Yanji, Jilin, China. *Microbiol Immunol*. 1990; 34:551-555.
30. Dong Z, Li Y, Liu R. IgG and IgM antibodies of Herpes Simplex Virus type-1 and type-2 in 233 maternal and neonatal sera. *Int J Gynaecol Obstet*. 1998; 63:69-70.
31. Qu JB, Zhang ZW, Shimbo S, Watanabe T, Nakatsuka H, Matsuda-Inoguchi N, Higashikawa K, Ikeda M. Urban-rural comparison of HBV and HCV infection prevalence in eastern China. *Biomed Environ Sci*. 2000; 13:243-253.
32. Bao YP, Liu ZM. Systematic review of HIV and HCV infection among drug users in China. *Int J STD AIDS*. 2009; 20:399-405.
33. Chang Y, Cesarman E, Pessin MS, Lee F, Culpepper J, Knowles DM, Moore PS. Identification of herpesvirus-like DNA sequences in AIDS-associated Kaposi's sarcoma. *Science*. 1994; 266:1865-1869.
34. Serraino D, Toma L, Andreoni M, Buttò S, Tchangmena O, Sarmati L, Monini P, Franceschi S, Ensoli B, Rezza G. A seroprevalence study of human herpesvirus type 8 (HHV8) in eastern and Central Africa and in the Mediterranean area. *Eur J Epidemiol*. 2001; 17:871-876.
35. Whitby D, Howard MR, Tenant-Flowers M, Brink NS, Copas A, Boshoff C, Hatzioannou T, Suggett FE, Aldam DM, Denton AS, *et al*. Detection of Kaposi sarcoma associated herpesvirus in peripheral blood of HIV-infected individuals and progression to Kaposi's sarcoma. *Lancet*. 1995; 346:799-802.
36. Min J, Katzenstein DA. Detection of Kaposi's sarcoma-associated herpesvirus in peripheral blood cells in human immunodeficiency virus infection: Association with Kaposi's sarcoma, CD4 cell count, and HIV RNA levels. *AIDS Res Hum Retroviruses*. 1999; 15:51-55.

(Received January 7, 2011; Revised January 28, 2011; Accepted February 7, 2011)

Invasion of carcinoma cells into reconstituted type I collagen gels: Visual real-time analysis by time-lapse microscopy

Keiko Sakai¹, Taisuke Kurokawa¹, Yoshihiro Furui¹, Yuh Kuronuma¹, Masaru Sekiguchi¹, Jun Ando¹, Yoshinori Inagaki², Wei Tang², Munehiro Nakata¹, Yoko Fujita-Yamaguchi^{1,*}

¹Department of Applied Biochemistry, Tokai University, Hiratsuka, Kanagawa, Japan;

²Hepato-Biliary-Pancreatic Surgery Division, Department of Surgery, Graduate School of Medicine, The University of Tokyo, Tokyo, Japan.

Summary

Stromal-epithelial interactions play a critical role in promoting tumorigenesis and invasion. To obtain detailed information on cancer cell behaviors on the stroma and kinetics of cell migration, which cannot be observed by conventionally-used Boyden chamber assays, this study was aimed at analyzing the cell invasion process *in vitro* using time-lapse microscopic observation. Serum-free conditions and reconstituted type I collagen gels which provided a basal membrane-stroma-like microenvironment were used to first establish a basal condition. Time-lapse microscopic observation for 30 h of cell invasion into the collagen gel revealed kinetic parameters and individualistic behavior of cancer cells. Of breast cancer MDA-MB-231 or MCF-7 cells and colon cancer LS180 or HT29 cells examined, MDA-MB-231 cells most rapidly disappeared from the collagen gel surface under basal conditions. Estrogen-dependent MCF-7 cells disappeared at a rate approximately two times slower than that of MDA-MB-231 cells under serum- and phenol red-free conditions. By the addition of 10 nM β -estradiol to the basal medium, MCF-7 cell invasion was facilitated to a rate similar to that of MDA-MB-231 cells. Microscopic analyses of collagen gel-sections demonstrated that most of the MDA-MB-231 and MCF-7 cells remained within 60 μ m from the gel top under basal conditions, which is consistent with the observation obtained using Boyden chambers that no cells could cross the collagen I gel barrier unless 1% fetal calf serum was added to basal conditions. In summary, this study demonstrated future applicability of this method to understand the initial phase of cancer cell invasion processes.

Keywords: Cancer cell invasion, reconstituted type I collagen gel, time-lapse microscopy, real-time analysis

1. Introduction

Biological behavior of epithelial cells is restricted by the surrounding microenvironment such as the basement membrane (BM) and cell-cell interaction (1-3). The basement membrane is a thin extracellular matrix (ECM) that underlies epithelia and separates cells from the stroma. Malignant cells must cross this membrane to invade stroma and eventually establish

distant metastases. Complex interactions between cancer cells and regulatory factors within the tumor microenvironment function cooperatively to control tumor cell invasion and eventual metastasis. Several genetic and epigenetic factors, both in the cell and in the microenvironment, contribute to the progression of cancer cells towards metastases. The escape of cancer cells from primary to distant sites is first established by producing proteases (4) that degrade ECM, consisting of basement membrane and stromal components. In addition, hormones and growth factors may also regulate motility and invasion of some types of carcinoma such as breast carcinoma. It has been shown that acquisition of cell invasion ability requires epithelial-to-mesenchymal transition (EMT) and that

*Address correspondence to:

Dr. Yoko Fujita-Yamaguchi, Department of Applied Biochemistry, Tokai University, 4-1-1 Kitakaname, Hiratsuka, Kanagawa 259-1292, Japan.
e-mail: yamaguch@keyaki.cc.u-tokai.ac.jp

induction of EMT in breast carcinoma cells can be associated with hormones such as estrogen (5).

Of *in vitro* models currently available, those using Matrigel as a biologically active basement membrane model for *in vitro* invasion assays have been used for two decades (6,7). In those assays, tumor cells are placed in the upper chamber of a Boyden migration chamber. The upper and lower chambers are separated by a porous membrane coated with Matrigel. A chemoattractant in the lower well stimulates migration. After an interval, tumor cells are recovered from or counted on the lower surface of the membrane. Although useful and convenient, the Boyden chamber assay cannot provide detailed information on cell invasion parameters such as kinetics of cell migration and migration behavior of cells on the BM-stroma in the presence of stimuli. In order to study cell invasion processes under different conditions reflecting the *in vivo* situation, we developed a real-time assay system that should allow direct visualization and assessment of cancer cell invasion processes.

Reconstituted gels with type I collagen, a major component forming a lattice structure in stroma (8), were used in the present study to observe migration of colorectal and breast carcinoma cells. That is, cancer cells were inoculated on a reconstituted 0.08% collagen gel (1.2 mm-thick) in phenol red-free Dulbecco's modified Eagle medium (DMEM) supplemented with 0.1% Bovine Serum Albumin (BSA) (the basal medium) and how the cells disappeared from the visible field were observed under a time-lapse phase contrast microscope. As the first step, the basal assay system in the absence of fetal calf serum (FCS) and phenol red, which mimics estrogen effects (9), was used to obtain information on the basal invasion of the tested cancer cells. Once the basal condition was established, effects of various parameters on invasion, such as changes in ECM components and/or addition of stimulants, can readily be assessed.

Time-lapse microscopic observation for 30 h of cell invasion into the collagen gel revealed kinetic parameters and individualistic behaviors of various cancer cells. Of breast cancer MDA-MB-231 or MCF-7 cells and colon cancer LS180 or HT29 cells examined, MDA-MB-231 cells most rapidly disappeared from the collagen gel surface under the basal conditions. Estrogen-dependent MCF-7 cells disappeared at a rate approximately two times slower than that of MDA-MB-231 cells under serum- and phenol red-free conditions. The effect of estrogen on invasion of estrogen-dependent MCF-7 breast carcinoma cells was then evaluated, which revealed that MCF-7 cell invasion was facilitated by the addition of 10 nM β -estradiol to the basal medium and had a rate similar to that of MDA-MB-231 cells. These results demonstrated future applicability of this real-time analysis to understand the cancer cell invasion processes.

2. Materials and Methods

2.1. Cell lines and cell culture conditions

Human breast carcinoma cells (MDA-MB-231 and MCF-7) and human colon carcinoma cells (LS180 and HT-29) were obtained from American Type Culture Collection (ATCC, Rockville, MD, USA). MDA-MB-231 and MCF-7 cells were maintained in low glucose DMEM containing 5% FCS (Sigma-Aldrich Japan, Tokyo, Japan) and high glucose DMEM containing 10% FCS, respectively, supplemented with penicillin, streptomycin, and 2 mM glutamine. LS180 cells were cultured in Minimum Essential Medium (MEM) containing 10% FCS. HT-29 cells were cultured in McCoy's 5A Medium (Invitrogen, Carlsbad, CA, USA) containing 10% FCS. These cells were cultured at 37°C in a 5% CO₂ atmosphere.

2.2. Preparation of a collagen gel bed for observation of cancer cell invasion

Type I collagen (collagen I) extracted from bovine skin by acetic acid was purchased from Koken Co. Ltd., Tokyo, Japan. To construct a collagen gel bed, 0.1% collagen I in 1 mM HCl was mixed with 10 times-concentrated phenol red-free DMEM, and neutralized with 100 mM HEPES (collagen I : DMEM : HEPES = 8:1:1, v/v/v) which was kept on ice. Two or 5 mL of the 0.08% collagen I solution were added to each plastic dish (ϕ 3.5 cm) quickly followed by incubation at 37°C until gels solidified with an approximate 1.2 mm thickness.

2.3. Assessment of cancer cell invasion by time-lapse microscopy

The invasion process of cancer cells on collagen gel culture model was monitored by a phase contrast time-lapse microscope ECLIPSE TE300 (Nikon, Kawasaki, Japan) housed in a temperature-controlled (37°C) CO₂ gassed chamber with water inside to maintain humidity. Breast or colon cancer cell lines were starved in FCS-free medium overnight, then harvested from plastic dishes by non-enzymatic separation solution (Invitrogen). Cells were seeded on the surface of the collagen gels at a concentration of 1×10^5 cells/mL in phenol red-free DMEM supplemented with 0.1% BSA and then placed in a chamber of the microscope adjusted to 37°C and a 5% CO₂ atmosphere. Cells remaining on the collagen gels were recorded at a 200 magnification every 1 h for 30 h. To evaluate the effect of the hormone on MCF-7 cell invasion, 10 nM β -estradiol was added to the basal medium.

The rate of cell invasion into the collagen gels was determined by plotting cell numbers remaining on the gel surface against incubation time. Data at each time point was collected from 4 to 10 independent experiments

for each condition tested. Statistical compilation was performed using StatView 5.0J (Abacus Concepts, Berkeley, CA, USA) software. The initial and maximum rates of invasion velocity were determined from the compiled data.

2.4. Migration of cells across the collagen gel

Collagen gels were similarly prepared on 24-well Boyden chambers with 8 μm pore size polycarbonate membranes (BD Biosciences, San Jose, CA, USA) as described above. Two hundred fifty μL of MDA-MB-231 or MCF-7 cell in DMEM with 1% FCS (6×10^5 cells/mL) was placed on the collagen gel. After cells were incubated for 18 h in a 5% CO_2 atmosphere, the collagen gel on the upper surface was gently removed from the chamber. The cells were then fixed with 5% formaldehyde and stained with Diff-Quik (Dade Behring, Deerfield, IL, USA) according to the manufacturer's protocol. Cells that migrated from the collagen gel surface to the underside of the filter were counted under a microscope.

2.5. Sectioning of collagen gels after cancer cell invasion

Collagen gels were prepared on 8-chamber slide glasses (1×1 cm, Nalgen Nunc International KK, Tokyo, Japan) as described above. Two hundred fifty μL of MDA-

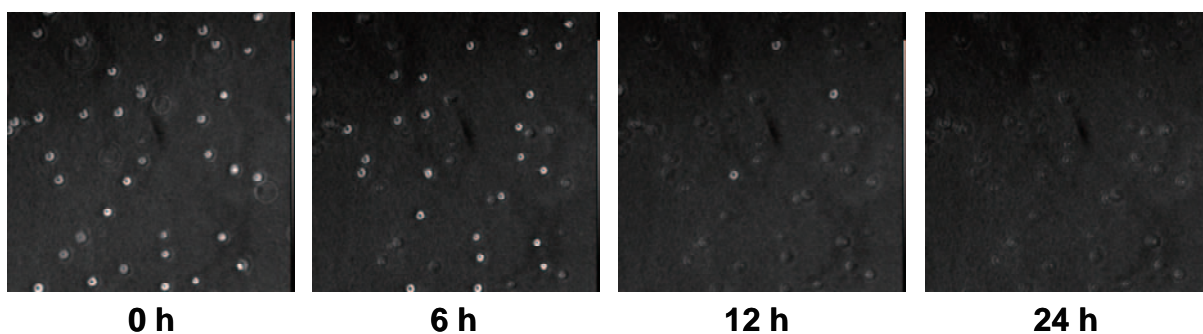
MB-231 or MCF-7 cell suspension (3×10^5 cells/mL) were placed on the surface of the collagen gel in phenol red-free DMEM supplemented with 0.1% BSA. After 3 h incubation at 37°C in a 5% CO_2 atmosphere, gels were gently washed with phosphate-buffered saline, soaked into Tissue-Tsk O.C.T. Compound (Sakura Finetechnical, Tokyo, Japan) and frozen at -80°C . The frozen gel was sliced using a cryostat (Leica Microsystems GmbH, Wetzlar, Germany) set at 20 μm thickness. The sections were then placed on a slide glass, fixed with 4% formalin, and stained with hematoxylin-eosin for observation under an optical microscope.

3. Results

3.1. Visualization of breast cancer cells invading collagen gels

Invasion of breast carcinoma MDA-MB-231 and MCF-7 cells into collagen gels under the serum- and phenol red-free conditions were recorded by time-lapse microscopy. Figure 1 shows representative photo images at the indicated incubation times after the cells were placed on the collagen gel surface. Both cell types gradually disappeared from the gel surface during the time course. MDA-MB-231 cells shown in Figure 1A apparently migrated into the collagen gel faster than MCF-7 cells

(A) MDA-MB-231



(B) MCF-7

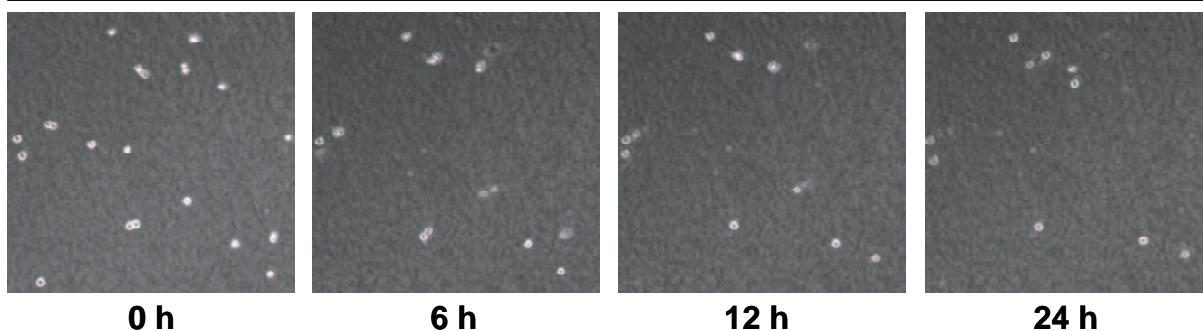


Figure 1. Visualization of breast carcinoma cell invasion into collagen gels. Reconstituted 0.08% collagen gel (1.2 mm-thick) was prepared in culture dish ($\phi 3.5$ cm), and then cells were inoculated on the gel at a concentration of 1×10^5 cells/mL in phenol red-free DMEM supplemented with 0.1% BSA (the basal medium). The dish was placed under a time lapse phase contrast microscope to observe the disappearance of the cells from the visible field. The photos present MDA-MB-231 (A) and MCF-7 (B) cells which remained on the gel surface at the indicated incubation time.

(Figure 1B). The traces of cells which migrated into the collagen gel were clearly marked on the surface (Figure 1).

Whether or not these cells actually moved through the collagen gels was examined using a collagen gel-coated conventional Boyden chamber as described in Materials and Methods. When the experiments were carried out under the serum- and phenol red-free condition as above, which was used throughout this study for the time-lapse recording method, none of the cells migrated across the filter (data not shown). Thus, 1% FCS was used to induce migration of cells in the Boyden chamber invasion assays. As seen in Figure 2A, a significant number of MDA-MB-231 cells (33.7 cells/60 μm^2) appeared on the underside of the membrane filter, and very few of the MCF-7 cells (5.7 cells/60 μm^2) were seen on the underside of the filter (Figure 2B) in which the 8 μm pores of the polycarbonate membrane are visible in the background. These results suggest that both the MDA-MB-231 and MCF-7 cells are capable of migrating into and through the collagen gel in the presence of 1% FCS, but that the degree of migration potential seems to be dependent on the individual characteristics of the cancer cell lines.

3.2. Detection of migrated cells into collagen gels

Time-lapse microscopic observations of the cells

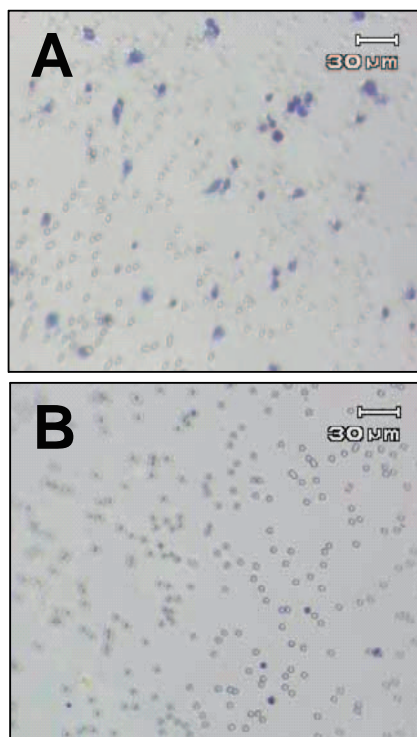


Figure 2. Migration of breast carcinoma cells across collagen gel to underside of the membrane in a 24-well Boyden chamber. Reconstituted collagen gel was prepared with a thickness of 1.2 mm on the membrane in chambers. MDA-MB-231 cells (A) or MCF-7 cells (B) were inoculated on the collagen gel, and then cultured for 18 h. Cells migrating to the underside of the membrane were stained with Trypan Blue and observed by microscopy (magnification $\times 200$). Representative fields of the membrane with migrated cells are shown.

disappearing from the image obviously indicated the occurrence of cell migration into collagen gels under the basal conditions (Figure 1). Few cells migrated, however, from the collagen gel surface to underside of the filter even though 1% FCS was used to induce migration (Figure 2). Thus, the distance cells migrated was determined by histocytochemically examining the sectioned collagen gels. After 20 h or 18 h culture, the collagen gels into which MDA-MB-231 and MCF-7 cells migrated were cryosectioned to visualize distribution of cells inside the collagen gels. Figures 3A-3D shows representative

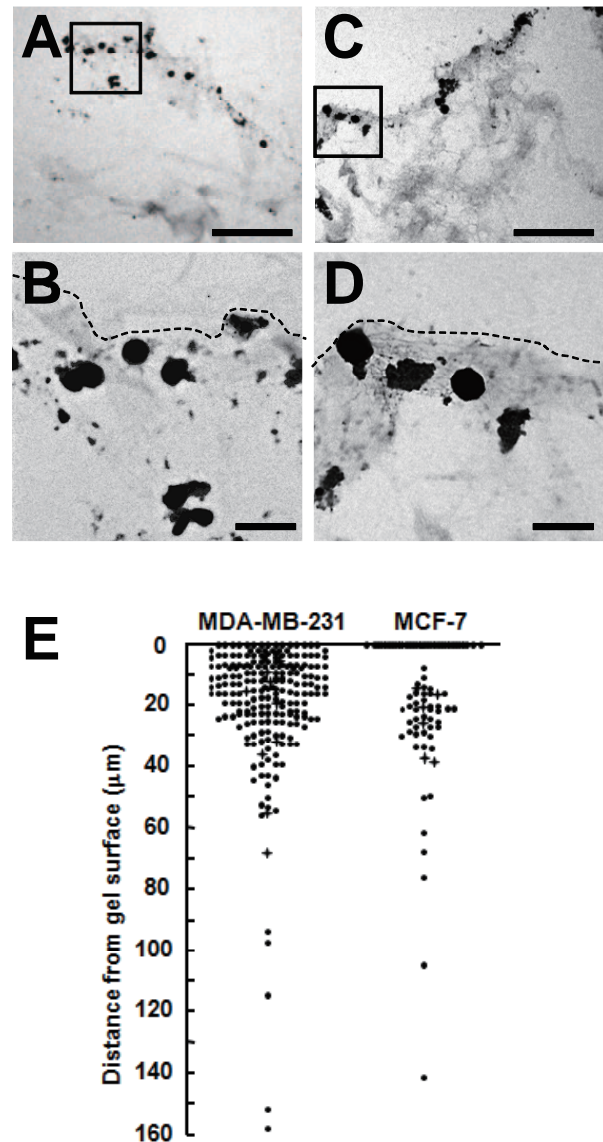


Figure 3. Histocytochemical observation of breast carcinoma cells in reconstituted collagen gels. MDA-MB-231 (A and B) and MCF-7 cells (C and D) in phenol red-free DMEM supplemented with 0.1% BSA (the basal medium) were incubated on collagen gels for 18 h at 37°C in 5% CO₂ atmosphere. The gels were frozen and sliced with a cryostat set at a 20 μm thickness. Sections were fixed and stained with hematoxylin-eosin. Areas around the gel surfaces were photographed with an optical microscope (Bars: 100 μm in A and C; 20 μm in B and D). Dotted lines in B and D represent the gel surfaces. In E, distribution of distances from the gel surface for each cell observed ($n = 214$ for MDA-MB-231 cells and $n = 75$ for MCF-7 cells) was plotted.

microscopic photos of the collagen gel sections stained with hematoxylin and eosin stain.

Migration distances of MDA-MB-231 and MCF-7 cells from the top of collagen gels measured were plotted as shown in Figure 3E. Of the 214 MDA-MB-231 cells observed, 199 (93%) cells invaded and were widely distributed in the gel. In contrast, of the 75 MCF-7 cells observed, 25 cells (33%) remained on the gel surface whereas 45 cells (60%) migrated to around 20-30 μm from the gel surface. The distances of cell migration into collagen gels are summarized in Table 1. The results suggest that cell migration certainly occurs under serum- and phenol red-free conditions, but that migration of both MDA-MB-231 and MCF-7 cells was only to 157 and 141 μm from the gel top, respectively. This result is consistent with the observation obtained by Boyden chamber assays that no cells migrated through the filter under the same conditions as used above (Figure 2).

3.3. Invasion kinetics of breast and colon cancer cells

Invasion rates of both breast and colon carcinoma cells into collagen gels are measured by counting the number of cells remaining in the same microscopic field that had been recorded by a time-lapse microscope every hour for 30 h (Figure 4). In the case of breast carcinoma cells, MDA-MB-231 cells showed a much higher disappearing rate than MCF-7 cells (Figure 4A), suggesting that MDA-MB-231 has a higher invasion potential than MCF-7 cells under the conditions used. The major difference was seen at around 25 h after cells were placed on the collagen gel, at which time nearly 100% of MDA-MB-231 cells invaded the collagen gel whereas on average $27.9 \pm 4.4\%$ ($n = 5$) of MCF-7 cells still remained on the gel surface (Figure 4A, closed and open circles, respectively). In the case of colon carcinoma cells, LS180 cells invaded more quickly than HT29 cells (Figure 4B).

In general, cell invasion started at 1-2 h of incubation after cells were seeded on the gel. The invasion process appears to be a characteristic of each cancer cell line. For example, MDA-MB-231 breast carcinoma cells disappeared with the highest invasion rate among the four cell lines examined. In addition, all of the MDA-MB-231 cells migrated into the collagen gel before 30 h incubation whereas in the case of the

other three cell lines, $22.4 \pm 3.4\%$ ($n = 5$), $15.0 \pm 2.2\%$ ($n = 10$), and $38.4 \pm 3.1\%$ ($n = 5$) seeded of MCF-7, LS180, and HT-29 cells, respectively, still remained on the gel surface at the 30 h incubation time (Figure 4). Although the invasion process showed at least two phases, when the initial phase invasion rates were taken, invasion rates of 10.01 ± 2.53 , 4.08 ± 1.19 , 6.08 ± 1.95 , and $3.48 \pm 0.73\%/h$ for MDA-MB-231, MCF-7, LS180 and HT-29 cells, respectively, were calculated. These results may reflect the malignancy of the cells.

3.4. Invasion kinetics of breast and colon cancer cells

The real-time invasion assays described above were

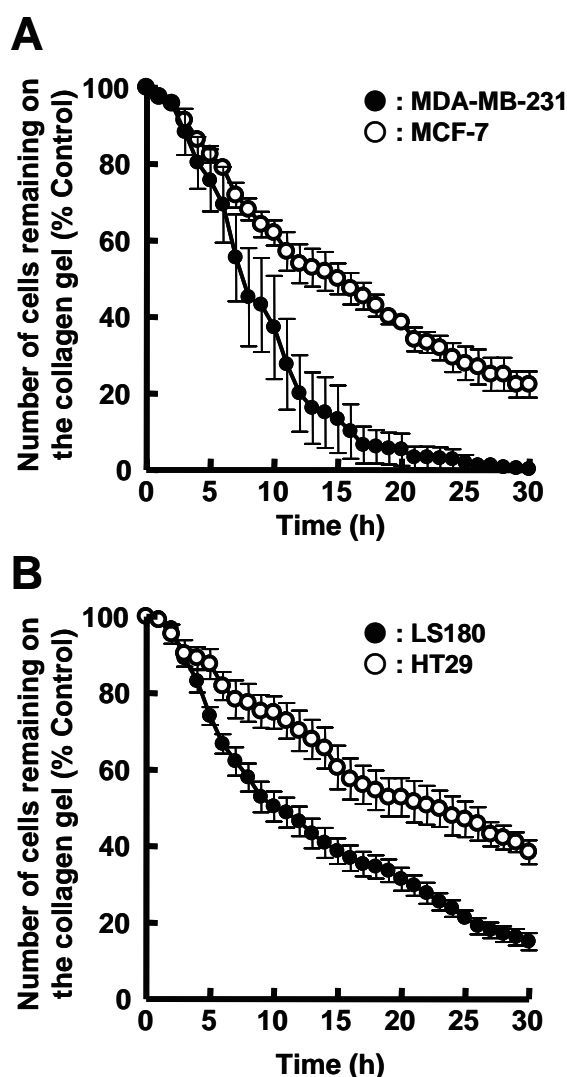


Figure 4. Invading rates of breast and colon carcinoma cells. Breast carcinoma MDA-MB-231 and MCF-7 cells and colon carcinoma LS180 and HT-29 cells were incubated on reconstituted collagen gels and the invasion was monitored under the time lapse microscope as described in Figure 1. The number of cells remaining on gel surface was counted and plotted against incubation time. In (A), results of breast carcinoma cell invasion are shown, MDA-MB-231 (●, $n = 5$) and MCF-7 (○, $n = 5$); the difference is statistically significant ($p = 0.0015$). In (B), results of colon carcinoma cell invasion are shown, LS180 (●, $n = 10$) and HT-29 (○, $n = 5$); difference is statistically significant ($p = 0.0004$).

Table 1. Migration distances of MDA-MB-231 and MCF-7 cells from the gel surface

	Migration distance (μm)	
	MDA-MB-231	MCF-7
Average	31.4	20.1
Maximum	157	141
75th percentile	24.2	32.9
50th percentile	14.9	24.2
25th percentile	7.1	18.7

under basal conditions, in which FCS and phenol red with estrogen-like effects were omitted (9). Although the growth of MCF-7 cells is dependent on estrogen, estrogen dependency is known to be reduced as passage numbers increase (10). Therefore, we examined the effects of β -estradiol on invasion of MCF-7 cells which had been cultured approximately for 10, 25, or 40 passages. As shown in Figure 5, under basal conditions, the invasion rates did not change among early, middle, and late passages of MCF-7 cells, and was on average $4.08 \pm 1.19\%/h$ ($n = 5$) as described above (Figure 4A, open circle). The addition of 10 nM β -estradiol to the basal medium significantly facilitated the migration of MCF-7 cells with early passages (~ 10) into the collagen gels (Figure 5, closed circle) as compared to that of the cells in the absence of β -estradiol (Figure 5, open circle). Although the effect of β -estradiol on the MCF-7 cell invasion was seen with the cells in middle and late passages (Figure 5, triangle and square, respectively), the effect seemed to be less significant as the passage number increased (Figure 5).

4. Discussion

In this study, we established a simple procedure for real-time observation of the initial step of the cancer cell invasion process. The real-time assay method could provide not only information on invasion rates but also migratory behaviors of individual cancer cells into the

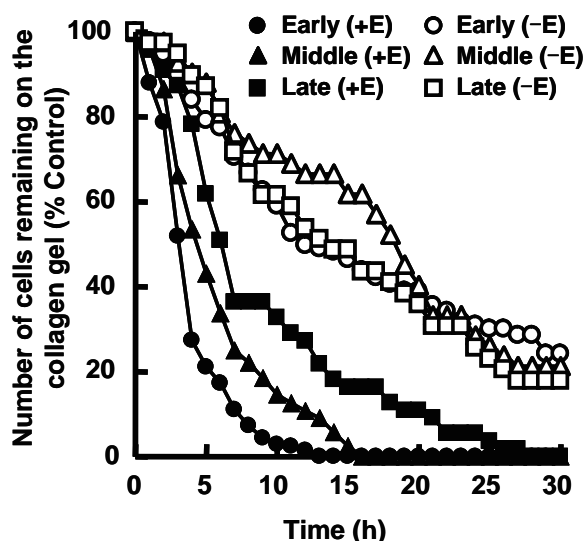


Figure 5. Effect of β -estradiol on MCF-7 cells invasion. MCF-7 cells with different passage numbers 10 (\bullet , \circ), 25 (\blacktriangle , \triangle), and 40 (\blacksquare , \square) were incubated on reconstituted collagen gels in the presence (\bullet , \blacktriangle , \blacksquare : +E) or absence (\circ , \triangle , \square : -E) of 10 nM β -estradiol (E). Invasion was monitored under the time lapse microscope as described in Figure 1. The number of cells remaining on gel surface was counted and plotted against incubation time. Shown are averages of three experiments for early (-E and +E) and two experiments for middle (+E) passages whereas the result of one experiment was shown for middle (-E) and late (-E and +E) passages (statistical evaluation was not done).

collagen I gel. The Boyden chamber assay which is handy and popularly used cannot provide such detailed information although our preliminary study using Boyden chambers provided useful information that, without 1% FCS, cancer cells were not able to cross the collagen I gel under basal conditions. In contrast, this study observing the disappearance of cancer cells from the collagen I gel surface clearly demonstrated that cancer cells penetrate into the collagen I gel under basal conditions without FCS. Obviously, under the conditions used, cells did not move much on the gel surface but rather attached on the collagen gel surface and moved into the gel. Most of the cells penetrating into the gel apparently remained within 60 μ m from the gel surface, which certainly indicated that cancer cells need stimuli to cross the collagen I barrier and further invade into ECM. The real-time assay system should thus allow not only direct visualization and assessment of the cancer cell invasion processes, but also study of cell invasion processes under different conditions reflecting *in vivo*.

Recording cell migration on or into the collagen gel was reported over three decades ago. Earlier studies using fibroblasts suggested the possible implication of this assay for cancer cell invasion (8,11). After rapid advances in cancer biology, several 3-dimensional culture systems have been reported for studying cancer cell invasion (12-16). Of those, the real-time assay system under basal conditions described in this report is the most basic and simplest *in vitro* model for effectively assessing the invasive behaviors of individual cancer cells. The earlier study by Erkell and Schirmacher (12) attempted to devise simplified systems to investigate the mechanisms of invasion based on the same concept as our study. It is the idea that since collagen I is a main component of normal tissue stroma, the ability to penetrate such a gel would be expected to reflect their metastatic potential. Their system was similar to our Boyden chamber methods with collagen I gel layered except that they counted cells which penetrated into and remained in the gel. In the Boyden chamber assays, we observed that both MCF-7 and MDA-MB-231 cancer cells did not reach the membrane under basal conditions whereas inclusion of 1% FCS in the medium induced invasion of these cancer cells to appear on the bottom side of the membrane (Figure 2).

The real-time invasion assays described here have used basal conditions, in which FCS and phenol red with estrogen-like effects were omitted. To observe effects of β -estradiol on invasion of MCF-7 cells whose growth is estrogen-dependent, three sets of MCF-7 cells from approximately 10, 25, or 40 passages were used. Although no significant difference on invasion was observed with early to late passage cells under basal conditions, the addition of 10 nM β -estradiol to the basal medium most significantly facilitated

the migration of MCF-7 cells from early passages (~ 10) into the collagen gels compared to those from middle- and late-passages. These results are consistent with a gradual loss of estrogen receptors during the progression from estrogen-dependent to -independent phenotypes (17).

In conclusion, the present method utilizing time-lapse microscopy is less involved and simpler than the previous methods (14,16), thus providing a useful system for further evaluating major components of ESM, growth factors, cytokines, and other possible microenvironment factors. Preliminary results on effects of ESM components and insulin-like growth factor-I on MCF-7 invasion have been previously presented at 12th International Congress of Endocrinology in 2004 (18). Further studies are in progress.

Acknowledgements

Authors are grateful to Atsuko Takeuchi for her excellent technical assistance and to Yuko Ohnishi and Tetsuyuki Kono for contributing to the initial phase of this study.

References

- Hanahan D, Weinberg RA. The hallmarks of cancer. *Cell*. 2000; 100:57-70.
- Liotta LA, Kohn EC. The microenvironment of the tumour-host interface. *Nature*. 2001; 411:375-379.
- Cretu A, Brooks PC. Impact of the non-cellular tumor microenvironment on metastasis: Potential therapeutic and imaging opportunities. *J Cell Physiol*. 2007; 213:391-402.
- Chang C, Werb Z. The many faces of metalloproteases: Cell growth, invasion, angiogenesis and metastasis. *Trends Cell Biol*. 2001; 11:S37-S43.
- Planas-Silva MD, Waltz PK. Estrogen promotes reversible epithelial-to-mesenchymal-like transition and collective motility in MCF-7 breast cancer cells. *J Steroid Biochem Mol Biol*. 2007; 104:11-21.
- Albini A, Benelli R, Noonan DM, Brigati C. The "chemoinvasion assay": A tool to study tumor and endothelial cell invasion of basement membranes. *Int J Dev Biol*. 2004; 48:563-571.
- Simon N, Noël A, Foidart JM. Evaluation of *in vitro* reconstituted basement membrane assay to assess the invasiveness of tumor cells. *Invasion Metastasis*. 1992; 12:156-167.
- Schor SL, Allen TD, Harrison CJ. Cell migration through three-dimensional gels of native collagen fibers: Collagenolytic activity is not required for the migration of two permanent cell lines. *J Cell Sci*. 1980; 46:171-186.
- Berthois Y, Katzenellenbogen JA, Katzenellenbogen BS. Phenol red in tissue culture media is a weak estrogen: Implications concerning the study of estrogen-responsive cells in culture. *Proc Natl Acad Sci U S A*. 1986; 83:2496-2500.
- Katzenellenbogen BS, Kendra KL, Norman MJ, Berthois Y. Proliferation, hormonal responsiveness, and estrogen receptor content of MCF-7 human breast cancer cells grown in the short-term and long-term absence of estrogens. *Cancer Res*. 1987; 47:4355-4360.
- Bard JB, Hay ED. The behavior of fibroblasts from the developing avian cornea. Morphology and movement *in situ* and *in vitro*. *J Cell Biol*. 1975; 67:400-418.
- Erkell LJ, Schirrmacher V. Quantitative *in vitro* assay for tumor cell invasion through extracellular matrix or into protein gels. *Cancer Res*. 1988; 48:6933-6937.
- Weaver VM, Fischer AH, Peterson OW, Bissell MJ. The importance of the microenvironment in breast cancer progression: Recapitulation of mammary tumorigenesis using a unique human mammary epithelial cell model and a three-dimensional culture assay. *Biochem Cell Biol*. 1996; 74:833-851.
- Duong HS, Le AD, Zhang Q, Messadi DV. Novel 3-dimensional culture system as an *in vitro* model for studying oral cancer cell invasion. *Int J Exp Pathol*. 2005; 86:365-374.
- Yamada KM, Cukierman E. Modeling tissue morphogenesis and cancer in 3D. *Cell*. 2007; 130:601-610.
- Hazgui S, Bonnet N, Cutrona J, Nawrocki-Raby B, Polette M, Chouchane L, Birembaut P, Zahm JM. 3D culture model and computer-assisted videomicroscopy to analyze migratory behavior of noninvasive and invasive bronchial epithelial cells. *Am J Physiol Cell Physiol*. 2005; 289:C1547-C1552.
- Clarke R, Brünner N, Katzenellenbogen BS, Thompson EW, Norman MJ, Koppi C, Paik S, Lippman ME, Dickson RB. Progression of human breast cancer cells from hormone-dependent to hormone-independent growth both *in vitro* and *in vivo*. *Proc Natl Acad Sci U S A*. 1989; 86:3649-3653.
- Sakai K, Ohnishi Y, Kono T, Fujita-Yamaguchi Y. Proceeding of 12th International Congress of Endocrinology. Lisbon, Portugal, August 31-September 4, 2004; pp. 703-707.

(Received September 28, 2010; Revised November 23, 2010; Re-revised December 1, 2010; Accepted December 3, 2010)

Expression, purification, and S-nitrosylation of recombinant histone deacetylase 8 in *Escherichia coli*

Jinhong Feng¹, Fanbo Jing², Hao Fang¹, Lichuan Gu³, Wenfang Xu^{1,*}

¹ Institute of Medicinal Chemistry, School of Pharmaceutical Sciences, Shandong University, Ji'nan, Shandong, China;

² The Affiliated Hospital of Medical College, Qingdao University, Qingdao, Shandong, China;

³ State Key Laboratory of Microbial Technology, School of Life Sciences, Shandong University, Ji'nan, Shandong, China.

Summary

Histone deacetylase (HDAC) 8 is a zinc ion dependent enzyme involved in removing the acetyl group from the core histones and other proteins which belong to Class I HDACs. It was reported that nitric oxide (NO) is a key regulator of HDAC function and S-nitrosylation of HDAC2 induces chromatin remodelling in neurons. This work reports the successful recombinant expression of human HDAC8 in *Escherichia coli* with two plasmids and the purification and S-nitrosylation *in vitro*. It was found that HDAC8 can be S-nitrosylated by the NO donor S-nitrosoglutathione (GSNO) *in vitro*, and the activity of HDAC8 was significantly inhibited when incubated with GSNO and S-nitrosocysteine in a time- and dosage-dependent manner, but sodium nitroprusside (SNP), and dithiothreitol cannot reverse this inhibition. These observations support and extend the concept that NO may regulate HDAC8 function by S-nitrosylation.

Keywords: Histone deacetylase 8, S-nitrosylation, nitric oxide, S-nitrosoglutathione, S-nitrosocysteine

1. Introduction

Histone deacetylases (HDACs) which remove the acetyl group of ϵ -amino groups of lysine residues in the N-terminal extension of core histones play an important role in many biological processes such as: DNA replication, transcription, differentiation, and apoptosis. HDACs comprise a family of 18 members in humans and are divided into four classes according to amino acid sequence and number of catalytic active sites (1). Class I includes HDAC1, HDAC2, HDAC3, and HDAC8, which are expressed ubiquitously, localized predominantly to the nucleus, and display high enzymatic activity toward histone substrates. They possess relatively simple structures, consisting of a conserved deacetylase domain with short amino- and carboxy-terminal extensions (2). HDAC1 and HDAC2 are nearly identical and are generally found together in repressive complexes such as the Sin3,

NuRD, CoResT, and PRC2 complexes (3). HDAC3 is found in distinct complexes such as the N-CoR-smRT complex, whereas no complex has been described for HDAC8 (4). Generally, the Zn²⁺-dependent HDACs are more important to modulate transcription and gene expression, and most HDAC inhibitors are designed to act on these HDACs (5). The zinc-dependent HDAC8 catalyzes the removal of acetyl moieties from histone tails, and is critically involved in regulating chromatin structure and gene expression (6). Recently, it was reported that HDAC8-selective inhibitors are available, and HDAC8 may be a potential drug target for neuroblastoma differentiation therapy using selective inhibitors, avoiding nonspecific side effects (7). The activity evaluation of HDAC inhibitors needs pure HDACs, so the expression, purification, and characterization of HDACs are very necessary.

Nitric oxide (NO) is a free-radical product of mammalian cell metabolism that plays diverse and important roles in the regulation of cell function. Protein S-nitrosylation refers to the reversible attachment of the NO moiety to specific cysteine residue(s) on selected proteins, producing labile S-nitrosothiol structure and functional alterations (8,9). S-nitrosylation is involved in the regulation of a diverse array of

*Address correspondence to:

Dr. Wenfang Xu, School of Pharmaceutical Sciences, Shandong University, Wen-hua-xi Road No. 44, Ji'nan 250012, Shandong, China.
e-mail: xuwenf@sdu.edu.cn

protein functions and plays a dominant role in many signaling pathways. It is increasingly accepted that *S*-nitrosylation of proteins serves as a critical cellular regulation mechanism similar to *O*-phosphorylation (10). Besides the physiological importance, dysfunction in maintaining the homeostasis of *S*-nitrosylation has been linked to many disease states (11). Recently, it was reported that *S*-nitrosylation of HDAC2 induces chromatin remodelling in neurons (12). Moreover, NO donors markedly reduced the enzymatic activity of HDAC2, minimally influenced that of HDAC1, and were ineffective on HDAC3. NO regulates the enzymatic activity of HDAC2 by *S*-nitrosylation, but not that of HDAC1 and HDAC3, as was detected in C2C12 myoblasts exposed to NO donors (13). As HDAC8 also belongs to the Class I HDACs group, whether NO can affect the activity of HDAC8 was not yet clear. In this study, we cloned, expressed, and purified recombinant human HDAC8, and examined whether NO can affect the activity of human HDAC8 by *S*-nitrosylation.

2. Materials and Methods

2.1. Materials

hHDAC8 gene (1-377 residues, NCBI accession No. NM_018486.1) was purchased from FulenGen (Guangzhou, China). Plasmids pGEX-6p-1 and pET21b were purchased from Invitrogen (Carlsbad, CA, USA). All enzymes, restriction endonucleases, and DNA markers were from Takara Biotechnology (Dalian, China). The plasmid purification kit and gel extraction kit were from Tiangen Biotech (Beijing, China). Sequencing primers were synthesized by Invitrogen China (Shanghai, China). Novagen[®] competent BL21 (DE3) *Escherichia coli* cells were from Merck (Darmstadt, Germany). *N*-[6-(Biotinamido)hexyl]-3'-(2'-pyridyldithio)propionamide (biotin-HPDP) were from Thermo Scientific Pierce Protein Research Products (Rockford, IL, USA). Boc-Lys (acetyl)-AMC and AMC were purchased from Bachem AG (Bubendorf, Switzerland). Streptavidin-peroxidase polymer ultrasensitive, glutathione (GSH), cysteine (Cys), Sodium nitroprusside (SNP), agarose and all other chemicals were of analytical grade and purchased from Sigma-Aldrich (St Louis, MO, USA).

2.2. Construction of plasmid pGEX-6p-1-*hHDAC8*, expression of glutathione *S*-transferase (*GST*)-*hHDAC8* fusion protein and purification of *hHDAC8*

HDAC8 gene (1-377 residues, GenBank accession No. AF230097) was amplified by using a polymerase chain reaction (PCR) with a forward primer 5'-TCAG GATCCATGGAGGAGCCGGAGGAACCG-3' and a reverse primer 5'-TTACTCGAGCTAGACCACATG

CTTCAGATTCCC-3', the products were subcloned into pGEX-6p-1 plasmid (Invitrogen). The constructs were used to transform *Escherichia coli* cells, the transformed cells were streaked on a Luria-Bertani (LB) agar plate containing 100 µg/mL ampicillin. Positive clones were selected by colony PCR and DNA sequencing. The recombinant human HDAC8 proteins with an *N*-terminal GST-tag were overexpressed in *Escherichia coli* strain BL21 (DE3). The full-length HDAC8 proteins were purified using a GST column (GE Healthcare Bio-Sciences, Piscataway, NJ, USA) as described previously (14). Source Q and Superdex-200 columns (GE Healthcare Bio-Sciences) were used for further purification of human HDAC8.

2.3. Construction of plasmid pET21b-*hHDAC8*, expression, and purification of *hHDAC8*

Construction and expression of plasmid pET21b-*hHDAC8* were similar to those of plasmid pGEX-6p-1-*hHDAC8* just with a forward primer 5'-ATACATATG ATGGAGGAGCCGGAGGAACCG-3' and a reverse primer 5'-TTACTCGAGGACCACATGCTTCAGATTC CC-3', which contained Nde I and Xho I restriction sites. The constructs were transformed into *Escherichia coli* cells and the ampicillin-resistant colonies were selected by colony PCR and DNA sequencing. The recombinant human HDAC8 proteins with an *N*-terminal six His-tag were overexpressed in *Escherichia coli* strain BL21 (DE3). The *hHDAC8* were first purified using a Ni-NTA resin column (GE Healthcare Bio-Sciences), then Source Q and Superdex 200 columns were used for further purification.

2.4. *hHDAC8* activity assay

Fluorescence analysis was used for the *hHDAC8* activity assay (15). HDAC8 releases the acetate moiety from 3-acetylated lysine residues of the substrate peptides, the deacetylated peptides containing unprotected lysine residues are recognized by trypsin and subsequently cleaved to release 7-amino-4-methylcoumarin (AMC). The fluorescence measurement was done at an excitation of 390 nm and emission of 460 nm by fluorometry (Varioskan; Thermo Fisher Scientific, Waltham, MA, USA). A standard curve of the cleavage product AMC was used to convert the fluorescence readings into micromolar products and calculate the specific activity of HDAC8 which was purified using two different recombinant plasmids (pGEX-6p-1-*hHDAC8* and pET21b-*hHDAC8*).

2.5. Synthesis of *S*-nitrosoglutathione (*GSNO*) and *S*-nitrosocysteine (*Cys-NO*) and detection of their effect on *HDAC8*

GSNO was synthesized by combining 200 mM NaNO₂

and 200 mM reduced glutathione in 0.5 M HCl in the dark at room temperature for 10 min. The solution was neutralized to pH 7.2 with 1 M NaOH, and its concentration determined by absorbance at 334 nm using an extinction coefficient of $900 \text{ M}^{-1}\cdot\text{cm}^{-1}$ (16). The synthesis of Cys-NO was similar to GSNO using cysteine to replace the glutathione. The recombinant HDAC8 was incubated with GSNO, Cys-NO, or SNP at a concentration gradient range for 30, 60, and 90 min at room temperature. Samples were desalted with Bio-Spin columns to remove excessive GSNO, Cys-NO, or SNP. To half of the samples at the 60 min incubation time, 1 mM dithiothreitol (DTT) was added for 15 min. The assay of HDAC8 activity was done as described above.

2.6. Western blot to detect the S-nitrosylation of HDAC8 *in vitro*

To induce S-nitrosylation *in vitro*, the recombinant HDAC8 proteins were incubated with freshly prepared GSNO (100 μM) in the dark for 30 min. Acetone precipitation was used to remove excessive GSNO. The Biotin-switch method was carried out essentially in the dark as detailed previously (17). Briefly, free protein thiols were blocked with 4 volumes of HEN buffer (250 mM Hepes-NaOH pH 7.7, 1 mM EDTA, 0.1 mM neocuproine) containing 2.5% SDS and 20 mM methyl methanethiol sulfonate at 50°C for 30 min. Proteins were precipitated with cold acetone and suspended in HEN buffer containing 1% SDS. Ascorbate (1 mM) was added to specifically reduce the SNO bond to free protein thiols, which were then labeled with biotin-HPDP (4 mM) for 1 h at room temperature. Proteins were added with SDS-PAGE sample buffer without boiling and DTT, and SDS-PAGE was performed. After transferring to a poly(vinylidene fluoride) membrane for immunoblotting, biotinylated proteins were detected with anti-biotin mouse monoclonal antibody.

3. Results

3.1. Clone, expression, and purification of human HDAC8

The expressed *h*HDAC8 was about 42 kDa and the expression level was approximately 1.2% of the total bacteria proteins for the pGEX-6p-1-*h*HDAC8 plasmid (Figure 1A), and approximately 0.5% of the total bacteria proteins for the pET21b-*h*HDAC8 plasmid (Figure 1B). SDS-PAGE analysis revealed that most target proteins existed in insoluble fractions. This indicated that the target proteins were mainly expressed as inclusion bodies in *Escherichia coli*. PreScission Protease (PPase) which specifically recognized LeuGluValLeuPheGln/GlyPro was used to resection the GST-tag from the *h*HDAC8 fused with GST and

combined to the GST-column. His-*h*HDAC8 combined to the Ni-NTA resin column was eluted with 250 mM imidazole. After affinity purification, the purity of *h*HDAC8 and His-*h*HDAC8 was over 90% (Figure 1). After further ion chromatography using a Source Q column and a final molecular sieve chromatography with Superdex-200, the purity of *h*HDAC8 was above 95% on SDS-PAGE stained with Coomassie brilliant blue. The HDAC8 purified from these two recombinant plasmids were all active proteins, and the specific activity of *h*HDAC8 from pGEX-6p-1-*h*HDAC8 plasmid was $0.73 \pm 0.23 \text{ U/mg}$ and His-*h*HDAC8 from pET21b-*h*HDAC8 plasmid was $1.39 \pm 0.44 \text{ U/mg}$. The higher specific activity of His-*h*HDAC8 may indicate that the N-terminal six his tag may stabilize the structure of HDAC8, since the already known crystal structures of *h*HDAC8 were mostly purified from pET21b plasmid in *Escherichia coli* (18).

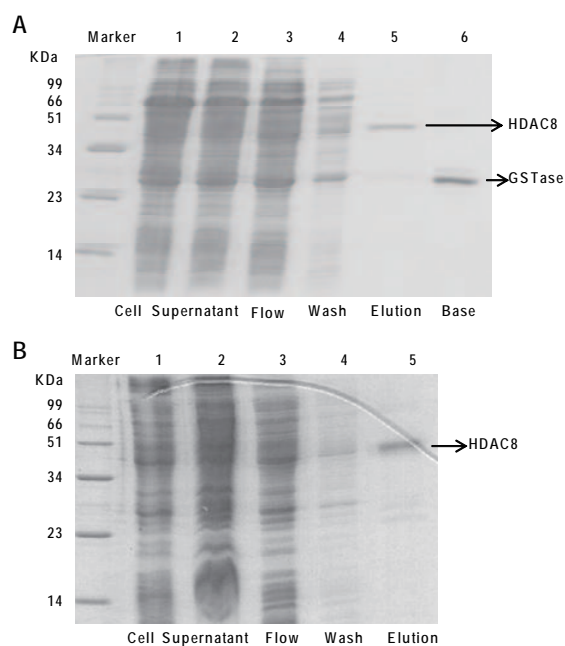


Figure 1. Expression and purification of *h*HDAC8. Ten microliters of proteins from each step were loaded. (A) Expression and purification of *h*HDAC8 from pGEX-6p-1-*h*HDAC8 plasmid. Lane 1, Isopropyl- β -D-thiogalactopyranoside (IPTG)-induced cells (arrow indicates GSTase-*h*HDAC8); lane 2, soluble lysate from induced cells; lane 3, soluble lysate after GST column flow-through; lane 4, proteins after GST column flow-through with wash buffer (25 mM Tris-HCl, pH 8.0, containing 150 mM NaCl); lane 5, *h*HDAC8 eluted from GST column by using pre-scission protease (PPase) to resection the GST-tag; lane 6, GSTase left on GST column base. (B) Expression and purification of *h*HDAC8 from pET21b-*h*HDAC8 plasmid. Lane 1, IPTG-induced cells (arrow indicates His-*h*HDAC8); lane 2, soluble lysate from induced cells; lane 3, soluble lysate after Ni-NTA resin column flow-through; lane 4, proteins after Ni-NTA resin column flow-through with wash buffer (25 mM Tris-HCl, pH 8.0, containing 5 mM imidazole and 150 mM NaCl); lane 5, His-*h*HDAC8 eluted from Ni-NTA resin column by 25 mM Tris-HCl, pH 8.0, containing 250 mM imidazole, 150 mM NaCl.

3.2. The activity of *h*HDAC8 can be inhibited by GSNO, Cys-NO but not SNP

It was reported that Class I HDACs which include HDAC1, HDAC2, and HDAC3 can be the targets for *S*-nitrosylation and that NO donors significantly reduced the enzymatic activity of HDAC2, minimally influenced that of HDAC1, and were ineffective on HDAC3 (13). However, the effect of NO donors on HDAC8 has not been reported. In this study, we tested whether NO donors caused functional changes in HDAC8. As shown in Figure 2, GSNO (50-1,000 μ M) caused concentration- and time-dependent inhibition of *h*HDAC8 activity, and the same inhibition also occurred with Cys-NO (75-800 μ M), but not SNP. From our synthesis of GSNO and Cys-NO, the GSNO we used might contain a small amount of GSH, NaNO₂, and oxidized glutathione disulfide (GSSG), while the Cys-NO might contain a small amount of cysteine and NaNO₂ (19). We tested whether these compounds could cause HDAC8 inhibition. We found that GSH, cysteine, NaNO₂, and GSSG at concentrations of 50-1,000 μ M had no detectable effects on HDAC8 activity (data not shown), suggesting that the contaminating compounds did not contribute to the inhibitory effects of GSNO

and Cys-NO. When DTT, a reagent that effectively decomposes *S*-nitrosothiol, was added to the GSNO or Cys-NO treated samples, HDAC8 activity was recovered completely to the original level (Figure 2), further supporting the hypothesis that *S*-nitrosylation plays a role in controlling HDAC8 activity.

3.3. HDAC8 can be *S*-nitrosylated *in vitro*

S-nitrosylation is involved in the regulation of a diverse array of protein functions and plays a dominant role in many signaling pathways. It was reported that *S*-nitrosylation of HDAC2 induced chromatin remodeling and emerged as an important regulatory mechanism for signal-dependent control of gene expression (12). In this study, we found the activity of *h*HDAC8 can be inhibited by GSNO and Cys-NO which existed in physiological conditions but not SNP. Therefore we used the biotin switch method to detect protein *S*-nitrosylation *in vitro*. As shown in Figure 3, HDAC8 obtained from two plasmids can be *S*-nitrosylated *in vitro* by incubation with 100 μ M GSNO. These results indicated that HDAC8 can be *S*-nitrosylated *in vitro*, and NO may regulate HDAC8 function by protein *S*-nitrosylation.

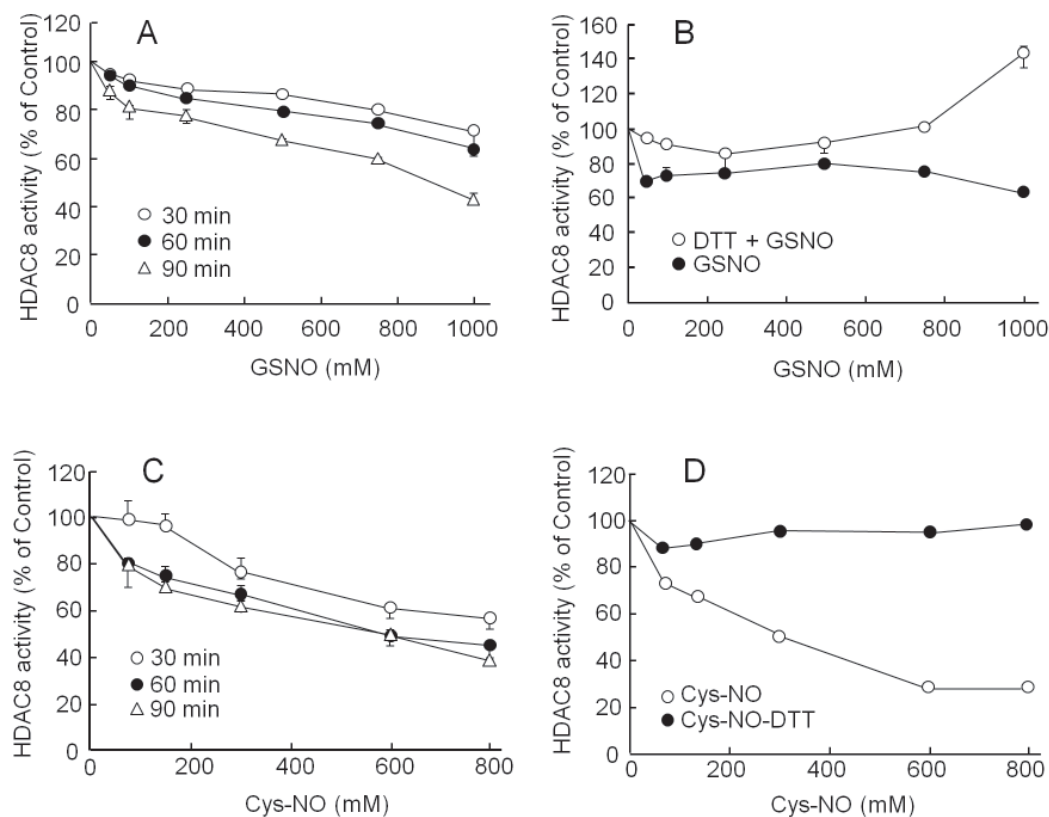


Figure 2. The activity of *h*HDAC8 was inhibited by GSNO and Cys-NO, and the inhibition was reversed by adding DTT. (A) HDAC8 activity was significantly inhibited by incubating with GSNO at final concentrations of 0, 50, 100, 250, 500, 750, and 1,000 μ M for 30, 60, and 90 min. **(B)** 1 mM DTT was added to the sample HDAC8 incubated with GSNO for 60 min. **(C)** HDAC8 activity was significantly inhibited by incubating with Cys-NO at final concentration of 0, 75, 150, 300, 600, and 800 μ M for 30, 60, and 90 min. **(D)** 1 mM DTT was added to the sample HDAC8 incubated with Cys-NO for 60 min. The result is representative of three different experiments.

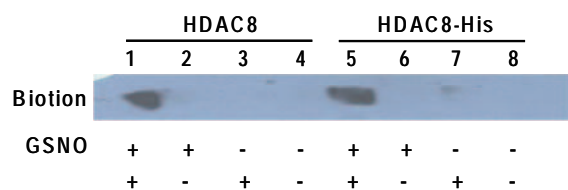


Figure 3. Western blot analysis of S-nitrosylated HDAC8. HDAC8 can be S-nitrosylated by incubation with GSNO (100 μ M) *in vitro*. HDAC8 used on lines 1, 2, 3, and 4 was purified from pGEX-6p-1-hHDAC8 plasmid, while HDAC8 on lines 5, 6, 7, and 8 was purified from pET-21b-hHDAC8 plasmid. First, samples were divided into two parts, half incubated with 100 μ M GSNO (lines 1, 2, 5, and 6), while the other with an equal volume of water (lines 3, 4, 7, and 8). Then, at the step of biotin-HPDP labelling on the SNO, samples were divided into two parts again, half was labeled with biotin-HPDP (lines 1, 3, 5, and 7), while the other half with solvent (lines 2, 4, 6, and 8). The result is representative of three different experiments.

4. Discussion

HDAC8, a eukaryotic zinc-dependent HDAC, is important for the growth of human tumor cell lines and has a distinct inhibition pattern that differs from that of HDAC1 and HDAC3, which both share 43% sequence identity with HDAC8 (18). It was reported that HDAC8 expression correlates with a poor outcome in neuroblastoma and selective HDAC8 inhibition induces cell differentiation (7), therefore, HDAC8 may be a potential drug target for neuroblastoma differentiation therapy using HDAC8-selective inhibitors. The cloning, expression and purification of human HDAC8 will help to screen for HDAC8 selective inhibitors.

Biological actions of NO arise as a direct consequence of chemical reactions between NO or NO-derived species and protein targets (10). NO exerts its action through addition to the transition metal ions which normally function as protein cofactors. However, more and more often direct structural modifications of peptidyl amino acid residues are being studied, such as the modifications of cysteine (S-nitrosylation) and tyrosine (nitration) residues, with respect to their putative signaling functions (20). It was reported that S-nitrosylation of histone deacetylase 2 induces chromatin remodelling in neurons (13). Moreover, NO decreases the enzymatic activity of a subgroup of neuronal HDACs *in vitro* and indicates that NO is a key regulator of HDAC function in mammalian neurons (21). In this study, we found NO donors markedly reduced the enzymatic activity of HDAC8 in a time and concentration dependent manner. The NO donors, GSNO and Cys-NO, which exist in the physiological state could inhibit the activity of HDAC8 and DTT can reverse this inhibition, but SNP has no effect. This may indicate that NO effects on HDAC8 needs a special structure to transfer the NO molecule, and this inhibition is reversible.

In this study, we further found HDAC8 can be

S-nitrosylated when incubated with a NO donor (GSNO) at a physiological concentration. Herein, we only found that HDAC8 can be S-nitrosylated, but the cysteine modified site of HDAC8 was not determined. In general, there has been a delay in adequate appreciation of the role of S-nitrosylation in biological signaling by NO. This lag is attributed to a poor understanding of the basis for selective targeting of NO to particular thiols, and methodological limitations in accurately quantifying this modification. Of course recent breakthroughs in concepts and methods diminish these barriers, such as the SNO-SID method (10,22). There are nine cysteine residues in the HDAC8 sequence, therefore, the identification of cysteine S-nitrosylation sites is very necessary for further research. In addition, we only found S-nitrosylation of HDAC8 *in vitro* but did not detect S-nitrosylation of HDAC8 in physiological and pathological processes *in vivo*. Since HDAC8 associates with smooth muscle alpha-actin, is essential for smooth muscle cell contractility (23), and induces neuroblastoma cell differentiation (7), study of the S-nitrosylation level of HDAC8 in these processes may be helpful to understand the role of the molecular mechanisms.

In conclusion, we cloned, expressed, and purified active human HDAC8 from two plasmids in *Escherichia coli*, and first found NO may regulate the activity of HDAC8 by S-nitrosylation *in vitro*. These findings should give some insight into the further research of HDAC8 in disease.

Acknowledgements

This work was greatly supported by State Key Laboratory of Microbial Technology, School of Life Sciences in Shandong University. This work was also supported by National High Technology Research and Development Program of China (863 project, Grant No. 2007AA02Z314) and Important National Science & Technology Specific Projects of China (No. 2009ZX09103-118).

References

1. Gregoret IV, Lee YM, Goodson HV. Molecular evolution of the histone deacetylase family: Functional implications of phylogenetic analysis. *J Mol Biol.* 2004; 338:17-31.
2. Haberland M, Montgomery RL, Olson EN. The many roles of histone deacetylases in development and physiology: Implications for disease and therapy. *Nat Rev Genet.* 2009; 10:32-42.
3. Yang XJ, Seto E. Collaborative spirit of histone deacetylases in regulating chromatin structure and gene expression. *Curr Opin Genet Dev.* 2003; 13:143-153.
4. Yang XJ, Seto E. The Rpd3/Hda1 family of lysine deacetylases: From bacteria and yeast to mice and men. *Nat Rev Mol Cell Biol.* 2008; 9:206-218.
5. Marks PA, Xu WS. Histone deacetylase inhibitors: Potential in cancer therapy. *J Cell Biochem.* 2009;

- 107:600-608.
6. Wu R, Wang S, Zhou N, Cao Z, Zhang Y. A proton-shuttle reaction mechanism for histone deacetylase 8 and the catalytic role of metal ions. *J Am Chem Soc.* 2010; 132:9471-9479.
 7. Oehme I, Deubzer HE, Lodrini M, Milde T, Witt O. Targeting of HDAC8 and investigational inhibitors in neuroblastoma. *Expert Opin Investig Drugs.* 2009; 18:1605-1617.
 8. Simon DI, Mullins ME, Jia L, Gaston B, Singel DJ, Stamler JS. Polynitrosylated proteins: Characterization, bioactivity, and functional consequences. *Proc Natl Acad Sci U S A.* 1996; 93:4736-4741.
 9. Jaffrey SR, Erdjument-Bromage H, Ferris CD, Tempst P, Snyder SH. Protein S-nitrosylation: A physiological signal for neuronal nitric oxide. *Nat Cell Biol.* 2001; 3:193-197.
 10. Lane P, Hao G, Gross SS. S-nitrosylation is emerging as a specific and fundamental posttranslational protein modification: Head-to-head comparison with O-phosphorylation. *Sci STKE.* 2001; 2001:re1.
 11. Foster MW, McMahon TJ, Stamler JS. S-nitrosylation in health and disease. *Trends Mol Med.* 2003; 9:160-168.
 12. Nott A, Watson PM, Robinson JD, Crepaldi L, Riccio A. S-nitrosylation of histone deacetylase 2 induces chromatin remodelling in neurons. *Nature.* 2008; 455:411-415.
 13. Colussi C, Mozzetta C, Gurtner A, *et al.* HDAC2 blockade by nitric oxide and histone deacetylase inhibitors reveals a common target in Duchenne muscular dystrophy treatment. *Proc Natl Acad Sci U S A.* 2008; 105:19183-19187.
 14. Guan KL, Dixon JE. Eukaryotic proteins expressed in *Escherichia coli*: An improved thrombin cleavage and purification procedure of fusion proteins with glutathione S-transferase. *Anal Biochem.* 1991; 192:262-267.
 15. Wegener D, Wirsching F, Riester D, Schwienhorst A. A fluorogenic histone deacetylase assay well suited for high-throughput activity screening. *Chem Biol.* 2003; 10:61-68.
 16. Hogg N. Biological chemistry and clinical potential of S-nitrosothiols. *Free Radic Biol Med.* 2000; 28:1478-1486.
 17. Jaffrey SR, Snyder SH. The biotin switch method for the detection of S-nitrosylated proteins. *Sci STKE.* 2001; 2001:pl1.
 18. Vannini A, Volpari C, Filocamo G, Casavola EC, Brunetti M, Renzoni D, Chakravarty P, Paolini C, De Francesco R, Gallinari P, Steinkühler C, Di Marco S. Crystal structure of a eukaryotic zinc-dependent histone deacetylase, human HDAC8, complexed with a hydroxamic acid inhibitor. *Proc Natl Acad Sci U S A.* 2004; 101:15064-15069.
 19. Becker K, Gui M, Schirmer RH. Inhibition of human glutathione reductase by S-nitrosoglutathione. *Eur J Biochem.* 1995; 234:472-478.
 20. Szuba A, Wojtaszek P. Structural modifications of proteins induced by nitric oxide. *Postepy Biochem.* 2010; 56:107-114. (in Polish)
 21. Watson PM, Riccio A. Nitric oxide and histone deacetylases: A new relationship between old molecules. *Commun Integr Biol.* 2009; 2:11-13.
 22. Hao G, Derakhshan B, Shi L, Campagne F, Gross SS. SNOSID, a proteomic method for identification of cysteine S-nitrosylation sites in complex protein mixtures. *Proc Natl Acad Sci U S A.* 2006; 103:1012-1017.
 23. Waltregny D, Glenisson W, Tran SL, North BJ, Verdin E, Colige A, Castronovo V. Histone deacetylase HDAC8 associates with smooth muscle alpha-actin and is essential for smooth muscle cell contractility. *FASEB J.* 2005; 19:966-968.

(Received January 6, 2011; Accepted February 7, 2011)

Nrf2-mediated protection against UVA radiation in human skin keratinocytes

Feifei Tian*, Feifei Zhang*, Xiangdong Lai, Lijuan Wang, Li Yang, Xiang Wang, Gurinder Singh, Julia Li Zhong**

The "111 Project" Laboratory of Biomechanics & Tissue Repair Engineering; Key Laboratory of Biorheological Science and Technology, Ministry of Education, College of Bioengineering, Chongqing University, Chongqing, China.

Summary

Ultraviolet A (UVA, 320-400 nm) radiation is an oxidizing agent that causes significant damage to cellular components and that leads to photoaging and cancer. It strongly induces NF-E2-related factor 2 (Nrf2) expressions in cultured FEK4 human skin fibroblasts but weakly induces it in transformed HaCaT skin keratinocytes. Nrf2 silencing increases cell damage at a moderate dose of UVA irradiation ($250 \text{ kJ}\cdot\text{m}^{-2}$) in FEK4 fibroblasts, but whether a decrease in Nrf2 sensitizes HaCaT keratinocytes to a moderate to high dose ($250\text{-}500 \text{ kJ}\cdot\text{m}^{-2}$) of UVA irradiation (*i.e.*, $400 \text{ kJ}\cdot\text{m}^{-2}$, peak emission 365 nm) is currently unknown. A moderate to high dose of UVA irradiation only slightly increased Nrf2 expression in HaCaT skin keratinocytes. Knockdown of Nrf2 by specific silencing of Nrf2 (siNrf2) strongly increased cell damage as gauged by membrane damage (LDH) and cell viability (MTT assay) following this dose of UVA irradiation. These results suggest that decreased Nrf2 significantly increased UVA irradiation-induced cell damage in skin keratinocytes. Nrf2 may play a role in protecting human skin keratinocytes from UVA radiation-induced damage.

Keywords: UVA, Nrf2, HaCaT skin keratinocytes

1. Introduction

The major source of human exposure to ultraviolet (UV) radiation is *via* sunlight or artificial sources such as cosmetic tanning spas that use artificial UV lamps (1,2). UV light that reaches the surface of the earth primarily consists of (> 90%) ultraviolet A (UVA) radiation (320-400 nm), which produces reactive oxygen species (ROS) and has been linked to lipid, protein, and nucleic acid damage (3,4). The skin acts as a physiological barrier to protect an organism against environmental UV radiation, chemical pollutants, and physical injury. Skin is equipped with an elaborate system of antioxidants and enzymes that maintain the balance between oxidative stress and anti-oxidant defense (1,5). The most significant enzymes, *e.g.* hemeoxygenase 1 (HO-1) and the phase II detoxification enzymes peroxiredoxin

1 (Prx I), NAD(P)H quinone oxidoreductase 1 (NQO1), glutamate-cysteine ligase, aldo-keto reductase, and thioredoxin reductase, are crucial to protect skin cells from exogenous toxicity, oxidative stress, and carcinogenesis (1,5). NF-E2-related factor 2 (Nrf2) is a member of the "cap 'n' collar" family of transcription factors, which also include Nrf1 and Nrf3. Upon heterodimerization with leucine zipper proteins such as small Maf proteins, Nrf2 binds to antioxidant response elements (AREs) or Maf recognition elements of its target genes and coordinates transcriptional activation of various antioxidant enzymes (6,7). During normal cellular quiescence, Nrf2 is held in the cytoplasm by Kelch-like ECH-associated protein 1 (Keap1) but is released under stress conditions, although the mechanism of its activation may vary depending on the type of cells or tissues (6,7).

Recently, the role of Nrf2 in protecting against oxidative stress has been studied and reviewed (7). Nrf2 is involved in wound healing in mouse skin and Nrf2-deficient mice have an impaired oxidative stress defense (7,8). A study by Hirota and a previous study by the current authors also showed that UVA irradiation causes nuclear accumulation of Nrf2 in human and

*The first two authors contributed equally to this work.

**Address correspondence to:

Dr. Julia Li Zhong, College of Bioengineering, Chongqing University, Chongqing 400044, China.
e-mail: jzhonglyq@163.com or jlzhong@cqu.edu.cn

mouse fibroblasts, respectively, and a deficiency of Nrf2 in these skin fibroblasts significantly increases cell damage caused by low (50-100 kJ•m⁻²) to moderate (250 kJ•m⁻²) doses of UVA irradiation (9,10). Nrf2 may be involved in protection of HaCaT human skin keratinocytes from UVA irradiation by quercetin, an antioxidant (11). Therefore, increased cellular antioxidant or detoxification capacity as a result of increased Nrf2 levels may help with cellular defense.

As the top layer of skin, epidermal keratinocytes encounter more UV irradiation and are more resistant to UVA irradiation-mediated cell damage than fibroblasts (12,13). Nrf2 knockout mice have a prolonged inflammatory response after skin injury (8). Previously, a significant increase in Nrf2 was not detected in human HaCaT skin keratinocytes following a low to moderate dose (50-250 kJ•m⁻²) of UVA irradiation (14,15). However, down-regulation of Nrf2 expression may suppress cellular functions, such as antioxidant response, so cells may be more susceptible to oxidative damage, including UVA irradiation (5,7,8).

Nrf2 may protect human keratinocytes against UVA exposure and enhanced protection of cells by Nrf2 may prevent radiation damage caused by sunbathing/tanning. The current study investigated the cell response to different doses of UVA irradiation. Earlier studies found that a moderate dose (250 kJ•m⁻²) of UVA irradiation did not activate Nrf2 in HaCaT human skin keratinocytes while a high dose (> 500 kJ•m⁻²) of UVA irradiation caused significant damage to these cells (13). Therefore, a moderate to high dose (400 kJ•m⁻²) of UVA irradiation was used to examine Nrf2 accumulation following irradiation. Further, the effect of Nrf2 silencing on cell damage by this dose of UVA irradiation was investigated in HaCaT human skin keratinocytes.

2. Materials and Methods

2.1. Cell culture and antibodies

Human immortalized skin keratinocytes (HaCaT cells) (14) were maintained in Dulbecco's Modified Eagle's Medium (DMEM) supplemented with 10% heat-inactivated fetal calf serum (FCS). Antibodies against Nrf2 (H300, sc-13032), and β -actin (sc-9104) were obtained from Santa Cruz Biotechnology (Santa Cruz, CA, USA). Anti-vinculin was purchased from Upstate Biotechnology (Waltham, MA, USA). Anti-mouse and anti-rabbit IgG secondary antibodies were from Sigma-Aldrich China (Shanghai, China) (10,14). A lactate dehydrogenase (LDH) cytotoxicity assay kit was obtained from Roche Diagnostics (Mannheim, Germany). 3-(4,5-dimethylthiazol-2-yl)-2,5-diphenyltetrazolium bromide (MTT) for a cell viability assay was purchased from Sigma-Aldrich.

2.2. Irradiation of cells with UVA

Cells were irradiated with a broad-spectrum UV lamp (ultraviolet B (UVB) was blocked with an appropriate filter) with a peak wavelength at 365 nm (MUA-165, Beijing Normal University, Beijing, China). The lamp exposure time was calculated using a radiometer (Beijing Normal University). The irradiation time normally took less than one hour. Prior to UVA irradiation, the growth medium was removed from the cells and retained; each dish was washed twice with phosphate-buffered saline (PBS) and cells were irradiated in PBS. In order to maintain a consistent temperature of 25°C, irradiation of cells with UVA was performed in an air-conditioned room as previously described (10,14). Non-irradiated cells were covered with foil to prevent exposure and used as a background control (sham = 0 kJ•m⁻²). After UVA irradiation, PBS was removed and cells were re-incubated in retained conditional medium for a period of time (normally 4-8 h).

2.3. RNA Interference

Small interfering RNAs were used to knock down Nrf2 protein levels. All small interfering RNAs (siRNAs) and scrambled control siRNAs (Sb) were obtained from Ambion siRNAs (Ambion, Austin, TX, USA): Sb: Silencer Negative Control siRNA (AM4611), siNrf2: NM_006164. #1: ID 115764, #2: ID 115763.

For siRNA transfection, sub-confluent cells were detached and transfected with siRNAs using siPORT™ NeoFX™ Transfection Agent (AM4511, Ambion). For HaCaT cells, siRNA was diluted in 50 μ L OPT medium (A) while 3 μ L NeoFX was diluted in 50 μ L OPT medium (B); the respective solutions were incubated for 10 min and then A and B were mixed well and incubated further for 10 min to allow the formation of siRNA complex (100 μ L). All steps were carried at room temperature (RT). The siRNA complex was then plated into 6-well plates. Then 1×10^5 cells within 1.5 mL normal cell growth medium were added to reach a total volume of 1.6 mL, and cells were then incubated at 37°C and 95% humidity with 5% CO₂. The following day, a half volume (0.8 mL) of fresh medium was added and cells were incubated for a total of 48 h before use (10,14).

2.4. Western blotting

After cells were incubated for a period of time (normally 8-12 h) following UVA irradiation, cell lysates were collected as described before (14). Equal amounts of proteins were mixed with loading buffer and subjected to electrophoresis using 8% (w/v) SDS-polyacrylamide gels. Separated proteins were transferred onto polyvinylidene fluoride (PVDF) membranes (Amersham Pharmacia Biotech, Little Chalfont, UK) and non-

specific bindings were blocked with 5% (w/v) non-fat dried-milk dissolved in tris-buffered saline with Tween (TBS-T) buffer. The membranes were then incubated for 1 h at RT with Nrf2 and actin antibodies, respectively. Subsequently, the membranes were incubated with related horseradish peroxidase conjugated secondary antibodies for 1 h at RT. Protein bands were visualized on X-ray film activated by chemiluminescence using an ECL Western blotting system (Amersham Pharmacia Biotech). The intensity of bands was quantified by digital densitometry using NIH Image J 1.33 software. Data were normalized to actin and expressed as the percentage or fold change compared to the corresponding control, which was set at 1 (10,14).

2.5. Immunofluorescence

HaCaT cells were cultured on glass coverslips. Four hours after irradiation, cells were washed twice with PBS, fixed with 4% (w/v) paraformaldehyde for 10 min at RT, permeabilized with ice-cold methanol for another 10 min, and then washed twice with PBS. They were then blocked with Image-iT™ Fx signal enhancer (Alexa-Fluor system, Invitrogen, Carlsbad, CA, USA) and incubated at RT for 1 h with the primary antibody Nrf2 (1:200) or vinculin (1:50) and washed twice in PBS for 30 min; afterwards, cells were incubated with secondary antibody Alexa Fluor 488-conjugated goat anti-rabbit or anti-mouse IgG or (1:1,000, Invitrogen) for 1 h, washed again in PBS, and mounted onto glass microscope slides using VECTASHIELD® Hard_Set™ Mounting Medium. Cells were analyzed under a Nikon Eclipse TE2000-U epifluorescence microscope. Images were recorded using the software program UltraVIEW (10,14).

2.6. LDH assay

The percentage of extracellular LDH leakage served as an indicator of membrane damage. LDH was determined using a cytotoxicity detection kit (Cat. No. 11644793001, Roche Diagnostics) following the instructions supplied. SiNrf2-treated cells (7,500) were seeded onto 96-well plates for 48 h, irradiated with UVA, and then re-incubated for 4 h. LDH release was then measured as described previously (8,10). The fraction of extracellular LDH was represented as the percentage of total LDH and expressed as the fold increase relative to the sham-irradiated scrambled siRNA-treated control, which was set at 1.

2.7. Cell viability assay

HaCaT cells were transfected with siRNA as described above and seeded onto 96-well plates (200 μ L, 7,500 cells/well). Cells were grown for 48 h and then were exposed to 100-500 $\text{kJ}\cdot\text{m}^{-2}$ of UVA light. After

irradiation, the cells were cultured in conditional culture medium again for a further 4 h. Each well then received 50 μ L of MTT (0.5 mg/mL) in serum-free medium. The plates were incubated for 2.5 h at 37°C and MTT solution was discarded. Fifty μ L of dimethyl sulfoxide was added to each well and the plates were shaken at 200 rpm on an orbital shaker for 5 min before colorimetric analysis. The absorbance at 570 nm was measured in a microplate reader and expressed as the percentage of surviving cells compared to the vehicle control group. The absorbance levels, an indicator of cell viability, were plotted and compared to the sham-irradiated scrambled siRNA-treated control, which was set at 100.

2.8. Statistical analyses

Statistical analyses were carried out using a two-tailed *t* test and *p* values below 0.05 were considered statistically significant. The values in the graphs correspond to the mean and the error bars indicate standard error (S.E.).

3. Results

3.1. Resistance of human skin keratinocytes to UVA-induced morphological changes

Human primary skin keratinocytes are more resistant to UVA-induced damage, as gauged by membrane damage and morphological changes, than matching fibroblasts from the same biopsy (12). To investigate the effect of various doses of UVA irradiation on cell morphology, the HaCaT cells were examined by vinculin staining for focal adhesion following the various doses of UVA irradiation.

HaCaT cells were sham-irradiated and served as the positive control. Staining with vinculin showed that, following a low (100 $\text{kJ}\cdot\text{m}^{-2}$) to moderate dose (250 $\text{kJ}\cdot\text{m}^{-2}$) of UVA irradiation, cell morphology was maintained without changes and that dot-like focal adhesion of molecules did not alter (Figure 1). The overall cell shape was maintained following the higher dose (500 $\text{kJ}\cdot\text{m}^{-2}$) of UVA irradiation, absent some specific and non-specific staining. This indicates that a moderate dose of UVA irradiation did not significantly alter the cell morphology or the staining pattern of focal adhesion molecules, *e.g.* vinculin, while a higher dose of UVA irradiation did alter cell morphology and the focal adhesion molecule vinculin in HaCaT keratinocytes. This result is consistent with previous reports that a moderate dose of UVA irradiation did not significantly alter the morphology of primary skin keratinocytes (12).

3.2. UVA irradiation did not significantly increase Nrf2 protein in skin keratinocytes

Low and moderate doses (100 and 250 $\text{kJ}\cdot\text{m}^{-2}$) of

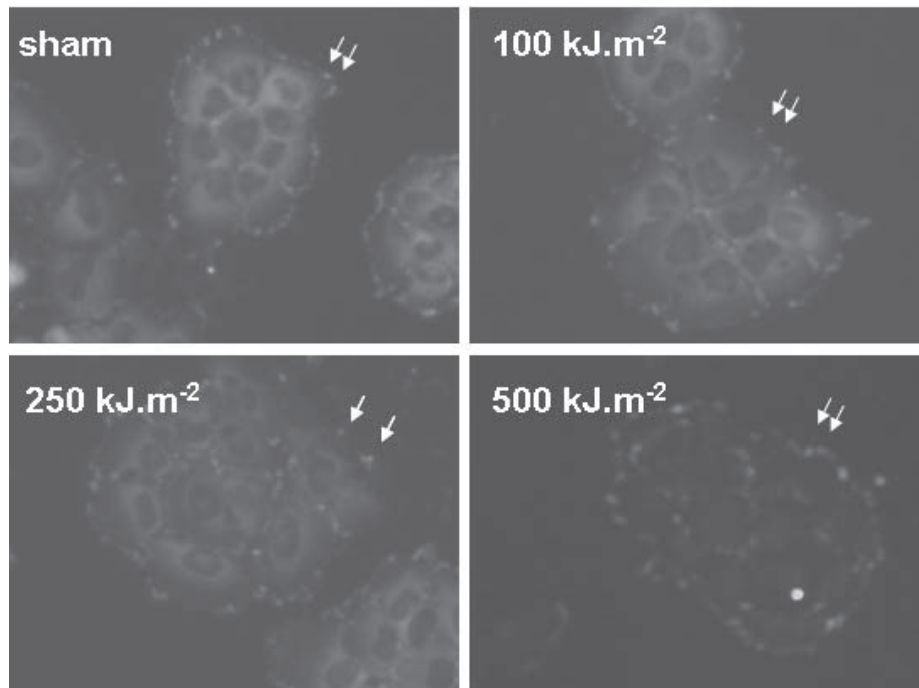


Figure 1. Immunocytochemical analysis of morphology and vinculin pattern following UVA irradiation of HaCaT cells. Cells were non-irradiated (sham) or irradiated with the doses indicated and then fixed and subjected to vinculin immunostaining for 4 h following UVA irradiation, as described in the Materials and Methods.

UVA irradiation are strong inducers of Nrf2 in FEK4 human skin fibroblasts but weak inducers of Nrf2 in human skin keratinocytes (10,14,15). To investigate if a moderate to high dose ($400 \text{ kJ}\cdot\text{m}^{-2}$) of irradiation altered Nrf2 localization, HaCaT was exposed to this dose of irradiation. Results revealed a less than 2-fold increase in Nrf2 protein levels in HaCaT cells 4 and 8 h after UVA irradiation (Figure 2A). Immunostaining analysis showed that Nrf2 protein was maintained in the nucleus of non-irradiated control cells, and it accumulated slightly in cells 4 and 8 h after this dose of irradiation. This result indicates that despite its activation in skin fibroblasts (10,14) Nrf2 was not significantly activated in human skin keratinocytes following UVA irradiation.

3.3. Reduction of Nrf2 increased cell damage induced by $400 \text{ kJ}\cdot\text{m}^{-2}$ of UVA in HaCaT cells

A study demonstrated that a moderate dose ($250 \text{ kJ}\cdot\text{m}^{-2}$) of UVA irradiation significantly induced the expression of Nrf2 in skin fibroblasts and that Nrf2 protected the cells against this dose of UVA irradiation-mediated membrane damage, which was measured with an LDH assay (10). Nrf2 was expected to protect HaCaT skin keratinocytes, though UVA irradiation caused only a slight increase in Nrf2 protein levels and nuclear accumulation in these cells (Figure 2).

To demonstrate the importance of Nrf2 in UVA irradiation-mediated cell damage, the Nrf2 gene was

knocked down in HaCaT cells using siRNA. Knock down of Nrf2 protein levels was confirmed by Western blotting analysis, which revealed a significant decrease in Nrf2 protein levels following siRNA transfection (Figure 3).

Cell damage was demonstrated by the loss of the integrity of the membrane, as gauged by LDH release and viability (MTT assay). HaCaT Cells were pretreated with vehicle or scrambled siRNA and siNrf2 during plating and grown to 90% confluence. Cells were then either sham or UVA ($400 \text{ kJ}\cdot\text{m}^{-2}$)-irradiated and further incubated in normal medium for 4 h. As shown in Figure 4, without UVA irradiation siRNA had a negligible effect on the leakage of LDH and viability of HaCaT cells, but $400 \text{ kJ}\cdot\text{m}^{-2}$ of UVA irradiation caused a 1.7-fold increase in LDH leakage, representing a significant increase (Figure 4A). This dose of UVA irradiation caused a 10% decrease in cell viability (Figure 4B), representing a significant reduction in viability. UVA-induced LDH leakage was further increased to 2.3- and 2.5-fold by pre-treatment with 10 and 50 nM of siNrf2, respectively ($p < 0.05$) (Figure 4A). UVA-induced loss of viability was further increased to 15% and 20% by pre-treatment with 10 and 50 nM of siNrf2, respectively ($p < 0.05$) (Figure 4B). A different exon targeting siNrf2 also provided similar results (data not shown). These results indicate that loss of Nrf2 significantly increased cell damage in human HaCaT keratinocytes irradiated with a moderate to high dose ($400 \text{ kJ}\cdot\text{m}^{-2}$) of UVA.

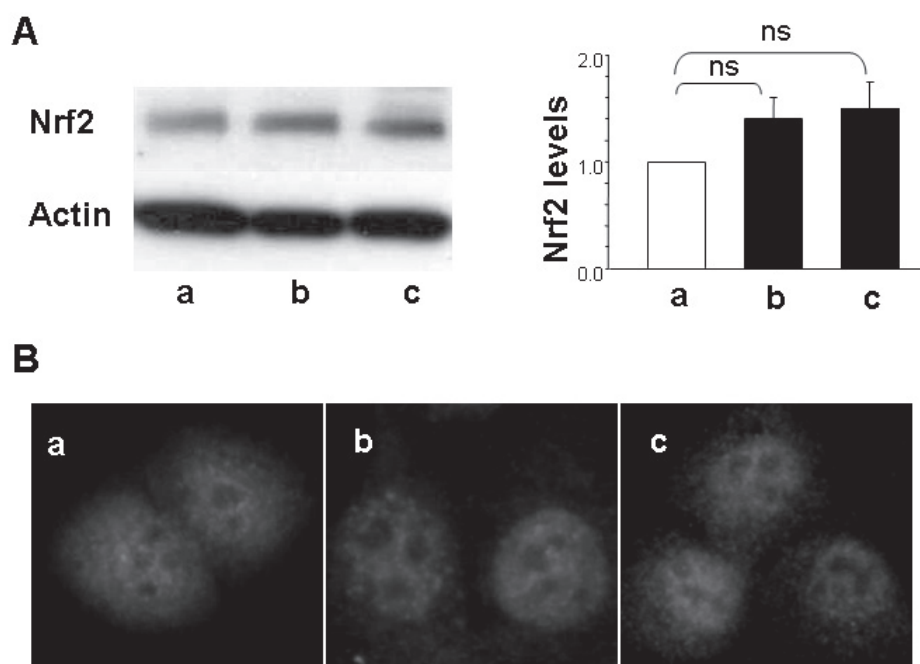


Figure 2. UVA irradiation slightly induced Nrf2 protein expression and nuclear accumulation in HaCaT. HaCaT cells were subjected to $400 \text{ kJ}\cdot\text{m}^{-2}$ UVA irradiation and re-incubated for the time indicated and then subjected to Western blotting (A) and immunofluorescence (B) analysis using Nrf2 antibody, as described in the Materials and Methods. The result shown is representative of 3 independent experiments. In the densitometric analysis of the Western blotting data, Nrf2 expression was normalized to actin and the sham-irradiated control was set to 1. Each bar represents the mean \pm S.E.M., $n = 3$. $p > 0.05$. a, sham-irradiated; b, 4 h after UVA; c, 8 h after UVA.

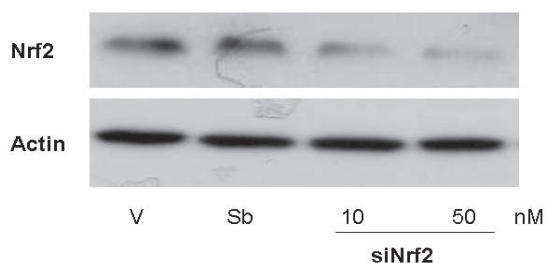


Figure 3. Silencing of Nrf2 reduced Nrf2 protein levels. HaCaT cells were transfected with vehicle control (V), 50 nM of negative scrambled control siRNA (Sb), and siNrf2 using siPORT NeoFX transfection reagent (Ambion), as described in the Materials and Methods. Cells were grown on 6-well plates for 48 h and collected and then Nrf2 levels were analyzed using Western blotting.

4. Discussion

Exposure to excessive UV irradiation in the form of sunlight adversely affects the skin, causing erythema, sunburn, pigmentation, hyperplasia, immunosuppression, skin aging, and cancer (2,3). In recent years, air pollution has caused ozone layer depletion, leading to increased exposure to UV. As a result, the incidence of skin ailments, such as skin aging and skin cancer, has dramatically increased worldwide (1,3). Therefore, a natural area of interest would be to identify protective molecules, including those in natural products, that can activate cellular defense, *i.e.*,

via activation of Nrf2 to protect against UVA-induced oxidative stress.

Earlier work demonstrated that HaCaT keratinocytes are resistant to UVA-mediated membrane damage at lower doses of radiation (13,14). Study of cell morphology found that low and moderate doses (100 and $250 \text{ kJ}\cdot\text{m}^{-2}$) of UVA irradiation did not alter cell focal adhesions and overall cell morphology, which is consistent with results of an earlier study indicating that human primary keratinocytes are generally resistant to UVA-mediated damage as gauged by LDH and cell morphology (12).

Nrf2 is ubiquitously expressed in a wide range of tissues and cell types, including keratinocytes (14). Nrf2 is involved in wound healing in mouse skin and Nrf2-deficient mice have an impaired oxidative stress defense (8). Previous studies have shown that UVA causes nuclear accumulation of Nrf2 in murine fibroblasts (9). Nrf2 is activated by UVA irradiation, and silencing of Nrf2 significantly increases UVA-mediated membrane damage in human primary skin fibroblasts (10). However, a recent study by the current authors showed that moderate dose of UVA irradiation did not significantly increase Nrf2 protein levels in HaCaT skin cells (14). UVA irradiation also has no effect on Nrf2 expression levels in murine skin keratinocytes, though electrophilic chemicals activate Nrf2 and induce Nrf2-mediated gene expression (15).

Nrf2 may play an important role in protecting skin

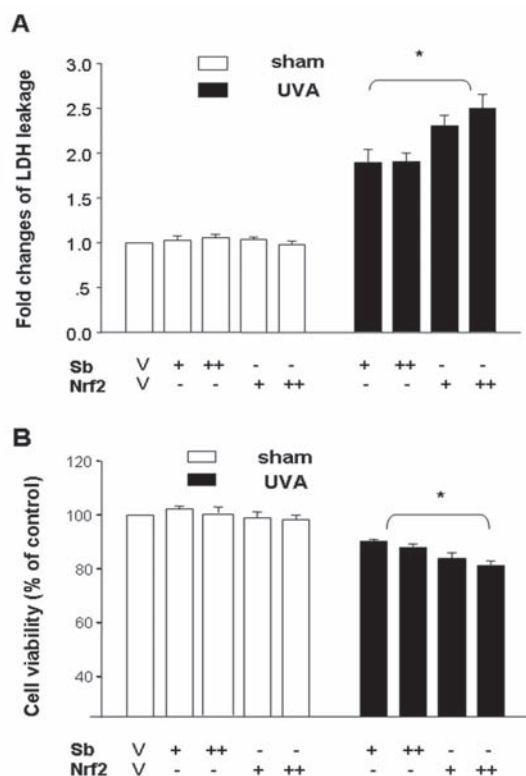


Figure 4. Silencing of Nrf2 increased UVA irradiation-mediated damage. HaCaT cells were transfected as described in Figure 3 and in the Materials and Methods. Cells grown on 96-well plates were sham or UVA-irradiated and re-incubated and assayed for 4 h following irradiation for LDH (A) and MTT (B). The control value was set at 1 and 100 for A and B, respectively. Values are means \pm S.E. ($n = 4$). *, $p < 0.05$ vs. relevant sample. V, vehicle control; Sb, scrambled control; +, 10 nM siRNA; ++, 50 nM siRNA.

cells against oxidative stress, which includes UVA irradiation-induced damage (10,11). A moderate to high dose ($400 \text{ kJ}\cdot\text{m}^{-2}$) of UVA irradiation slightly increased Nrf2 protein levels, although not significantly, and immunostaining also revealed that Nrf2 accumulated only slightly in the nucleus following this dose of UVA irradiation, the same as happens at $250 \text{ kJ}\cdot\text{m}^{-2}$ (14) and $500 \text{ kJ}\cdot\text{m}^{-2}$ (data not shown). The current results are supported by those of Durchdewald's study that observed no activation of Nrf2 following a low to moderate dose of UVA radiation (15). Further, cells sensitized to Nrf2 suffered more UVA irradiation-mediated cell damage, as demonstrated by a decrease in cell viability and increase in the release of LDH. This supports the notion that Nrf2 plays a role in protecting both skin keratinocytes and fibroblasts from exposure to UVA irradiation (10,11).

Skin is a major target of exposure to UVA irradiation and the chronic toxic and carcinogenic effects of different substances. Oxidative damage plays a role in many age-related chronic degenerative diseases like aging of the skin, which is induced by UVA irradiation, so further understanding of the protection offered by Nrf2 expression may provide clues to new modalities

for *in vivo* skin protection and prevention of skin disorders (7). A decline in Nrf2 function also sensitizes cells to oxidative stress during aging; increased Nrf2 levels are noted in the cells of long-lived mice and high Nrf2 levels protect these cells against oxidant-induced damage (7,16-20). Liu demonstrated that Nrf2 levels increased by the suppression of Keap1 can therefore protect human keratinocytes against UVA-induced damage (21). Although the mechanisms underlying Nrf2 protection of skin cells must be evaluated further, there is evidence that it may protect skin keratinocytes from damage to the cell membrane caused by UVA irradiation by maintaining membrane integrity and enhancing cell survival (12).

In summary, the current study has provided the evidence that Nrf2 protects skin keratinocytes from damage caused by UVA irradiation. Since epidermal keratinocytes are constantly exposed to UVA irradiation, activation of Nrf2 may prove to be critical to the effective protection of human skin cells. Increased Nrf2 levels may be a desirable action of skin care supplements or sun protection products.

Acknowledgements

This work was supported by the Natural Science Foundation of Chongqing (CSTC, 2009BB5044), the Key Program of International Cooperation in Science and Technology of Chongqing (2009AA5045), and the National Natural Science Foundation of China (11032012). The authors wish to thank Dr. Rex Tyrrell (University of Bath, UK) and Dr. Joerg Bartsch (King's College London) for their valuable comments.

References

1. Tyrrell RM. Solar ultraviolet radiation: An oxidizing skin carcinogen that activates heme oxygenase-1. *Antioxid Redox Signal*. 2004; 6:835-840.
2. Young AR. Acute effects of UVR on human eyes and skin. *Prog Biophys Mol Biol*. 2006; 92:80-85.
3. Svobodova A, Walterova D, Vostalova J. Ultraviolet light induced alteration to skin. *Biomed Pap Med Fac Univ Palacky Olomouc Czech Repub*. 2006; 150:25-38.
4. Pourzand C, Watkin RD, Brown JE, Tyrrell RM. Ultraviolet A radiation induces immediate release of iron in human primary skin fibroblasts: The role of ferritin. *Proc Natl Acad Sci U S A*. 1999; 96:6751-6756.
5. MacLeod AK, McMahon M, Plummer SM, Higgins LG, Penning TM, Igarashi K, Hayes JD. Characterization of the cancer chemopreventive NRF2- dependent gene battery in human keratinocytes: Demonstration that the KEAP1-NRF2 pathway, and not the BACH1-NRF2 pathway, controls cytoprotection against electrophiles as well as redox-cycling compounds. *Carcinogenesis*. 2009; 30:1571-1580.
6. Itoh K, Mimura, J Yamamoto M. Discovery of the negative regulator of Nrf2, Keap1: A historical overview. *Antioxid Redox Signal*. 2010; 13:1665-1678.

7. Sykietis GP, Bohmann D. Stress-activated cap'n'collar transcription factors in aging and human disease. *Sci Signal*. 2010; 3:112-116.
8. Braun S, Hanselmann C, Gassmann MG, auf dem Keller U, Born-Berclaz C, Chan K, Kan YW, Werner S. Nrf2 transcription factor, a novel target of keratinocyte growth factor action which regulates gene expression and inflammation in the healing skin wound. *Mol Cell Biol*. 2002; 22:5492-5505.
9. Hirota A, Kawachi Y, Itoh K, Nakamura Y, Xu X, Banno T, Takahashi T, Yamamoto M, Otsuka F. Ultraviolet A irradiation induces NF-E2-related factor 2 activation in dermal fibroblasts: Protective role in UVA-induced apoptosis. *J Invest Dermatol*. 2005; 124:825-832.
10. Zhong JL, Edwards GP, Raval C, Li H, Tyrrell RM. The role of Nrf2 in ultraviolet A mediated heme oxygenase 1 induction in human skin fibroblasts. *Photochem Photobiol Sci*. 2010; 9:18-24.
11. Kimura S, Warabi E, Yanagawa T, Ma D, Itoh K, Ishii Y, Kawachi Y, Ishii T. Essential role of Nrf2 in keratinocyte protection from UVA by quercetin. *Biochem Biophys Res Commun*. 2009; 387:109-114.
12. Applegate LA, Noël A, Vile G, Frenk E, Tyrrell RM. Two genes contribute to different extents to the heme oxygenase enzyme activity measured in cultured human skin fibroblasts and keratinocytes: Implications for protection against oxidant stress. *Photochem Photobiol*. 1995; 61:285-291.
13. Zhong JL, Yiakouvakis A, Holley P, Tyrrell RM, Pourzand C. Susceptibility of skin cells to UVA-induced necrotic cell death reflects the intracellular level of labile iron. *J Invest Dermatol*. 2004; 123:771-780.
14. Zhong JL, Raval C, Edwards GP, Tyrrell RM. A role of Bach1 and HO-2 in suppression of basal and UVA-induced HO-1 expression in human skin keratinocytes. *Free Radic Biol Med*. 2010; 48:196-206.
15. Durchdewald M, Beyer TA, Johnson DA, Johnson JA, Werner S, auf dem Keller U. Electrophilic chemicals but not UV irradiation or reactive oxygen species activate Nrf2 in keratinocytes *in vitro* and *in vivo*. *J Invest Dermatol*. 2007; 127:646-653.
16. Nguyen T, Nioi P, Pickett CB. The Nrf2-antioxidant response element signaling pathway and its activation by oxidative stress. *J Biol Chem*. 2009; 284:13291-13295.
17. Taguchi K, Maher JM, Suzuki T, Kawatani Y, Motohashi H, Yamamoto M. Genetic analysis of cytoprotective functions supported by graded expression of Keap1. *Mol Cell Biol*. 2010; 30:3016-3026.
18. Gruber F, Mayer H, Lengauer B, Mlitz V, Sanders JM, Kadl A, Bilban M, de Martin R, Wagner O, Kensler TW, Yamamoto M, Leitinger N, Tschachler E. NF-E2-related factor 2 regulates the stress response to UVA-1-oxidized phospholipids in skin cells. *FASEB J*. 2010; 24:39-48.
19. Leiser SF, Miller RA. Nrf2 signaling, a mechanism for cellular stress resistance in long-lived mice. *Mol Cell Biol*. 2010; 30:871-884.
20. Yin F, Liu J, Zheng X, Guo L, Xiao H. Geniposide induces the expression of heme oxygenase-1 *via* PI3K/Nrf2-Signaling to enhance the antioxidant capacity in primary hippocampal neurons. *Biol Pharm Bull*. 2010; 33:1841-1846.
21. Liu Y, Chan F, Sun H, Yan J, Fan D, Zhao D, An J, Zhou D. Resveratrol protects human keratinocytes HaCaT cells from UVA-induced oxidative stress damage by downregulating Keap1 expression. *Eur J Pharmacol*. 2011; 650:130-137.

(Received January 14, 2011; Accepted February 5, 2011)

Influence of glutathione levels and activity of glutathione-related enzymes in the brains of tumor-bearing mice

Kaikai Shen¹, Lili Ji^{1,2,*}, Ying Chen¹, Qianming Yu¹, Zhengtao Wang^{1,2,*}

¹The MOE Key Laboratory for Standardization of Chinese Medicines and the SATCM Key Laboratory for New Resources and Quality Evaluation of Chinese Medicines, Institute of Chinese Materia Medica, Shanghai University of Traditional Chinese Medicine, Shanghai, China;

²Shanghai R&D Centre for Standardization of Chinese Medicines, Shanghai, China.

Summary

Oxidative stress takes place due to an imbalance between the production of reactive oxygen species (ROS) and the protection provided by cellular antioxidants. High levels of ROS are caused by tumor cells during tumor progression and may affect the functions of other important organs. The present study sought to investigate whether non-primary brain tumors affect reduced glutathione (GSH) levels and the activity of related enzymes in the brain. GSH contents, the activity of glutathione peroxidase (GPx), glutathione-*s*-transferase (GST), glutathione reductase (GR) as well as glutamate cysteine ligase (GCL) were determined in the brains of normal and tumor-bearing mice treated with the chemotherapy drug 5-Fluorouracil (5-Fu) or not. The results in S180 and H22 tumor-bearing mice showed that GSH levels and the activity of GPx, GST, and GCL all decreased while GR activity markedly increased in the brains of tumor-bearing mice compared to those of normal mice. Further investigation found that 5-Fu, a typical chemotherapy drug, significantly inhibited tumor growth but did not improve the loss of redox homeostasis in the brain caused by non-primary brain tumors. Overall, these results suggest that non-primary brain tumors can induce an ROS burden in the brain that cannot be reversed by the chemotherapy drug 5-Fu.

Keywords: Tumor, brain, reduced glutathione, glutathione peroxidase (GPx), glutathione-*s*-transferase (GST), glutathione reductase (GR), glutamate cysteine ligase (GCL)

1. Introduction

Oxidative stress takes place due to the disturbance of the balance between the formation of reactive oxygen species (ROS) and the defense provided by cellular antioxidants (1). Reduced glutathione (GSH), ubiquitously distributed in all mammalian cells, is a reducing sulfhydryl (-SH) tripeptide and plays important roles in the endogenous antioxidant system because it conjugates toxic substances (2). Intracellular GSH and

its related enzymes, such as glutathione peroxidase (GPx), glutathione-*s*-transferase (GST), glutathione reductase (GR), and glutamate cysteine ligase (GCL), constitute the cellular glutathione antioxidant system and represent a crucial defensive system to protect cells against ROS.

The presence of tumors in the human body or in experimental animals is known to affect various functions of vital organs even when the site of the tumor is not close to the organ (3). There are two characteristics of tumor cells compared to normal cells: one is the increased generation of ROS and the other is the decreased capacity to eliminate ROS, leading to damage to other normal tissues (4). The GSH concentration in the brain is lower than that in the liver, kidney, spleen, and small intestine. Furthermore, there is a large concentration of unsaturated lipids and a high rate of oxidative metabolism in the brain (5,6), so the brain is especially vulnerable to oxidative stress injury compared to other organs (7). However, whether or not a high level of ROS caused by the progression of a non-

*Address correspondence to:

Dr. Lili Ji and Zhengtao Wang, The MOE Key Laboratory for Standardization of Chinese Medicines and the SATCM Key Laboratory for New Resources and Quality Evaluation of Chinese Medicines, Institute of Chinese Materia Medica, Shanghai University of Traditional Chinese Medicine, 1200 Cailun Road, Shanghai 201210, China
e-mail: lily0913@yahoo.cn; wangzht@hotmail.com

primary brain tumor affects the glutathione antioxidant system in the brain remains unclear.

Since brain tissue cannot be obtained from cancer patients with non-primary brain tumors, a mice model with clinical features was established to investigate whether non-primary brain tumors affect GSH levels and the activity of GSH-related enzymes in the brain. The present study sought to compare GSH levels and the activity of GSH-related enzymes in the brains of a control group and model and 5-Fluorouracil (5-Fu) groups using mouse models of transplanted S180 and H22 tumors.

2. Materials and Methods

2.1. Experimental animals

Specific pathogen-free male ICR mice (6-8 weeks age) from the Chinese Academy of Science were housed in plastic cages, kept on a light-dark rhythm of 12 h-12 h at a constant temperature ($22 \pm 1^\circ\text{C}$) and humidity ($65 \pm 5\%$), and allowed free access to water and a standard diet during the experiment. Animal handling procedures were carried out in accordance with Chinese state legislation on the use and care of laboratory animals and this study was approved by the Experimental Animal Ethical Committee of the Shanghai University of Traditional Chinese Medicine. All efforts were made to minimize animals' suffering and to reduce the number of animals used.

2.2. Experimental mice protocol

Thirty ICR male mice were randomly divided into three groups, with each group consisting of 10 mice. One group was the control group, one was a model group (untreated), and one was a 5-Fu group (treated). Each mouse was subcutaneously injected in the right axilla with S180 or H22 ascites tumor cells (approximately 2×10^6 cells/mouse) except the control group. Twenty-four hours after implantation, the 5-Fu group served as the treatment group and was intraperitoneally administered a 5-Fu dose of 25 mg/kg/2d a total of five times. The control and model groups were treated with the same volume of normal saline. Fourteen days after implantation, the animals were sacrificed. Tumor tissue was totally excised from the animal and accurately weighted. Meanwhile, the brain was excised from the animal and stored at -80°C . The tumor inhibition ratio (%) = $[(A-B)/A] \times 100$, where A is the average tumor weight for the model group and B is that for the 5-Fu group.

2.3. Measurement of GSH content

Brain homogenates were prepared in a cold phosphate buffer, pH 7.0, containing 1mM EDTA and 5% metaphosphoric acid, sonicated twice at 4°C , and then

centrifuged at 10,000 g at 4°C for 10min. The GSH contents in the brain homogenate were determined in accordance with a reported method (8) with minor modifications. The reaction mixture contained 1mM EDTA, NADPH (0.24 mM), glutathione reductase (0.06 Units), DTNB (86 μM), and the sample. Yellow 5-thio-2-nitrobenzoic acid (TNB) formation was monitored at 412 nm. GSSG was determined after elimination of GSH with 2-vinylpyridine. The levels of GSH were calculated from the difference between concentrations of total glutathione (GSH + GSSG) and GSSG. Values are expressed as mM/g protein of brain tissue homogenates used.

2.4. Measurement of GPx enzymatic activity

Brain homogenates were prepared in ice-cold PBS (pH 7.0), sonicated twice at 4°C , and then centrifuged at 4°C , 3,000 g for 5 min. The supernatant was transferred to new tubes for GPx enzymatic activity assay. GPx activity was determined from brain tissue homogenate in accordance with a previously reported method (9) with minor modifications. The enzymatic activity of GPx was expressed as Unit/mg protein, where 1 Unit of GPx activity was defined as 1 μM GSH depleted per minute.

2.5. Measurement of GST enzymatic activity

Brain homogenates were prepared in ice-cold PBS (pH 7.0), sonicated twice at 4°C , and then centrifuged at 4°C , 3,000 g for 5 min. The supernatant was transferred to new tubes for GST enzymatic activity assay. GST activity was measured from brain tissue homogenate in accordance with a previously reported method (10) with minor modifications. The enzymatic activity of GST was expressed as Unit/mg protein, where 1 Unit of GST activity was defined as 1 μM GSH depleted per minute.

2.6. Measurement of GR enzymatic activity

Brain homogenates were prepared in ice-cold PBS (pH 7.0), sonicated twice at 4°C , and then centrifuged at 4°C , 3,000 g for 5 min. The supernatant was transferred to new tubes for GR enzymatic activity assay. GR activity from brain tissue homogenate was assayed in accordance with a reported method (11) with minor modifications. The enzymatic activity of GR was expressed as mUnit/mg protein, where 1 Unit of GR activity was defined as 1 mM GSSG catalyzed per minute.

2.7. Measurement of GCL enzymatic activity

Brain homogenates were prepared in ice-cold PBS (pH 7.0), sonicated twice at 4°C , and then centrifuged

at 4°C, 10,000 g for 5 min. The supernatant was transferred to new tubes for GCL enzymatic activity assay. GCL activity was assayed in accordance with a previously reported method (12). The enzymatic activity of GCL was expressed as Unit/min/mg protein, where 1 Unit of GCL activity was equal to the amount of enzyme that oxidized the reduction of 1 mM NADPH per minute.

2.8. Statistical analysis

Data from all experiments are expressed as means \pm S.E.M. Statistical comparisons were subjected to an analysis of variance (ANOVA) and LSD-test using SPSS version 11.5, and $p < 0.05$ was considered a statistically significant difference. All statistical analyses were performed using SigmaPlot version 10.0 software.

3. Results

3.1. Comparison of GSH levels in the brains of non-tumor-bearing mice and tumor-bearing mice treated with 5-Fu and not treated with 5-Fu

The results in Figure 1A show that administration

of 5-Fu significantly inhibited tumor growth in S180 tumor-bearing mice; the ratio of tumor growth inhibition was 81.9%. Similar results were observed in H22 tumor-bearing mice as shown in Figure 1B. The current results are consistent with those of previous studies indicating that 5-Fu markedly inhibited tumor growth (13,14).

GSH is a ubiquitously distributed antioxidant that can exacerbate exogenous toxic injury, enhance defense against oxygen free radicals, and regulate immune function (15). GSH levels in the brains of S180 tumor-bearing mice treated with 5-Fu or not and normal mice were investigated. As shown in Figure 2A, the GSH levels in the brains of the model group declined significantly compared to levels in the control group ($p < 0.01$). Meanwhile, the average brain GSH levels of the 5-Fu-treated group increased slightly but not significantly so compared to levels in the model group. Similar results with regard to the changes in GSH levels in the brains of different groups were also observed in H22 tumor-bearing mice, as shown in Figure 2B. The results of Figures 1 and 2 indicate that GSH levels decreased in the brains of mice bearing non-primary brain tumors. The chemotherapy drug 5-Fu significantly inhibited tumor growth but it did not improve GSH levels in the brain.

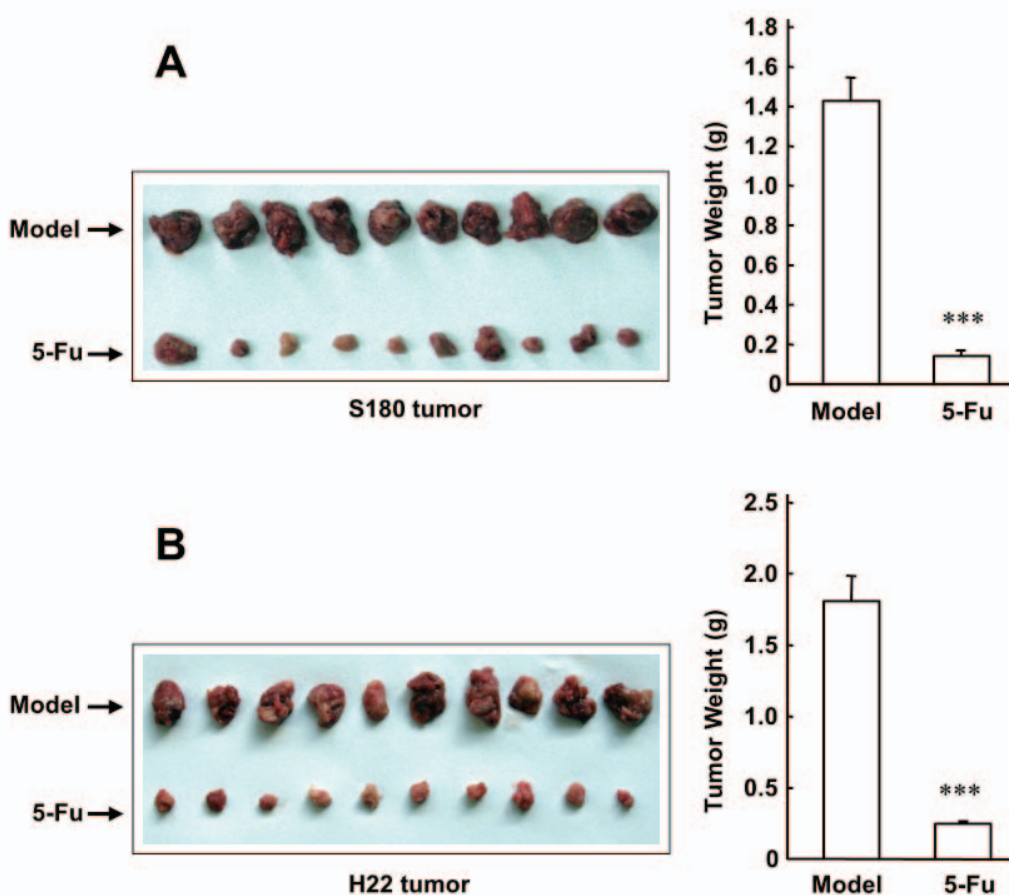


Figure 1. Decreased tumor area in S180 and H22 tumor-bearing mice treated with 5-Fu. (A) S180 tumor-bearing ICR mice; (B) H22 tumor-bearing ICR mice. ***, $p < 0.001$ vs. the model group.

3.2. Changes in GPx and GST activity in the brains of non-tumor-bearing mice and treated and untreated tumor-bearing mice

Previous studies have reported that GSH plays important roles in two forms of chemical detoxification and anti-oxidative defense: one is the inactivation of

ROS either via direct GSH-ROS interaction or via catalysis through GPx, and the other is the accelerated excretion of less toxic GSH-xenobiotic conjugates via GST (16,17). GPx and GST activity in the brains of S180 tumor-bearing mice treated with 5-Fu or not and normal mice was further investigated. As shown in Figure 3A, in S180 tumor-bearing mice GPx activity

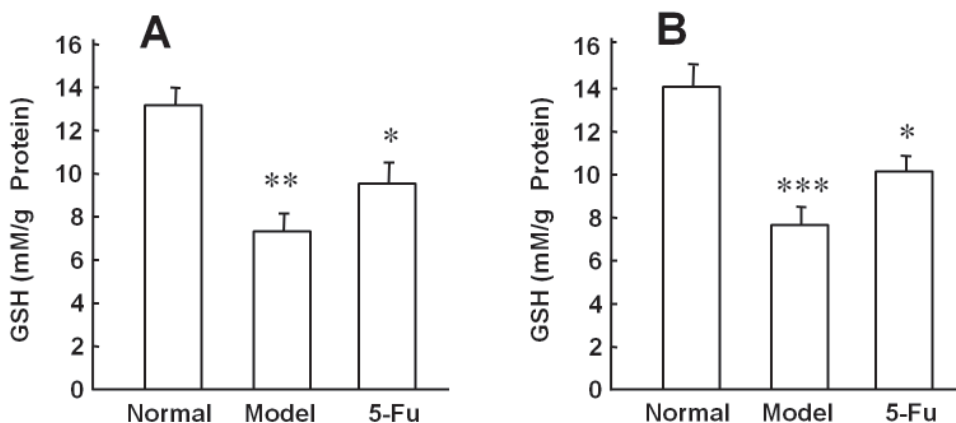


Figure 2. GSH levels in the brain tissues of each group. (A) GSH levels in brains of S180 tumor-bearing mice; (B) GSH levels in brains of H22 tumor-bearing mice. *, $p < 0.05$; **, $p < 0.01$; ***, $p < 0.001$ vs. the control group.

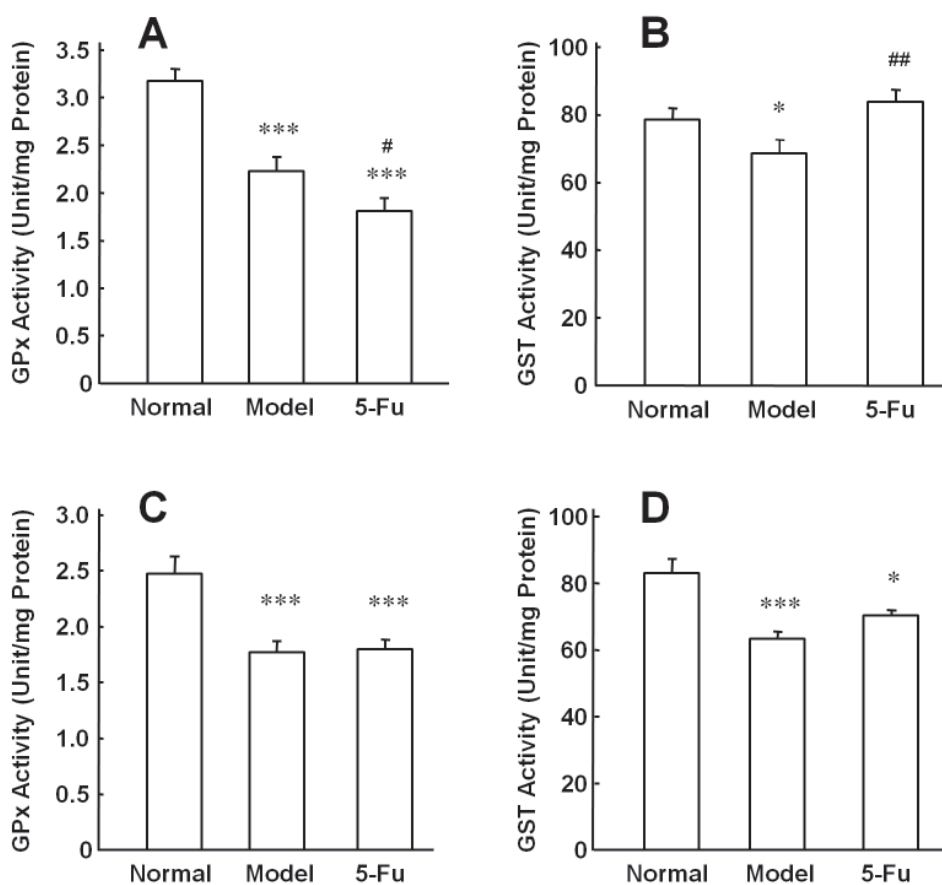


Figure 3. GPx and GST activity in the brain tissues of each group. (A) GPx activity in brains of S180 tumor-bearing mice; (B) GST activity in brains of S180 tumor-bearing mice; (C) GPx activity in brains of H22 tumor-bearing mice; (D) GST activity in brains of H22 tumor-bearing mice. *, $p < 0.05$; ***, $p < 0.001$ vs. the control group. #, $p < 0.05$; ##, $p < 0.01$ vs. the model group.

in the brain decreased significantly in the model group compared to the control group (2.23 Unit/mg protein vs. 3.18 Unit/mg protein, $p < 0.001$). Moreover, the GPx activity in the 5-Fu group was even lower than that in the model group (1.81 Unit/mg protein vs. 2.23 Unit/mg protein, $p < 0.05$). Further, results for H22 tumor-bearing mice (Figure 3C) showed that the model group had GPx activity of 1.77 Unit/mg protein while the 5-Fu-treated group had activity of 1.80 Unit/mg protein; there were no significant differences between the two. GPx activity in the brains of the model group and 5-Fu-treated group was lower than that in the control group, which had activity of 2.47 Unit/mg protein ($p < 0.001$). As shown in Figure 3B, in S180 tumor-bearing mice the GST activity in the brains of the model group declined significantly compared to activity in the control group ($p < 0.05$). Further, the decreased GST activity in tumor-bearing mice was reversed by 5-Fu to a level higher than that in the model group ($p < 0.01$). Similar data were obtained from H22 tumor-bearing mice except for GST activity, which increased little in the 5-Fu-treated group compared to the model group ($p \geq 0.05$) (Figure 3D).

3.3. Changes in GCL and GR activity in the brains of non-tumor-bearing mice and treated and untreated tumor-bearing mice

In order to identify the possible reasons for the change in GSH levels, the activity of GR and GCL, which are both main enzymes involved in the synthesis and regeneration of GSH, was measured. GR enzymatic activity was investigated in three groups of mice, *i.e.*, those bearing S180 tumors and administered 5-Fu, those bearing S180 tumors and not administered 5-Fu, and normal mice. The results shown in Figure 4A indicate that GR activity increased slightly in the brains of the model group in comparison to the control group ($p \geq 0.05$). Moreover, GR activity in the brains of the 5-Fu-treated group was much greater than that in brains of the control group ($p < 0.01$). Similarly, results for H22 tumor-bearing mice as shown in Figure 4C indicate that the activity of GR in the brains of mice treated with 5-Fu and mice not treated with 5-Fu was significantly greater than that in the control group, which had activity of 8.87 mUnit/mg protein ($p < 0.01$). Levels of GCL activity in the three groups were also investigated. As shown in

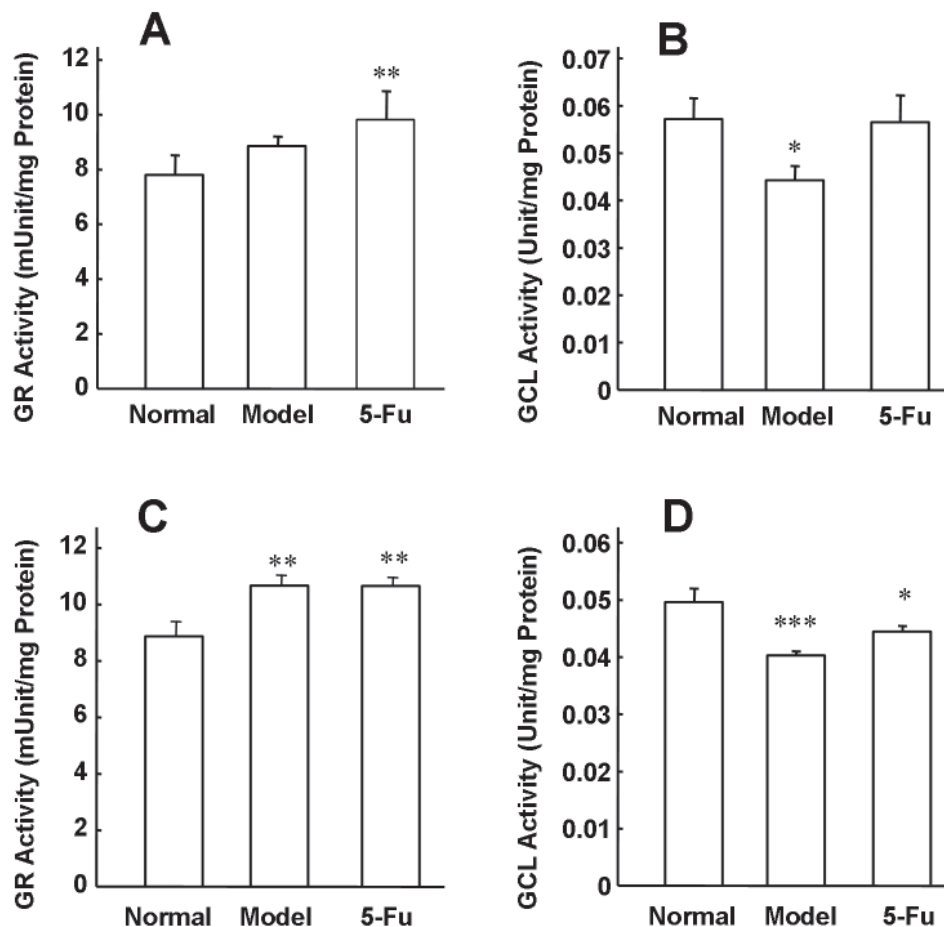


Figure 4. GR and GCL activity in the brain tissues of each group. (A) GR activity in brains of S180 tumor-bearing mice; (B) GCL activity in brains of S180 tumor-bearing mice; (C) GR activity in brains of H22 tumor-bearing mice; (D) GCL activity in brains of H22 tumor-bearing mice. *, $p < 0.05$; **, $p < 0.01$; ***, $p < 0.001$ vs. the control group.

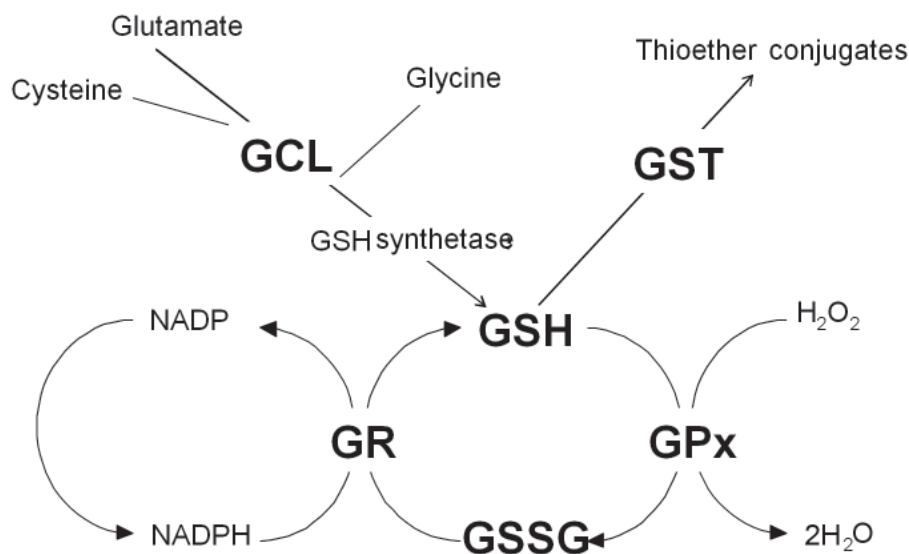


Figure 5. The whole GSH antioxidant system, including GSH, GPx, GST, GR, and GCL, is shown here.

Figure 4B, GCL activity in the brains of S180 tumor-bearing mice decreased slightly compared to that in the model group ($p < 0.05$). In addition, decreased GCL activity was slightly reversed by administration of 5-Fu ($p \geq 0.05$) and almost rose to the level in the control group. Similar results as shown in Figure 4D were also obtained for H22 tumor-bearing mice. Although GCL activity in the brains of the 5-Fu-treated group increased slightly in comparison to the model group, it was still lower than the level in the control group ($p < 0.05$).

4. Discussion

Tumors severely affect human health, and their incidence and mortality rates are increasing worldwide. 5-Fu is a typical chemotherapy drug for nonhematologic malignancies that is widely used in the treatment of a range of cancers (18,19). The present study selected 5-Fu since previous studies have used it to treat cancer (13,14). Xenografted S180 and H22 cells are typically both chosen when creating *in vivo* tumor models (20,21). In this regard, the present study used S180 and H22 ascites tumor cells subcutaneously injected into the right axilla of ICR mice to create a tumor model *in vivo*. The current results showed that 5-FU clearly inhibited S180 and H22 tumor growth.

Cancer cells can produce large amounts of reactive oxygen intermediates such as hydrogen peroxide that may injure surrounding healthy tissue and therefore promote tumor growth and invasion (4). Of the main organs in mammals, the brain is particularly susceptible to ROS damage due to its richness in polyunsaturated fatty acids (22-24). The whole GSH antioxidant system is shown in Figure 5, and GSH and its related enzymes

such as GPx, GST, GCL, and GR are the major components involved in this system. GSH, as a major antioxidant with a high concentration of approximately 2-3 mM, plays a crucial protective role in protecting the brain against ROS (6). The present study found that GSH levels in the brain clearly decreased in tumor-bearing mice but slightly increased in the brain with 5-Fu treatment, although the levels were still lower than those in the control group. These results demonstrate that non-primary brain tumors significantly decreased GSH levels in the brain and these decreased levels were not reversed by 5-Fu.

Cytosolic GPx is an enzyme containing four selenium-cofactors that protects tissues from damage by catalyzing the breakdown of hydrogen peroxide and organic hydroperoxides (25). The current results showed that brain GPx activity largely decreased in tumor-bearing mice compared to non-tumor-bearing mice, and this decrease was not reversed by administration of 5-Fu. In combination with the results of GSH analysis, results suggest that 5-Fu inhibited tumor growth but did not improve redox homeostasis. GST is a member of a family of detoxification enzymes that metabolizes a variety of carcinogens by conjugating GSH to a wide variety of xenobiotics, which can then be excreted out through thioether formation (26). In the present study, brain GST activity declined markedly in tumor-bearing mice compared to non-tumor-bearing mice. As mentioned above, these results suggest that non-primary brain tumors decrease the detoxification activity of xenobiotic and endobiotic compounds in the brains of tumor-bearing mice. Furthermore, decreased GST activity in tumor-bearing mice was reversed by administering 5-Fu, which indicates that 5-Fu may

increase the detoxification activity of GST in the brains of tumor-bearing mice. Previous studies have reported that increased GST activity is closely related to the resistance of tumor cells to cancer drugs used in cancer studies over the past three decades (27,28). In this regard, the current results indicate that GST activity increased by 5-Fu may enhance the resistance of tumor cells to chemotherapy drugs.

There are two major pathways involved in regulating cellular GSH contents: one is GR, which catalyzes the reduction of GSSG to GSH *via* consumption of NADPH (11); the other is GCL, which is the rate-limiting enzyme in GSH synthesis (29). The present study found that GR activity was highly elevated in treated and untreated tumor-bearing mice compared to the control group. Increased GR activity may conceivably be due to the body's self-feedback regulation. Results also indicated a marked decrease in GCL activity, and this may augment the depletion of GSH in the brains of tumor-bearing mice. Results also showed that 5-Fu slightly reversed this decline, indicating that 5-Fu may slightly increase GCL activity.

There are reports that oxidative stress is implicated in the pathogenesis of a broad range of neuropathological conditions, including ischemia, Alzheimer's disease (AD), Parkinson's disease (PD), multiple sclerosis, stroke, and seizure disorders (30-34). Additionally, oxidative stress injury caused by ROS seems to be closely related to the loss of neurons during stroke and neurodegenerative diseases, thereby increasing the ROS burden and consequently reducing antioxidant capacity (35). The present study found that non-primary brain tumors reduced antioxidant capacity and led to the loss of redox homeostasis in the brain. Excessive free radicals are capable of precipitating brain dysfunction. Although 5-Fu is, as a typical chemotherapy drug, able to inhibit tumor growth, it cannot, however, improve redox homeostasis and even increases the ROS burden in the brain.

Taken together, the current results are the first to show that non-brain primary tumors affect GSH levels and the activity of glutathione-related enzymes in the brain. This study also emphasizes the need for caution when choosing clinical agents for cancer treatment particularly for patients with a brain dysfunction. Further research on the exact mechanism through which how non-primary brain tumors increase the ROS burden in the brain is needed.

Acknowledgements

This project was financially supported by the National Natural Science Foundation of China (No. 30801544), the National Basic Research Program Foundation of China (No. 2006CB504704), and the Innovation

Program of the Shanghai Municipal Education Commission (No. 09ZZ125).

References

1. Schafer FQ, Buettner GR. Redox environment of the cell as viewed through the redox state of the glutathione disulfide/glutathione couple. *Free Radic Biol Med.* 2001; 30:1191-1212.
2. Winterbourn CC, Metodiewa D. The reaction of superoxide with reduced glutathione. *Arch Biochem Biophys.* 1994; 314:284-290.
3. DeWys WD. Pathophysiology of cancer cachexia: Current understanding and areas for future research. *Cancer Res.* 1982; 42:721s-726s.
4. Szatrowski TP, Nathan CF. Production of large amounts of hydrogen peroxide by human tumor cells. *Cancer Res.* 1991; 51:794-798.
5. Commandeur JN, Stijntjes GJ, Vermeulen NP. Enzymes and transport systems involved in the formation and disposition of glutathione-S-conjugates. Role in bioactivation and detoxication mechanisms of xenobiotics. *Pharmacol Rev.* 1995; 47:271-330.
6. Dringen R. Metabolism and functions of glutathione in brain. *Prog Neurobiol.* 2000; 62:649-671.
7. Aovama K, Watabe M, Nakaki T. Regulation of neuronal glutathione synthesis. *J Pharmacol Sci.* 2008; 108:227-238.
8. Sies H, Akerboom TP. Glutathione disulfide (GSSG) efflux from cells and tissues. *Methods Enzymol.* 1984; 105:445-451.
9. Rotruck JT, Pope AL, Ganther HE, Swanson AB, Hafeman DG, Hoekstra WG. Selenium: Biochemical role as a component of glutathione peroxidase. *Science.* 1973; 179:588-590.
10. Habig WH, Pabst MJ, Jakoby WB. Glutathione S-transferases. The first enzymatic step in mercapturic acid formation. *J Biol Chem.* 1974; 249:7130-7139.
11. Carlberg I, Mannervik B. Glutathione reductase. *Methods Enzymol.* 1985; 113:484-490.
12. Zheng S, Yumei F, Chen A. *De novo* synthesis of glutathione is a prerequisite for curcumin to inhibit hepatic stellate cell (HSC) activation. *Free Radic Biol Med.* 2007; 43:444-453.
13. Li XJ, Mao YX, Zhang HL, Wang JX, Liu FY. Study on effects of anticancer and immunoregulation of Fuganchun 6 on hepatoma of mouse. *Zhongguo Zhong Yao Za Zhi.* 2006; 31:1622-1625. (in Chinese)
14. Yu ZH, Wei PK, Xu L, Qin ZF, Shi J. Anticancer effect of jinlongshe granules on in situ-transplanted human MKN-45 gastric cancer in nude mice and xenografted sarcoma 180 in Kunming mice and its mechanism. *World J Gastroenterol.* 2006; 12:2890-2894.
15. DeLeve LD, Kaplowitz N. Glutathione metabolism and its role in hepatotoxicity. *Pharmacol Ther.* 1991; 52:287-305.
16. Lei XG. *In vivo* antioxidant role of glutathione peroxidase: Evidence from knockout mice. *Methods Enzymol.* 2002; 347:213-225.
17. Strange RC, Spiteri MA, Ramachandran S, Fryer A. Glutathione-S-transferase family of enzymes. *Mutat Res.* 2001; 482:21-26.
18. Longlev DB, Harkin DP, Johnston PG. 5-fluorouracil: Mechanisms of action and clinical strategies. *Nat Rev*

- Cancer. 2003; 3:330-338.
19. Muqgia FM, Peters GJ, Landolph JR Jr. XIII International Charles Heidelberger Symposium and 50 Years of fluoropyrimidines in cancer therapy held on September 6 to 8, 2007 at New York University Cancer Institute, Smilow Conference Center. *Mol Cancer Ther.* 2009; 8:992-999.
 20. Wang XB, Liu QH, Wang P, Zhang K, Tang W, Wang BL. Enhancement of apoptosis by sonodynamic therapy with protoporphyrin IX in isolate sarcoma 180 cells. *Cancer Biother Radiopharm.* 2008; 23:238-246.
 21. Yuan F, Zhang ZR, Yang YX, Huang Y. *In vitro* release study, *in vivo* evaluation of biodistribution and antitumor activity of HPMA copolymer-5-fluorouracil conjugates. *Yao Xue Xue Bao.* 2008; 43:1152-1156. (in Chinese)
 22. Choi BH. Oxygen, antioxidants and brain dysfunction. *Yonsei Med J.* 1993; 34:1-10.
 23. Halliwell B. Role of free radicals in the neurodegenerative diseases: Therapeutic implications for antioxidant treatment. *Drugs Aging.* 2001; 18:685-716.
 24. Olanow CW. A radical hypothesis for neurodegeneration. *Trends Neurosci.* 1993; 16: 439-444.
 25. Briquelius-Flohe R, Kipp A. Glutathione peroxidases in different stages of carcinogenesis. *Biochim Biophys Acta.* 2009; 1790:1555-1568.
 26. Dourado DF, Fernandes PA, Ramos MJ. Mammalian cytosolic glutathione transferases. *Curr Protein Pept Sci.* 2008; 9:325-337.
 27. McIlwain CC, Townsend DM, Tew KD. Glutathione *s*-transferase polymorphisms: Cancer incidence and therapy. *Oncogene.* 2006; 25:1639-1648.
 28. Ricci G, Caccuri AM, Lo Bello M, Parker MW, Nuccetelli M, Turella P, Stella L, Di Iorio EE, Federici G. Glutathione transferase P1-1: Self-preservation of an anti-cancer enzyme. *Biochem J.* 2003; 376(Pt 1):71-76.
 29. Griffith OW. Biologic and pharmacologic regulation of mammalian glutathione synthesis. *Free Radic Biol Med.* 1999; 27: 922-935.
 30. Banheqvi G, Mandl J, Csala M. Redox-based endoplasmic reticulum dysfunction in neurological diseases. *J Neurochem.* 2008; 107:20-34.
 31. Devi PU, Manocha A, Vohora D. Seizures, antiepileptics, antioxidants and oxidative stress: An insight for researchers. *Expert Opin Pharmacother.* 2008; 9:3169-3177.
 32. Kaur C, Ling EA. Antioxidants and neuroprotection in the adult and developing central nervous system. *Curr Med Chem.* 2008; 15:3068-3080.
 33. Maier CM, Chan PH. Role of superoxide dismutases in oxidative damage and neurodegenerative disorders. *Neuroscientist.* 2002; 8:323-334.
 34. Napoli C, Palinski W. Neurodegenerative diseases: Insights into pathogenic mechanisms from atherosclerosis. *Neurobiol Aging.* 2005; 26:293-302.
 35. Hyslop PA, Zhang Z, Pearson DV, Phebus LA. Measurement of striatal H₂O₂ by microdialysis following global forebrain ischemia and reperfusion in the rat: Correlation with the cytotoxic potential of H₂O₂ *in vitro*. *Brain Res.* 1995; 671:181-186.

(Received December 12, 2010; Revised January 6, 2011; Accepted February 17, 2011)

Environmental lead exposure as a risk for childhood aplastic anemia

Maqsood Ahamed^{1,*}, Mohd Javed Akhtar¹, Sanjeev Verma², Archana Kumar², Mohammad K.J. Siddiqui³

¹ Indian Institute of Toxicology Research, Lucknow, India;

² Chhatrapati Shahuji Maharaj Medical University, Lucknow, India;

³ Council of Science and Technology-UP, Lucknow, India.

Summary

Concern about environmental lead exposure as a significant public health threat has increased as evidence has accumulated regarding adverse health effects at successively lower levels. Aplastic anemia is a hematological disorder of unknown etiology with a high lethality rate. Lead is a known toxicant for the hematopoietic system. Oxidative stress appears to be the possible mode of lead toxicity. We evaluated the effects of blood lead level on oxidative stress parameters in children suffering from aplastic anemia disease. Seventeen children with aplastic anemia disease (15 male and 2 female, age 3-12 y) were recruited in the study group. Fifty one healthy children (45 male and 6 female, age 3-12 y) having normal blood profiles and not suffering from any chronic disease(s) were used as controls. Blood lead level and oxidative stress parameters were determined. Mean blood lead level was significantly higher while δ -aminolevulinic acid dehydratase (δ -ALAD) activity, a biomarker for lead exposure was significantly lower in the study group as compared to the control group ($p < 0.05$ for each). Thiobarbituric acid reactive species (TBARS), a marker of lipid peroxidation, was significantly higher while the antioxidant glutathione (GSH) level was significantly lower in the study group as compared to the control group ($p < 0.05$ for each). Activity of the antioxidant enzyme catalase (CAT) was significantly higher in the study group than in the control group ($p < 0.05$). There was a significant negative correlation of blood lead levels with δ -ALAD ($r = -0.45$; $p < 0.05$) and GSH ($r = -0.32$; $p < 0.05$), and a positive correlation with TBARS ($r = 0.41$; $p < 0.05$) and CAT ($r = 0.37$; $p < 0.05$). Although a causal pathway cannot be determined from this study, our results indicated that lead induces oxidative stress in children suffering from aplastic anemia. Lead-induced oxidative stress as an underlying mechanism for aplastic anemia warrants further research.

Keywords: Aplastic anemia, lead exposure, children, oxidative stress

1. Introduction

Aplastic anemia is a hematological disorder with a high lethality rate in which all cellular components of bone marrow origin are deficient (1). The annual incidence rate reported in the literature ranges from 1.5 to 24.6

cases per million with a range for more rigorous studies to be 1.5 to 5.0 (2). The determination of risk factors for aplastic anemia faces multiple difficulties. The evidence of myelotoxicity of several drugs, infectious agents, solvents, and other environmental toxins is circumstantial; there are no tests available that could confirm their cause-effect relationship. In addition, multiple exposures are the rule. For these reasons most cases are classified as idiopathic (3).

Exposure to lead can result in significant effects in multiple organs, with the hematopoietic system being an important target (4-6). Lead interferes with heme

*Address correspondence to:

Dr. Maqsood Ahamed, King Abdullah Institutes for Nanotechnology (KAIN), King Saud University, Box-2454, Riyadh-11451, KSA.

e-mail: maqsood@gmail.com

biosynthesis, and it affects formation and function of erythrocytes. A shortening of erythrocyte life span was observed by Terayama (7) in experiments with rats. Grandjean *et al.* (8) reported a lead-dependent delay for the regeneration of human erythrocytes. Lead, furthermore, interferes with iron utilization for heme formation, and radio-iron studies showed that lead competes with iron for incorporation into erythrocytes (9). If lead was indeed toxic to the hematopoietic system, one would expect the risk of aplastic anemia might be associated with lead exposure.

Children are more susceptible to lead exposure than adults because of their hand to mouth activity, increased respiratory rates and higher gastrointestinal absorption per unit body weight (10). In the 1960s, a blood lead level of 60 µg/dL was considered safe. Due to increased understanding of lead toxicology, the acceptable blood lead level was reduced to 25 µg/dL in 1985 and 10 µg/dL in 1991 by the Center for Disease Control (CDC), USA. Despite these changes, subclinical effects of lead exposure have been reported at blood lead levels less than 10 µg/dL (10). This issue is further complicated by the fact that there is no demonstrated biological function of lead in humans. As such, it is arguable that a "safe" blood lead level cannot be defined.

Evidence suggests that cellular damage mediated by oxidants may be involved in some of the pathophysiology of human diseases including aplastic anemia (11-13). Free radical generation seems to be the possible mechanism of lead toxicity (14-18). In the present study we evaluated the effect of blood levels on oxidative stress parameters in children suffering from aplastic anemia disease.

2. Materials and Methods

2.1. Chemicals

δ-Aminolevulinic acid (δ-ALA), reduced glutathione (GSH), 5,5'-dithio-bis-(2-nitro benzoic acid) (DTNB), thiobarbituric acid (TBA) and lead standards were purchased from Sigma Chemical Co., St. Louis, MO, USA. Hydrogen peroxide (H₂O₂) (30%) was obtained from E. Merck, Mumbai, India. All the other chemicals used were of the highest purity available from commercial sources.

2.2. Selection of patients

The study was designed to enroll children with aplastic anemia in the age group ≤ 12 y. A total of 17 cases of childhood aplastic anemia (15 male and 2 female, age 3-12 y) were enrolled at the Department of Pediatrics, Chhatrapati Shahuji Maharaj Medical University (CSMMU), Lucknow, India. Eligible patients were required to meet at least two of the following three criteria: white blood cell count ≤ 3.5 × 10⁹/L, platelet

count ≤ 50 × 10⁹/L, and hemoglobin concentration ≤ 10 g/dL or hematocrit ≤ 30%. If the latter criterion was one of the two fulfilled, a reticulocyte count ≤ 30 × 10⁹/L was also required. Definite diagnosis and final acceptance of the cases required a characteristic hypocellular bone marrow biopsy (marrow cellularity < 30%) without gross marrow fibrosis and absence of infiltration by leukemia, lymphomatous, or carcinoma cells. These defined criteria are identical to those used in the International Agranulocytosis and Aplastic Anemia Study (IAAAS) (19).

2.3. Selection of controls

Fifty one healthy children (45 male and 6 female, age 3-12 y) from a similar socio-economic environment were used as the controls. Inclusion criteria for the selection of controls were hemoglobin concentration (≥ 12 g/dL), hematocrit (40-47%), red blood cell count (4.0-5.5 × 10¹²/L), white blood cell count (4.0-11.0 × 10⁹/L), platelet count (200-500 × 10⁹/L) and not suffering from any chronic disease(s).

Parent's consent was obtained prior to sample collection and questionnaire administration. The Ethical Committee of CSMMU, Lucknow (India) approved the study. Parents of the subjects were interviewed by trained physicians or nurses to obtain relevant medical history, history of exposure to radiation, and a detailed case history of drug use. Patients who had received chemotherapy, immunotherapy or radiotherapy were not eligible as cases or controls. None of the subjects in either cases or controls were found enzyme-linked immunosorbent assay (ELISA) positive for anti-human immunodeficiency virus (HIV)-I and HIV-II antibody in the serum.

2.4. Blood collection and processing

Approximately 4.0 mL of venous blood was withdrawn from each subject. One milliliter was transferred to a vial containing ethylene diamine tetraacetic acid for routine blood investigation. Another 1.0 mL was transferred in a plain vial (without anticoagulant) for anti HIV-I and HIV-II antibody detection in serum by the ELISA method. These investigations were performed at the Department of Pathology, CSMMU, Lucknow. The remaining 2.0 mL blood was collected in pre-heparinized vials as coded samples, and transported under ice-cold conditions to the Analytical Toxicology Laboratory, Indian Institute of Toxicological Research (IITR), Lucknow for biochemical assays and analysis for lead.

A portion of the blood was used for the preparation of the lysate. Briefly, blood was centrifuged at 2,500 rpm for 15 min at 4°C and the supernatant aspirated. The erythrocyte rich precipitate was washed three times with physiological saline (3:1, v/v) and lysed

using double distilled water. The particulate material was centrifuged at 15,000 rpm for 90 min at 4°C, and the supernatant (erythrocyte lysate) was collected for the determination of catalase (CAT) activity. Another portion of the blood was utilized for assays of δ -aminolevulinic acid dehydratase (δ -ALAD), thiobarbituric acid reactive species (TBARS), GSH, and analysis of lead. The person analyzing for lead and carrying out biochemical assays was totally blind as to the case history of subjects.

2.5. Biochemical assays

The European standardized method was used to determine blood δ -ALAD activity using δ -ALA as a substrate and expressed as μmol porphobilinogen (PBG) formed/min/L blood (20). The extent of lipid peroxidation in whole blood was determined by measuring the formation of TBARS by the method of Stocks and Dormandy (21) and expressed as nmol TBARS formed per mL blood using a molar extinction coefficient of $1.56 \times 10^5 \text{ mol}^{-1} \text{ cm}^{-1}$. GSH was estimated in blood using Ellman's method (22) and expressed as $\mu\text{mol}/\text{mL}$ blood. CAT activity in hemolysate was assayed by the method of Sinha (23) using H_2O_2 as substrate and expressed as $\mu\text{mol H}_2\text{O}_2$ decomposed/min/g Hb.

2.6. Analysis of lead

Blood lead was determined using a graphite furnace atomic absorption spectrometer (Varian SpectraAA 250+, Varian Australia Pty Ltd., Victoria, Australia) (24). The instrument was calibrated using aqueous lead standards of 10, 20, 30, and 40 $\mu\text{g}/\text{L}$. The detection limit was 3 $\mu\text{g}/\text{L}$. Fifty microliters of blood were diluted 1:10 in the diluent in a 1.0-mL polystyrene auto-sampler tube. The diluent (Triton X-100, 0.1%, w/v; $\text{NH}_4\text{H}_2\text{PO}_4$, 0.2%, w/v; NH_3 , 0.14 M) was prepared in deionized water. The calibration blank used was 0.2% nitric acid, 0.2% $\text{NH}_4\text{H}_2\text{PO}_4$ solution and the reagent blank was the diluent solution. Results for duplicate analysis of blood samples agreed within $\pm 7\%$. Accuracy and precision of the method were checked by spiking the samples with known amounts of standard. Coefficients of variation were 6% and 4% at 10 and 40 $\mu\text{g}/\text{L}$, respectively.

The accuracy of the method for metal estimation was further controlled by participation in an inter-laboratory quality-assurance program (IITR, Lucknow) wherein coded samples were analyzed regularly and results scrutinized by the quality manager. Further, a quality check sample was always run with each set of samples for lead analysis to maintain accuracy.

2.7. Statistical evaluation

All the data were normally distributed. The significance

of differences of mean values of blood lead level and biochemical indices between the study and control groups were compared by Student's *t*-test. Linear regression analysis was performed to determine strength of relationship between the blood lead level and selected biochemical indices.

3. Results

All the subjects of this study were residents of Lucknow, India and its surroundings, where small-scale industries like smelting processes, recycling of batteries and their use in electronics might contribute substantial amounts of lead to the environment even after the phasing out of leaded-petrol (6,13). Table 1 represents the demographic covariates of the study and control groups. Age, sex, body mass index (BMI), and area of living in the two groups of children were not statistically different. Table 2 shows the comparison of blood lead level and biochemical indices between the study and control groups. Blood lead level was significantly higher in the study group when compared with the control group ($p < 0.05$). The δ -ALAD activity, a biomarker of lead exposure was significantly lower in the study group as compared to the control group ($p < 0.05$). Lipid peroxides in blood, as determined by TBARS level was significantly higher while the antioxidant molecule GSH was significantly lower in the study group than in the control group ($p < 0.05$ for each). Furthermore, antioxidant enzyme CAT activity was significantly higher in the children with aplastic anemia compared to the controls ($p < 0.05$).

Figure 1 indicates the relationship strength between blood lead level and biochemical indices. There were significant negative correlations of blood lead level with δ -ALAD ($r = -0.45$; $p < 0.05$) and GSH level ($r = -0.32$; $p < 0.05$) and a positive correlation with TBARS ($r = 0.41$; $p < 0.05$) and CAT ($r = 0.37$; $p < 0.05$) (See Figure 1).

4. Discussion

The hematopoietic system has been proposed as being one of the important targets of lead-toxicity (4,5). Erythrocytes have high affinity for lead and typically contain the majority of lead found in the blood stream (25). Exposure of children with pre-existing aplastic anemia to lead can have serious consequences, because lead can further impair their hematopoietic system. The existing experimental and epidemiological data on lead toxicity and the occurrence of significant levels of lead in the blood of Indian subjects, especially children, prompted us to study if there is an association between lead and childhood aplastic anemia (6,13,16,17). In the present study, we found that the blood lead level of aplastic anemia patients was significantly higher compared to

Table 1. Covariates of the study and control groups

Covariates	Control group (n = 51)	Study group (n = 17)	p value
Age in year (range)	7.49 ± 1.91 (3-12)	7.65 ± 2.80 (3-12)	0.792
BMI (kg/m ²)	14.0 ± 2.8	14.4 ± 3.7	0.672
Sex			
Male	45 (88)	15 (88)	1
Female	6 (12)	2 (12)	1
Area of living			
Rural	0 (0)	0 (0)	1
Urban	51 (100)	17 (100)	1

Values represent mean ± S.D. (% of subjects). Student's *t*-test was applied for determining statistical significance between the cases and controls.

Table 2. Blood lead level and biochemical indices of the study and control groups

Parameters	Control group (n = 51)	Study group (n = 17)	p value
Blood lead level (µg/dL)	4.23 ± 1.23	9.86 ± 2.04	< 0.05
δ-ALAD (µmol PBG formed/min/L blood)	4.10 ± 0.59	3.01 ± 0.31	< 0.05
TBARS (nmol/mL blood)	13.3 ± 3.9	23.3 ± 4.0	< 0.05
GSH (µmol/mL blood)	24.9 ± 5.2	16.2 ± 3.9	< 0.05
CAT (×10 ⁴ µmol H ₂ O ₂ decomposed/min/g Hb)	82.3 ± 8.7	119.7 ± 15.3	< 0.05

Values represent mean ± S.D. Student's *t*-test was applied for determining statistical significance between the study and control groups. Abbreviations: δ-ALAD, δ-aminolevulinic acid dehydratase; TBARS, thiobarbituric acid reactive species; GSH, glutathione; CAT, catalase.

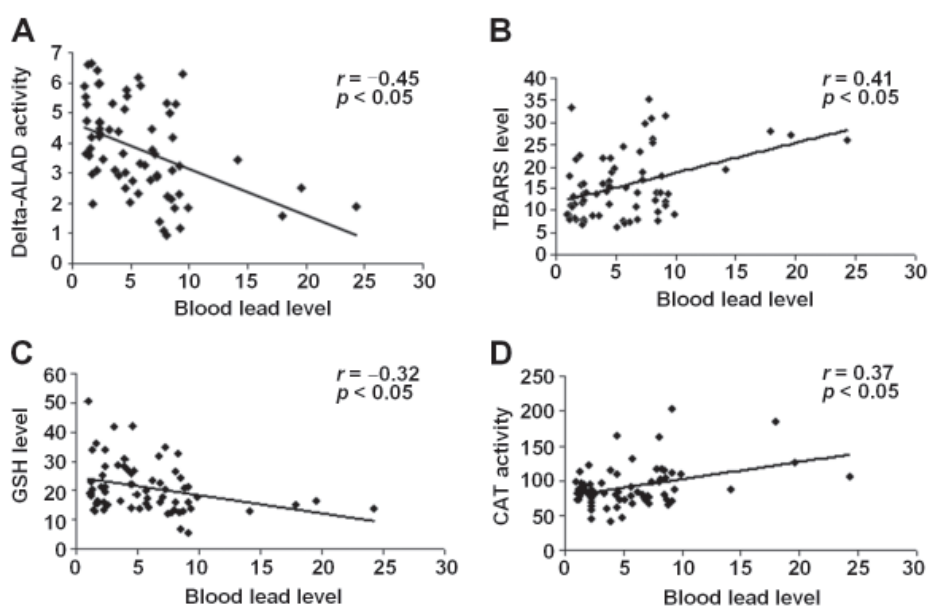


Figure 1. Statistically significant correlations of blood lead level with selected biochemical indices. (A) Blood δ-ALAD activity plotted as a function of blood lead levels. **(B)** Blood TBARS levels plotted against blood lead levels. **(C)** Erythrocyte CAT activity plotted against blood lead levels. **(D)** Blood GSH levels plotted against blood lead levels. Blood lead level, µg/dL; δ-ALAD, µmol PBG formed/min/L blood; TBARS, nmol/mL blood; GSH, µmol/mL blood; CAT, ×10⁴ µmol H₂O₂ decomposed/min/g Hb.

the control group.

Investigation of lead-induced oxidative stress as an underlying mechanism for aplastic anemia offers the potential to reveal more about the etiology of this complex disease and may provide opportunities for prevention of this disease of unknown etiology. Several lines of evidences suggest that cellular damage

mediated by oxidants may be involved in some of the pathogenesis associated with lead intoxication (26,27). Oxidation phenomena and/or the formation of free radicals have been suggested to be causally related to various diseases (11-13). In the present study, activity of the δ-ALAD enzyme was significantly lower in aplastic anemia cases than in the controls. It has been

suggested that inhibition of δ -ALAD enzyme by lead directs the accumulation of its substrate δ -ALA that can be rapidly oxidized to generate free radicals (6). On the other hand, lead per se has the capacity to stimulate ferrous ion initiated membrane lipid peroxidation (14). Lipid peroxides in the blood, as determined by TBARS level, were significantly correlated with blood lead levels in the children of the general population (16,28). In this study, TBARS level was significantly higher in aplastic anemia patients. Our finding is further supported by other experimental studies where blood TBARS level was higher due to lead exposure (14,15). Peroxidation of erythrocyte membrane lipids can be very damaging because it leads to alterations in the biological properties of the membrane, such as the degree of fluidity and can result in inactivation of membrane-bound receptors or enzymes, which in turn may impair normal cellular function, increase tissue permeability and shorten the life span of blood cells.

Lead can lower cellular concentrations of hemoproteins and GSH, thus reducing the redox buffering capacity of cells (29). In this study, GSH status significantly declined in the blood of aplastic anemia patients as compared to the controls. GSH is a tri-peptide containing cysteine that has a reactive thiol group (-SH) with reductive potency. GSH acts as a non-enzymatic antioxidant by direct interaction of the -SH group with free radicals, or it can be involved in the enzymatic detoxification reactions for free radicals as a cofactor (30). Evidence for involvement of free radicals in the pathophysiology of aplastic anemia also arises from the significant increase of erythrocyte CAT activity in children with aplastic anemia. CAT has been suggested to provide an important pathway for H_2O_2 decomposition (18).

We also found significant correlations of blood lead level with the selected biochemical indices. It is therefore, interesting to note that in aplastic anemia patients lead-induced oxidative stress directs membrane lipid peroxidation with a concomitant decrease in antioxidants like GSH and activity of antioxidant enzymes such as CAT which increases to scavenge free radicals (12). However, it is anticipated that there may be a number of plausible reasons for increased oxidative stress in aplastic anemia patients and the results of this study may be limited due to limited statistical power but certainly form the basis for a larger sample size study with greater statistical power, taking into account all the known confounders of the disease.

Acknowledgements

Authors express their sincere thanks to Mrs. Poonam Saxena for her assistance in lead analysis. MA and MJA sincerely thank the Council of Scientific and Industrial Research-University Grant Commission (CSIR-UGC), New Delhi, India for financial support.

References

- Weiss DJ. Aplastic anemia in cats – clinico-pathological features and associated disease conditions 1996-2004. *J Feline Med Surgery*. 2006; 8:203-206.
- Ahamed M, Anand M, Kumar A, Siddiqui MK. Childhood aplastic anemia in Lucknow, India: Incidence, organochlorines in the blood and review of case reports following exposure to pesticides. *Clin Biochem*. 2006; 39:762-766.
- Brodsky RA, Jones RJ. Aplastic anaemia. *Lancet*. 2005; 365:1647-1656.
- Jacob B, Ritz B, Heinrich J, Hoelscher B, Wichmann HE. The effects of low level of blood lead on hematological parameters in children. *Environ Res*. 2000; 82:150-159.
- Gurer-Orhan H, Sabir HU, Ozgüneş H. Correlation between clinical indicator of lead poisoning and oxidative stress parameters in controls and lead-exposed workers. *Toxicology*. 2004; 195:147-154.
- Ahamed M, Singh S, Behari JR, Kumar A, Siddiqui MK. Interaction of lead with some essential trace metals in the blood of anemic children from Lucknow India. *Clin Chim Acta*. 2007; 377:92-97.
- Terayama K. Effects of lead on electrophoretic mobility, membrane sialic acid, deformability and survival of rat erythrocytes. *Ind Health*. 1993; 31:113-126.
- Grandjean P, Jensen BM, Sandø SH, Jørgensen PJ, Antonsen S. Delayed blood regeneration in lead exposure: An effect on reserve capacity. *Am J Public Health*. 1989; 79:1385-1388.
- Labbé RF. Lead poisoning mechanisms. *Clin Chem*. 1990; 36:1870.
- Ahamed M, Siddiqui MK. Environmental lead toxicity and nutritional factors. *Clin Nutr*. 2007; 26:400-408.
- Liégeois JF, Bruhwiler J, Petit C, Damas J, Delarge J, Géczy J, Kauffmann JM, Lamy M, Meltzer H, Mouithys-Mickalad A. Oxidation sensitivity may be a useful tool for the detection of the hematotoxic potential of newly developed molecules: Application to antipsychotic drugs. *Arch Biochem Biophys*. 1999; 370:126-137.
- Dalle-Donne I, Rossi R, Colombo R, Giustarini D, Milzani A. Biomarkers of oxidative damage in human disease. *Clin Chem*. 2006; 52:601-623.
- Ahamed M, Fareed M, Kumar A, Siddiqui WA, Siddiqui MK. Oxidative stress and neurological disorders in relation to blood lead levels in children. *Redox Rep*. 2008; 13:117-122.
- Adonaylo VN, Oteiza PI. Lead intoxication: Antioxidant defenses and oxidative damage in rat brain. *Toxicology*. 1999; 135:77-85.
- Tandon SK, Singh S, Prasad S, Srivastava S, Siddiqui MK. Reversal of lead-induced oxidative stress by chelating agents, antioxidant or their combination in rat. *Environ Res*. 2002; 90:61-66.
- Ahamed M, Verma S, Kumar A, Siddiqui MK. Environmental exposure to lead and its correlation with biochemical indices in children. *Sci Total Environ*. 2005; 346:48-55.
- Ahamed M, Verma S, Kumar A, Siddiqui MK. Delta-aminolevulinic acid dehydratase inhibition and oxidative stress in relation to blood lead among urban adolescents. *Hum Exp Toxicol*. 2006; 25:547-553.
- Ahamed M, Siddiqui MK. Low levels lead exposure and oxidative stress: Current opinions. *Clin Chim Acta*. 2007; 383:57-64.

19. Kaufman DW, Kelly JP, Levy M, Shapiro S. The drug etiology of agranulocytosis and aplastic anemia: The International Agranulocytosis and Aplastic Anemia Study (IAAAS). Oxford University Press, New York, NY, USA, 1999.
20. Berlin A, Schaller KN. European standardized method for determination of delta-ALAD activity in blood. *Z Klin Chem Klin Biochem.* 1974; 12:389-390.
21. Stocks J, Dormandy TL. The auto-oxidation of human red cells lipid induced by hydrogen peroxide. *Br J Hematol.* 1971; 20:95-111.
22. Kuo CH, Maita K, Sleight SD, Hook JB. Lipid peroxidation: A possible mechanism of cephaloridine-induced nephrotoxicity. *Toxicol Appl Pharmacol.* 1983; 67:78-88.
23. Sinha AK. Colorimetric assay of catalase. *Anal Biochem.* 1972; 47:389-394.
24. Giri SK, Shields CK, Littlejohn D, Ottaway JM. Determination of lead in whole blood by electrothermal atomic-absorption spectrometry using graphite probe atomisation. *Analyst.* 1983; 108:244-253.
25. Leggett RW. An age-specific kinetic model of lead metabolism in humans. *Environ Health Perspect.* 1993; 101:598-616.
26. Hermes-Lima M, Pereira B, Bechara EJ. Are free radicals involved in lead poisoning? *Xenobiotica.* 1991; 21:1085-1090.
27. Patra RC, Swarup D, Dwivedi SK. Antioxidant effects of alpha tocopherol, ascorbic acid and L-methionine on lead induced oxidative stress to the liver, kidney and brain in rats. *Toxicology.* 2001; 162:81-88.
28. Diouf A, Garçon G, Thiaw C, Diop Y, Fall M, Ndiaye B, Siby T, Hannotiaux MH, Zerimech F, Ba D, Haguenoer JM, Shirali P. Environmental lead exposure and its relationship to traffic density among Senegalese children: A pilot study. *Hum Exp Toxicol.* 2003; 22:559-564.
29. Silbergeld EK, Waalkes M, Rice JM. Lead as a carcinogen: Experimental evidence and mechanisms of action. *Am J Ind Med.* 2000; 38:316-323.
30. Das M, Babu K, Reddy NP, Srivastava LM. Oxidative damage of plasma proteins and lipids in epidemic dropsy patients: Alterations in antioxidant status. *Biochim Biophys Acta.* 2005; 1722:209-217.

(Received September 21, 2010; Accepted November 23, 2010)

Dengue causing fulminant hepatitis in a hepatitis B virus carrier

Mukul P. Agarwal¹, Subhash Giri¹, Vishal Sharma^{2,*}, Ujjawal Roy¹, Komal Gharsangi¹

¹Department of Medicine, University College of Medical Sciences (University of Delhi) and GTB Hospital, Delhi, India;

²Department of Gastroenterology, PGIMER, Chandigarh, India.

Summary

Dengue is an acute febrile illness resulting from infection by a flavivirus transmitted by the *Aedes* mosquito. It is characterized by bleeding manifestations and a plasma leak syndrome. Hepatic involvement in the form of elevation in transaminases is common. However, acute hepatic failure is uncommon. It is not known how the presence of an underlying chronic hepatitis or liver disease affects the likelihood of severity of hepatitis from dengue. The present report is of a 33-year-old man, a carrier of hepatitis B virus, who presented with fever, altered sensorium, thrombocytopenia, and coagulopathy. He was diagnosed to have developed acute hepatic failure due to dengue. The patient improved with supportive measures.

Keywords: Dengue, acute liver failure

1. Introduction

Dengue is an arbo-viral disease transmitted by the bite of the *Aedes* mosquito. It is endemic in many areas of the world including India. Apart from causing fever and severe myalgias and arthralgias, dengue results in a phenomenon of plasma leak manifesting as hemoconcentration, serositis, and occasionally shock. Thrombocytopenia is common and can result in bleeding manifestations (1). Hepatic involvement in the form of raised transaminases is common but usually of no clinical importance. Sometimes dengue can cause acute hepatic failure (2). However, the effects of dengue infection on chronic liver disease or a chronic carrier state are not known.

2. Case report

A 33-year-old male, resident of Delhi (India) presented with a history of 5 days of fever. The fever was documented to be as high as 40°C. The fever was associated with chills and rigors. Two days prior to presentation there had been a gradual deterioration in his sensorium. He had started behaving abnormally and was irritable and abusive to his relatives. Around

eight hours prior to his presentation to us the patient had one episode of generalized tonic movements of the body associated with clenching of teeth. The patient had no associated rash, neck stiffness, cough, urinary, or bowel complaints. There was no past history of any seizures, jaundice, or long standing fever. There was no history of any herbal drug intake. Patient had taken paracetamol (500 mg three times per day) for two days prior to presentation.

On examination, the patient was unconscious. His blood pressure was 116/78 mmHg, pulse was 104/min, and regular oral temperature was 38.5°C. His oxygen saturation on room air was 98%. He had mild icterus. Chest auscultation revealed diminution of breath sounds on the right side with stony dullness on percussion. The cardiovascular examination was normal. On palpation of abdomen liver was palpable two fingers below costal margin, spleen was not palpable. He was unconscious and moved his limbs only to deep painful stimulus. There was no neck rigidity, pupils were normal size and reacted normally to light and the plantars were flexor.

His investigations revealed a hemoglobin of 18.4 g/dL (PCV-55%), total leukocytes of 2,600/mm³, and a platelet count of 18,000/mm³. His serum total bilirubin was 3.5 mg/dL, with a direct of 1.5 mg/dL (Table 1). Alanine transaminases (ALT), aspartate transaminase (AST), and serum alkaline phosphatase (SAP) were 768, 882, and 132 IU/L, respectively. Serum albumin was 3.5 g/dL (Table 1). His prothrombin time was 32 sec (control, 12 sec) (Table 1). His serologies for

*Address correspondence to:

Dr. Vishal Sharma, Department of Gastroenterology, PGIMER, Chandigarh 160012, India.
e-mail: docvishalsharma@gmail.com

Table 1. Trend of liver function tests during admission

Parameters	Days				
	D1	D3	D8	D10	D14
Bilirubin (total) (mg/dL)	3.5	2.6	1.8	1.6	1.5
Bilirubin (direct) (mg/dL)	1.5	1.2	0.6	0.3	0.3
ALT (IU/L)	768	308	112	80	35
AST (IU/L)	882	450	205	115	52
SAP (IU/L)	132	112	98	111	108
Albumin (g/dL)	3.5	3.2	3.2	3.5	3.4
prothrombin time (sec)*	32 (12)	–	–	–	15 (13)

* Control time is shown in parenthesis.

viral hepatitis including IgM anti-hepatitis A virus, IgM anti-hepatitis E virus, and anti-hepatitis C virus were negative. He was, however, positive for hepatitis B surface antigen (HBsAg). He was negative for hepatitis Be antigen (HBeAg) but positive for anti-hepatitis Be antibody. His IgM anti-hepatitis Bc (HBc) antibody was negative. A peripheral smear for malaria and a card test for parasite lactate dehydrogenase (pLDH) for *Plasmodium vivax* and *P. falciparum* were negative. His blood cultures were returned sterile. His chest roentgenogram was remarkable for presence of right sided pleural effusion. His ultrasound confirmed the presence of hepatomegaly. Presence of mild ascites and gall bladder wall edema was also noted. Magnetic resonance imaging of his brain was normal. IgM enzyme-linked immunosorbent assay (ELISA) for dengue was positive. The patient improved with conservative management (including fluid resuscitation, platelet transfusion, and anti-cerebral edema measures, *i.e.*, head end elevation, *i.v.* mannitol). Anti-virals (nucleoside analogues) were not administered. The patient was discharged after 2 weeks when his liver functions had returned to normal. The patient remained positive for HBsAg, with normal transaminases and hepatitis B virus (HBV) DNA of 1,880 IU/mL at six months.

3. Discussion

This patient presented with fever and altered sensorium. The differentials for this are broad and include among others meningitis, encephalitis, cerebral malaria, CNS tuberculosis, *etc.* The investigations in this patient were suggestive of leucopenia, thrombocytopenia, deranged liver functions especially transaminase elevation, and mild pleural effusion. These pointed to the possibility of dengue. Dengue was suspected as the patient presented with symptoms during an epidemic of dengue. The absence of IgM anti-HBc and low viral DNA levels argue against acute hepatitis B or an acute flare up of chronic hepatitis B. Also, the presence of severe thrombocytopenia and serositis argue against HBV as

the responsible etiological agent. The diagnosis was confirmed with a positive IgM ELISA for dengue.

Dengue is an arboviral disease caused by a member of flaviviridae. Dengue virus is a single strand RNA virus having four serotypes. Hepatitis is very common in dengue and can result in acute hepatic failure (3). Some reports have indicated that dengue is one of the most common etiologies responsible for acute hepatic failure in endemic areas (4).

However, not much is known about the effect of dengue coinfection in a HBV carrier state. There are some reports which have documented acute hepatitis resulting from dengue in a patient with chronic liver disease (5). However, it is not clear if dengue coinfection will result in more severe hepatitis or a higher likelihood of liver failure. A study in China examined the effect of co-infection of dengue on patients with HBV and found a difference of cytokine profiles in these patients. It noted that in cases of coinfection less interleukin (IL)-6 and tumor necrosis factor- α were formed whereas levels of IL-4, IL-10 and interferon- γ were similar (6). The clinical consequences of this difference are not clear and the study offered no evidence regarding any difference in liver function tests of dengue patients coinfecting with HBV. To the best of our knowledge the present report is the first one implicating dengue in causation of acute hepatic failure in a HBV carrier. The present case highlights the need to consider dengue as a possible cause of acute liver failure in endemic regions.

References

1. Teixeira MG, Barreto ML. Diagnosis and management of dengue. *BMJ*. 2009; 339:b4338.
2. Giri S, Agarwal MP, Sharma V, Singh A. Acute hepatic failure due to dengue: A case report. *Cases J*. 2008; 1:204.
3. Itha S, Kashyap R, Krishnani N, Saraswat VA, Choudhuri G, Aggarwal R. Profile of liver involvement in dengue virus infection. *Natl Med J India*. 2005; 18:127-130.
4. Poovorawan Y, Hutagalung Y, Chongsrisawat V, Boudville I, Bock HL. Dengue virus infection: A major cause of acute hepatic failure in Thai children. *Ann Trop Paediatr*. 2006; 26:17-23.
5. Souza LJ, Coelho JM, Silva EJ, Abukater M, Almeida FC, Fonte AS, Souza LA. Acute hepatitis due to dengue virus in a chronic hepatitis patient. *Braz J Infect Dis*. 2008; 12:456-459.
6. Tang Y, Kou Z, Tang X, Zhang F, Yao X, Liu S, Jin X. Unique impacts of HBV co-infection on clinical and laboratory findings in a recent dengue outbreak in China. *Am J Trop Med Hyg*. 2008; 79:154-158.

(Received November 12, 2010; Revised November 17, 2010; Re-revised November 29, 2010; Accepted November 30, 2010)

Guide for Authors

1. Scope of Articles

BioScience Trends is an international peer-reviewed journal. BioScience Trends devotes to publishing the latest and most exciting advances in scientific research. Articles cover fields of life science such as biochemistry, molecular biology, clinical research, public health, medical care system, and social science in order to encourage cooperation and exchange among scientists and clinical researchers.

2. Submission Types

Original Articles should be well-documented, novel, and significant to the field as a whole. An Original Article should be arranged into the following sections: Title page, Abstract, Introduction, Materials and Methods, Results, Discussion, Acknowledgments, and References. Original articles should not exceed 5,000 words in length (excluding references) and should be limited to a maximum of 50 references. Articles may contain a maximum of 10 figures and/or tables.

Brief Reports definitively documenting either experimental results or informative clinical observations will be considered for publication in this category. Brief Reports are not intended for publication of incomplete or preliminary findings. Brief Reports should not exceed 3,000 words in length (excluding references) and should be limited to a maximum of 4 figures and/or tables and 30 references. A Brief Report contains the same sections as an Original Article, but the Results and Discussion sections should be combined.

Reviews should present a full and up-to-date account of recent developments within an area of research. Normally, reviews should not exceed 8,000 words in length (excluding references) and should be limited to a maximum of 100 references. Mini reviews are also accepted.

Policy Forum articles discuss research and policy issues in areas related to life science such as public health, the medical care system, and social science and may address governmental issues at district, national, and international levels of discourse. Policy Forum articles should not exceed 2,000 words in length (excluding references).

Case Reports should be detailed reports of the symptoms, signs, diagnosis, treatment, and follow-up of an individual patient. Case reports may contain a demographic profile of the patient but usually describe an unusual or novel occurrence. Unreported or unusual

side effects or adverse interactions involving medications will also be considered. Case Reports should not exceed 3,000 words in length (excluding references).

News articles should report the latest events in health sciences and medical research from around the world. News should not exceed 500 words in length.

Letters should present considered opinions in response to articles published in BioScience Trends in the last 6 months or issues of general interest. Letters should not exceed 800 words in length and may contain a maximum of 10 references.

3. Editorial Policies

Ethics: BioScience Trends requires that authors of reports of investigations in humans or animals indicate that those studies were formally approved by a relevant ethics committee or review board.

Conflict of Interest: All authors are required to disclose any actual or potential conflict of interest including financial interests or relationships with other people or organizations that might raise questions of bias in the work reported. If no conflict of interest exists for each author, please state "There is no conflict of interest to disclose".

Submission Declaration: When a manuscript is considered for submission to BioScience Trends, the authors should confirm that 1) no part of this manuscript is currently under consideration for publication elsewhere; 2) this manuscript does not contain the same information in whole or in part as manuscripts that have been published, accepted, or are under review elsewhere, except in the form of an abstract, a letter to the editor, or part of a published lecture or academic thesis; 3) authorization for publication has been obtained from the authors' employer or institution; and 4) all contributing authors have agreed to submit this manuscript.

Cover Letter: The manuscript must be accompanied by a cover letter signed by the corresponding author on behalf of all authors. The letter should indicate the basic findings of the work and their significance. The letter should also include a statement affirming that all authors concur with the submission and that the material submitted for publication has not been published previously or is not under consideration for publication elsewhere. The cover letter should be submitted in PDF format. For example of Cover Letter, please visit <http://www.biosciencetrends.com/downcentre.php> (Download Centre).

Copyright: A signed JOURNAL PUBLISHING AGREEMENT (JPA) form must be provided by post, fax, or as a scanned file before acceptance of the article. Only forms with a hand-written signature are accepted. This copyright will ensure the widest possible dissemination of information. A form facilitating transfer of copyright can be downloaded by clicking the

appropriate link and can be returned to the e-mail address or fax number noted on the form (Please visit [Download Centre](#)). Please note that your manuscript will not proceed to the next step in publication until the JPA Form is received. In addition, if excerpts from other copyrighted works are included, the author(s) must obtain written permission from the copyright owners and credit the source(s) in the article.

Suggested Reviewers: A list of up to 3 reviewers who are qualified to assess the scientific merit of the study is welcomed. Reviewer information including names, affiliations, addresses, and e-mail should be provided at the same time the manuscript is submitted online. Please do not suggest reviewers with known conflicts of interest, including participants or anyone with a stake in the proposed research; anyone from the same institution; former students, advisors, or research collaborators (within the last three years); or close personal contacts. Please note that the Editor-in-Chief may accept one or more of the proposed reviewers or may request a review by other qualified persons.

Language Editing: Manuscripts prepared by authors whose native language is not English should have their work proofread by a native English speaker before submission. If not, this might delay the publication of your manuscript in BioScience Trends.

The Editing Support Organization can provide English proofreading, Japanese-English translation, and Chinese-English translation services to authors who want to publish in BioScience Trends and need assistance before submitting a manuscript. Authors can visit this organization directly at <http://www.iacmhr.com/iac-eso/support.php?lang=en>. IAC-ESO was established to facilitate manuscript preparation by researchers whose native language is not English and to help edit works intended for international academic journals.

4. Manuscript Preparation

Manuscripts should be written in clear, grammatically correct English and submitted as a Microsoft Word file in a single-column format. Manuscripts must be paginated and typed in 12-point Times New Roman font with 24-point line spacing. Please do not embed figures in the text. Abbreviations should be used as little as possible and should be explained at first mention unless the term is a well-known abbreviation (e.g. DNA). Single words should not be abbreviated.

Title Page: The title page must include 1) the title of the paper (Please note the title should be short, informative, and contain the major key words); 2) full name(s) and affiliation(s) of the author(s), 3) abbreviated names of the author(s), 4) full name, mailing address, telephone/fax numbers, and e-mail address of the corresponding author; and 5) conflicts of interest (if you have an actual or potential conflict of interest to disclose, it must be included as a footnote on the title page of the manuscript; if no conflict of

interest exists for each author, please state "There is no conflict of interest to disclose"). Please visit [Download Centre](#) and refer to the title page of the manuscript sample.

Abstract: A one-paragraph abstract consisting of no more than 250 words must be included. The abstract should briefly state the purpose of the study, methods, main findings, and conclusions. Abbreviations must be kept to a minimum and non-standard abbreviations explained in brackets at first mention. References should be avoided in the abstract. Key words or phrases that do not occur in the title should be included in the Abstract page.

Introduction: The introduction should be a concise statement of the basis for the study and its scientific context.

Materials and Methods: The description should be brief but with sufficient detail to enable others to reproduce the experiments. Procedures that have been published previously should not be described in detail but appropriate references should simply be cited. Only new and significant modifications of previously published procedures require complete description. Names of products and manufacturers with their locations (city and state/country) should be given and sources of animals and cell lines should always be indicated. All clinical investigations must have been conducted in accordance with Declaration of Helsinki principles. All human and animal studies must have been approved by the appropriate institutional review board(s) and a specific declaration of approval must be made within this section.

Results: The description of the experimental results should be succinct but in sufficient detail to allow the experiments to be analyzed and interpreted by an independent reader. If necessary, subheadings may be used for an orderly presentation. All figures and tables must be referred to in the text.

Discussion: The data should be interpreted concisely without repeating material already presented in the Results section. Speculation is permissible, but it must be well-founded, and discussion of the wider implications of the findings is encouraged. Conclusions derived from the study should be included in this section.

Acknowledgments: All funding sources should be credited in the Acknowledgments section. In addition, people who contributed to the work but who do not meet the criteria for authors should be listed along with their contributions.

References: References should be numbered in the order in which they appear in the text. Citing of unpublished results, personal communications, conference abstracts, and theses in the reference list is not recommended but these sources may be mentioned in the text. In the reference list, cite the names of all authors when there are fifteen or fewer authors; if there are sixteen or more authors, list the first three

followed by *et al.* Names of journals should be abbreviated in the style used in PubMed. Authors are responsible for the accuracy of the references. Examples are given below:

Example 1 (Sample journal reference):

Inagaki Y, Tang W, Zhang L, Du GH, Xu WF, Kokudo N. Novel aminopeptidase N (APN/CD13) inhibitor 24F can suppress invasion of hepatocellular carcinoma cells as well as angiogenesis. *Biosci Trends*. 2010; 4:56-60.

Example 2 (Sample journal reference with more than 15 authors):

Darby S, Hill D, Auvinen A, *et al.* Radon in homes and risk of lung cancer: Collaborative analysis of individual data from 13 European case-control studies. *BMJ*. 2005; 330:223.

Example 3 (Sample book reference):

Shalev AY. Post-traumatic stress disorder: diagnosis, history and life course. In: *Post-traumatic Stress Disorder, Diagnosis, Management and Treatment* (Nutt DJ, Davidson JR, Zohar J, eds.). Martin Dunitz, London, UK, 2000; pp. 1-15.

Example 4 (Sample web page reference):

Ministry of Health, Labour and Welfare of Japan. Dietary reference intakes for Japanese. <http://www.mhlw.go.jp/houdou/2004/11/h1122-2a.html> (accessed June 14, 2010).

Tables: All tables should be prepared in Microsoft Word or Excel and should be arranged at the end of the manuscript after the References section. Please note that tables should not in image format. All tables should have a concise title and should be numbered consecutively with Arabic numerals. If necessary, additional information should be given below the table.

Figure Legend: The figure legend should be typed on a separate page of the main manuscript and should include a short title and explanation. The legend should be concise but comprehensive and should be understood without referring to the text. Symbols used in figures must be explained.

Figure Preparation: All figures should be clear and cited in numerical order in the text. Figures must fit a one- or two-column format on the journal page: 8.3 cm (3.3 in.) wide for a single column, 17.3 cm (6.8 in.) wide for a double column; maximum height: 24.0 cm (9.5 in.). Please make sure that the symbols and numbers appeared in the figures should be clear. Please make sure that artwork files are in an acceptable format (TIFF or JPEG) at minimum resolution (600 dpi for illustrations, graphs, and annotated artwork, and 300 dpi for micrographs and photographs). Please provide all figures as separate files. Please note that low-resolution images are one of the leading causes of article resubmission and schedule delays. All color figures will be reproduced in full color in the online edition of the journal at no cost to authors.

Units and Symbols: Units and symbols conforming to the International System

of Units (SI) should be used for physicochemical quantities. Solidus notation (*e.g.* mg/kg, mg/mL, mol/mm²/min) should be used. Please refer to the SI Guide www.bipm.org/en/si/ for standard units.

Supplemental data: Supplemental data might be useful for supporting and enhancing your scientific research and BioScience Trends accepts the submission of these materials which will be only published online alongside the electronic version of your article. Supplemental files (figures, tables, and other text materials) should be prepared according to the above guidelines, numbered in Arabic numerals (*e.g.*, Figure S1, Figure S2, and Table S1, Table S2) and referred to in the text. All figures and tables should have titles and legends. All figure legends, tables and supplemental text materials should be placed at the end of the paper. Please note all of these supplemental data should be provided at the time of initial submission and note that the editors reserve the right to limit the size and length of Supplemental Data.

5. Submission Checklist

The Submission Checklist will be useful during the final checking of a manuscript prior to sending it to BioScience Trends for review. Please visit [Download Centre](#) and download the Submission Checklist file.

6. Online Submission

Manuscripts should be submitted to BioScience Trends online at <http://www.biosciencetrends.com>. The manuscript file should be smaller than 5 MB in size. If for any reason you are unable to submit a file online, please contact the Editorial Office by e-mail at office@biosciencetrends.com.

7. Accepted Manuscripts

Proofs: Galley proofs in PDF format will be sent to the corresponding author via e-mail. Corrections must be returned to the editor (proof-editing@biosciencetrends.com) within 3 working days.

Offprints: Authors will be provided with electronic offprints of their article. Paper offprints can be ordered at prices quoted on the order form that accompanies the proofs.

Page Charge: A page charge of \$140 will be assessed for each printed page of an accepted manuscript. The charge for printing color figures is \$340 for each page. The total charge may be reduced or waived in accordance with conditions in the country where the study took place.

(Revised February 2011)

Editorial and Head Office:

Pearl City Koishikawa 603
2-4-5 Kasuga, Bunkyo-ku
Tokyo 112-0003 Japan
Tel: +81-3-5840-8764
Fax: +81-3-5840-8765
E-mail: office@biosciencetrends.com

JOURNAL PUBLISHING AGREEMENT (JPA)

Manuscript No.:

Title:

Corresponding Author:

The International Advancement Center for Medicine & Health Research Co., Ltd. (IACMHR Co., Ltd.) is pleased to accept the above article for publication in BioScience Trends. The International Research and Cooperation Association for Bio & Socio-Sciences Advancement (IRCA-BSSA) reserves all rights to the published article. Your written acceptance of this JOURNAL PUBLISHING AGREEMENT is required before the article can be published. Please read this form carefully and sign it if you agree to its terms. The signed JOURNAL PUBLISHING AGREEMENT should be sent to the BioScience Trends office (Pearl City Koishikawa 603, 2-4-5 Kasuga, Bunkyo-ku, Tokyo 112-0003, Japan; E-mail: office@biosciencetrends.com; Tel: +81-3-5840-8764; Fax: +81-3-5840-8765).

1. Authorship Criteria

As the corresponding author, I certify on behalf of all of the authors that:

- 1) The article is an original work and does not involve fraud, fabrication, or plagiarism.
- 2) The article has not been published previously and is not currently under consideration for publication elsewhere. If accepted by BioScience Trends, the article will not be submitted for publication to any other journal.
- 3) The article contains no libelous or other unlawful statements and does not contain any materials that infringes upon individual privacy or proprietary rights or any statutory copyright.
- 4) I have obtained written permission from copyright owners for any excerpts from copyrighted works that are included and have credited the sources in my article.
- 5) All authors have made significant contributions to the study including the conception and design of this work, the analysis of the data, and the writing of the manuscript.
- 6) All authors have reviewed this manuscript and take responsibility for its content and approve its publication.
- 7) I have informed all of the authors of the terms of this publishing agreement and I am signing on their behalf as their agent.

2. Copyright Transfer Agreement

I hereby assign and transfer to IACMHR Co., Ltd. all exclusive rights of copyright ownership to the above work in the journal BioScience Trends, including but not limited to the right 1) to publish, republish, derivate, distribute, transmit, sell, and otherwise use the work and other related material worldwide, in whole or in part, in all languages, in electronic, printed, or any other forms of media now known or hereafter developed and the right 2) to authorize or license third parties to do any of the above.

I understand that these exclusive rights will become the property of IACMHR Co., Ltd., from the date the article is accepted for publication in the journal BioScience Trends. I also understand that IACMHR Co., Ltd. as a copyright owner has sole authority to license and permit reproductions of the article.

I understand that except for copyright, other proprietary rights related to the Work (*e.g.* patent or other rights to any process or procedure) shall be retained by the authors. To reproduce any text, figures, tables, or illustrations from this Work in future works of their own, the authors must obtain written permission from IACMHR Co., Ltd.; such permission cannot be unreasonably withheld by IACMHR Co., Ltd.

3. Conflict of Interest Disclosure

I confirm that all funding sources supporting the work and all institutions or people who contributed to the work but who do not meet the criteria for authors are acknowledged. I also confirm that all commercial affiliations, stock ownership, equity interests, or patent-licensing arrangements that could be considered to pose a financial conflict of interest in connection with the article have been disclosed.

Corresponding Author's Name (Signature):

Date:

